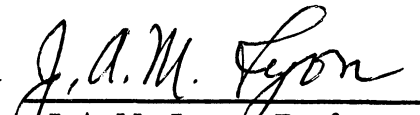## STUDY AND INVESTIGATION OF A UHF-VHF ANTENNA

Sixth Quarterly Report
1 April 1967 through 30 June 1967

August 1967

Prepared by

J. A. M. Lyon, C-C Chen, E. S. Greene
J. C. Parker and D. L. Smith

Approved by *J. A. M. Lyon*

J. A. M. Lyon, Professor
Electrical Engineering

Contract No. AF 33 (615)-3609
Project 6278, Task 627801
O. E. Horton, Project Monitor

Air Force Avionics Laboratory, AVWE
Research and Technology Division, AFSC
Wright-Patterson Air Force Base, Ohio

FOREWORD

ACKNOWLEDGEMENTS

ABSTRACT

This report discusses the activity and accomplishment of the various aspects of four assigned tasks of this project for a three month period. Under Task 1, studies have centered upon the development of a helical slow wave structure utilizing ferrite. The objective is to use this helical structure as a winding on a log conical spiral. In this way, the ferrite loading material would be associated with the conductor of the log conical spiral rather than as a core.

A ferrite loaded slot array is being studied under Task 2. Some preliminary results are given utilizing type Q-3 ferrite sticks in transmission line fed slots. As a result, the type of ferrite loaded slot arrays will be completely changed in future work. Individually ferrite slots will be used rather than those fed by a waveguide. The objectives under the new program of ferrite loaded arrays are described in some detail.

Under Task 3, studies have been made on ferrite rod antennas. Most of the work has been on analysis of such antennas. Simple experimental models have been fabricated, but test data are not yet available. Various analytical approaches are considered in the report. A review has been made of such analyses by other workers. An analysis more complete than any heretofore, is now underway. Principal considerations of this analysis are given.

Various types of antenna configurations useful down to 30 MHz are studied under Task 4. A discussion and analysis is given on the advantages of multi-linear elements. Experimental data are recorded upon the tuning of linear elements utilizing magnetic biasing. Multiple resonance behavior of composite slow wave structures is considered both experimentally and analytically.

Additional information is reported on the testing of ferrite materials. For the frequency ranges involved, previous test methods have not been entirely satisfactory. For this reason, a strip line cavity was fabricated.

LIST OF FIGURES

TABLE OF CONTENTS

I

INTRODUCTION

During this quarterly report period, progress has been made in each of the general areas designated as Tasks under this contract.

Task 1 dealing with the log conical spiral antenna has been given considerable emphasis during this period. A rather detailed study of slow wave structures, useful for winding such an antenna, has been made. The reduction in size possible, using a slow wave winding, involving a helical wire about a ferrite core, has approached the ratio of 4 : 1. This reduction factor has been observed upon the basis of radiation patterns at various frequencies. Radiation patterns taken on a cylindrical helix antenna wound with such a slow wave winding have been very satisfactory.

Efficiency tests on the antenna were not satisfactory. The efficiencies achieved were unexpectedly low. The efficiency can be contrasted with use of a ferrite core in a cylindrical helix wound with a simple circular conductor. Efficiency of the order of 60 percent was achieved for such cylindrical helical antennas. It is believed at this time that the slow wave structure utilizing ferrite is very much dependent upon the Q-factor of the ferrite; particularly, the magnetic Q is of extreme importance. The contribution of ferrite material in this slow wave structure can be considered to be provided by molecular currents in the ferrite. A slow wave structure could be formed by using more turns of solid copper conductor. Whether one structure is better than another will be very much dependent upon the losses of the structure.

Task 2, involves slot arrays utilizing ferrite loading. The activity under this task originally concentrated on a waveguide section utilizing a number of slots cut in the broad wall. However, difficulties were encountered due in large part to the fact that the type Q-3 ferrite sticks were not capable of operating at as high a frequency as indicated in the printed sales literature. For this reason, an unsatisfactory

design of an array developed. The actual cutoff frequency of this array was considerably above that which was calculated based upon published electrical characteristics of the type Q-3 material. After numerous efforts to modify this design, it was decided to embark on an entirely different design using separate ferrite filled slots. This change was in accordance with the desire of the contract monitor.

This task is now being studied, utilizing three slots in a linear array. The linear array will be arranged first so that the H-fields are collinear and later a similar linear array will be arranged so that the E-fields are collinear. Provision is being made so that magnetic bias can be applied in various amounts to the individual ferrite filled slots. Phase and amplitude control of the illumination of each of the slots will be by appropriate elements placed in the coaxial feed lines to each slot. Some control of either amplitude or phase or possibly both, may be achieved by the application of magnetic bias. Detailed arrangements of the magnetic bias schemes have yet to be worked out.

Under Task 3, a large amount of analysis has been made of ferrite rod radiators. The starting point for this analysis was the available analysis of dielectric rod radiators. In surveying the available analyses, it was found that each of the available analyses had considerable deficiencies due to the mathematical model used. The mathematical model available in the literature which seems closest to being satisfactory is the one designated in this report as Fradin's analysis. This analysis makes use of electric polarization currents on the boundary surface of the dielectric rod antenna. The analysis offered by this project is one which will make use of both electric and magnetic polarization currents on the boundary surface of a ferrite rod. A rather complete discussion of the merits and defects of presently available analysis of rod antennas is included in this report. The experimental part of this task is underway to the extent that some ferrite rod designs have been made and are ready for testing.

Effort has been continued under Task 4 in the development of antenna types suitable for operation down to 30 MHz. Both experimental and analytical studies have been made. This task has reviewed many types of configuration of radiating element with a view to use at this frequency range. In the present report, details are given on the study of multiple linear elements. Such multiple linear elements can use material loading as is indicated in the report. In the report, emphasis is placed on three different geometrical configurations, - a single helical monopole, a double helical monopole, and a folded helical monopole. These arrangements were tested with the helix having a hollow core with and without a filling of ferrite.

The study of linear elements was extended to the use of magnetic biasing. It was found that a direct current through an appropriate winding could sufficiently change the characteristics of a a ferrite core so that a shift of the resonant frequency of the linear element could be observed. Shifts in frequency of as much as 7 percent were obtained. This does not seem to constitute a limit..

Substantial work has been done on the measurements of materials. A new resonant cavity has been fabricated utilizing the TEM mode. It is believed that this resonant cavity will be best suited for the frequency range of interest, 100 MHz to 700 MHz. It also offers considerable advantage as far as requiring a minimum of time in preparing the samples for testing. The resonant cavity utilizes a strip line. The cavity has a length of approximately 5'. Tests on the cavity indicated an unloaded Q of approximately 300. Although this was sufficiently high for the determination of the real part of permeability of samples utilizing the perturbation method, it still left something to be desired. For this reason the cavity is now being silver plated in order to improve the unloaded Q. It is believed that if the unloaded Q is approximately 700, then it will be possible to have meaningful measurements of the imaginary part of complex permeability and complex permittivity.

In addition, another measurement circuit has been utilized. This measurement makes use of a sample holder that is really a shielded parallel plate capacitance. In this way measurements were made on the relative dielectric constant of Indiana General type Q-4 material. These measurements were made in the frequency range from 100 MHz to 200 MHz. The values of dielectric constant obtained appeared reasonable. This method has severe limitations as far as frequency and is generally not appropriate for frequencies above 200 MHz; in fact, it may very well be subject to severe limitations above 100 MHz. It is believed that these values so obtained should be checked by the resonant cavity method.

II
FERRITE LOADED CONICAL SPIRALS

2.1 Introduction

The objective of this task is to develop a ferrite filled conical spiral antenna that will cover the 200 to 600 MHz range and reduce to approximately one-third the size of an unloaded conical spiral antenna. The antenna is to have circular polarization with a broad forward directional main beam. The antenna should also be capable of employing both the transmit and receive modes simultaneously.

Throughout the course of this contract, emphasis has been placed on size reduction of helix antennas instead of conical spiral antennas. The reasons are two: 1) a helix is a special case of a conical spiral antenna that occurs when the cone angle is 0 degrees; 2) helix antennas are much easier to construct and analyze mathematically. Therefore more investigations can be made into reduction techniques with the time and money available.

During this report period, a helix antenna with a winding consisting of a ferrite filled helical slow wave structure winding was studied. Tests performed on this antenna indicate that it has good helix antenna patterns from 160 to 210 MHz corresponding approximately to a 4 to 1 reduction of the diameter of this antenna. The input impedance over this frequency range centers around $400 - j200$ ohms. However, the gain measurements indicate that the antenna is very lossy. Current distribution measurements indicate that a standing wave current distribution exists on the antenna instead of a traveling wave distribution attenuating rapidly from the tip as occurs for the conventional unloaded backward-fire helix antenna current. Thus, the helix antenna wound with a ferrite filled helical slow wave structure winding is a reduced size helix antenna of rather low efficiency. A higher magnetic Q of the ferrite filling could considerably improve the efficiency.

2.2 Antenna Description

The antenna is a 6-1/2 turn bifilar helix antenna. The conductor of the antenna is a smaller helix, wound on a 3/4" O.D. x 3/32" thick piece of Tygon

polyvinyl tubing with number 20 enameled copper wire. The small helix is wound at a ptich angle of 8°. The conductor is itself wound on a 3-1/8" O.D. x 1/16" thick piece of NEMA XXX (MIL-P-3115-PBE) paper phenolic tubing at a pitch of 4". The antenna was fed at the tip through an Anzac H-9 hybrid through two pieces of RG-58/U coaxial cable that had the sheilds tied together. Figure 2-1 dipicts the antenna with the windings filled with EAF-2 powdered ferrite. Figure 2-2 shows a cross section of the antenna and gives the dimensions.

Using the largest diametral dimension of the antenna (4-5/8") and the approximate formula that the center frequency of operation occurs when the circumference is approximately a wavelength, then the size of this antenna would correspond to a conventional helix operating at 800 MHz. This is the reference frequency used in the reduction figures given later on.

2.3 Experimental Results

The far field radiation patterns between 160 and 210 MHz for antenna 232 were very close to those observed for a conventional helix antenna, as is indicated in Fig. 2-3. Using the arithmetic average of 160 and 210, or 185 as the center frequency of operation, this would indicate a multiplicative size reduction factor of 0.231. Based on the center frequency of 185 MHz, the bandwidth of operation of antenna 232 is 27 per cent. This compares with a value of 50 percent frequently claimed for a conventional helix antenna.

According to Li and Beam (1957) the slowing factor for the coiled winding used on antenna 232 is 0.28. Thus the patterns are consistent with what is known about the problem.

A Smith Chart of the input impedance is illustrated in Fig. 2-4. The impedance was measured with a Hewlett-Packard Vector Voltmeter. Corrections were made in the data for the phase shift caused by the reference in the Vector Voltmeter arrangement not being at the tip of the antenna. No corrections were made for the attenuation of the cable between the reference and the antenna. The resultant
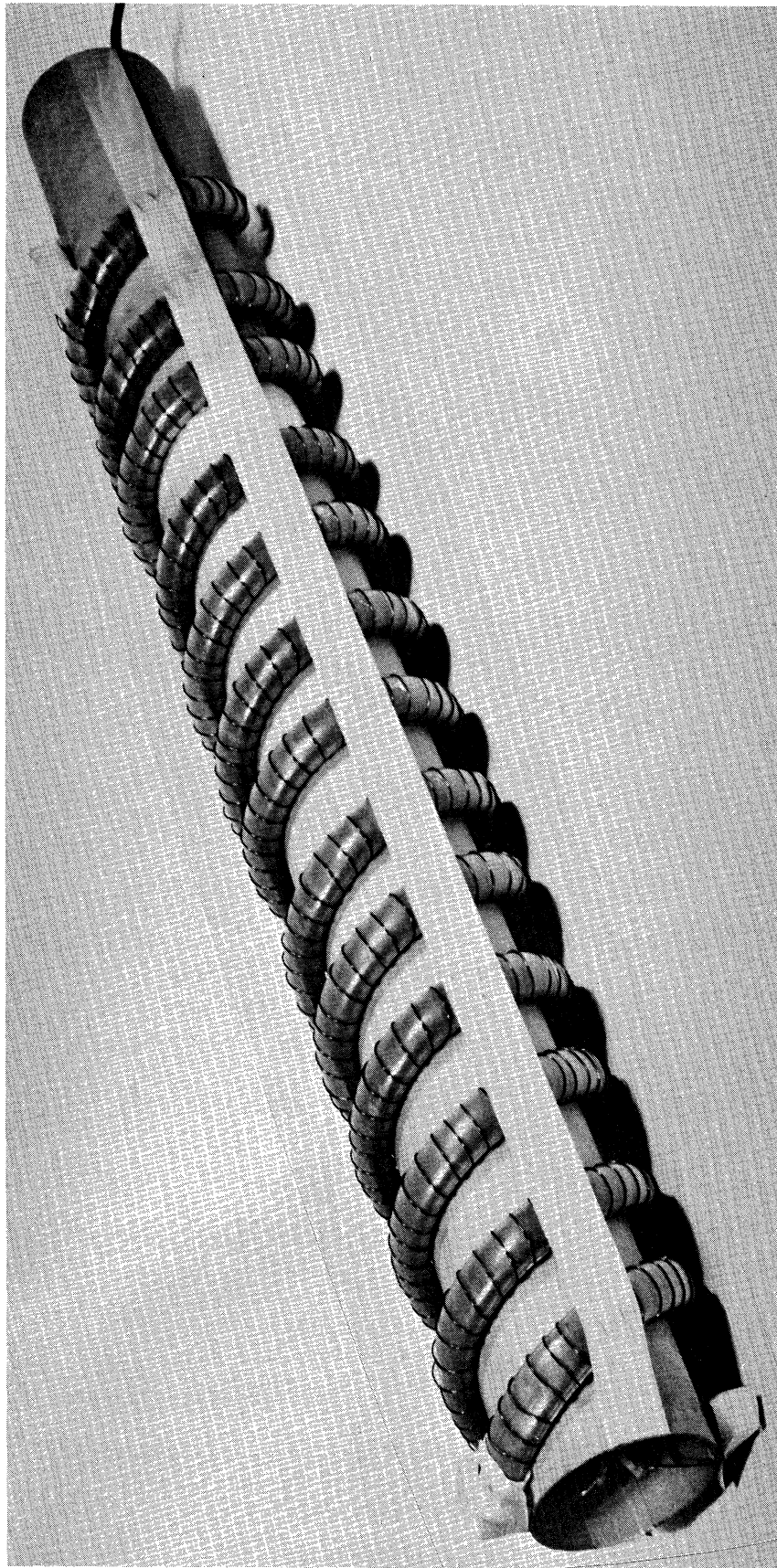
FIG. 2-1: ANTENNA 232 A BIFILAR HELIX ANTENNA WITH A HELIX SLOW
WAVE STRUCTURE WINDING FILLED WITH POWDERED EAF-2
FERRITE.

3/4" O.D. x 3/32" Thick
Tygon Polyvynal Tubing on
Which Antenna Winding is Wound.

NEMA XXX
(MIL-P-3115-PBE)
Paper Phenolic
Tubing

$3\frac{1}{8}"$ D

3" D

EAF-2
Powdered
Ferrite

4"
Antenna
Pitch

$3\frac{7}{8}"$ D

$4\frac{5}{8}"$ D
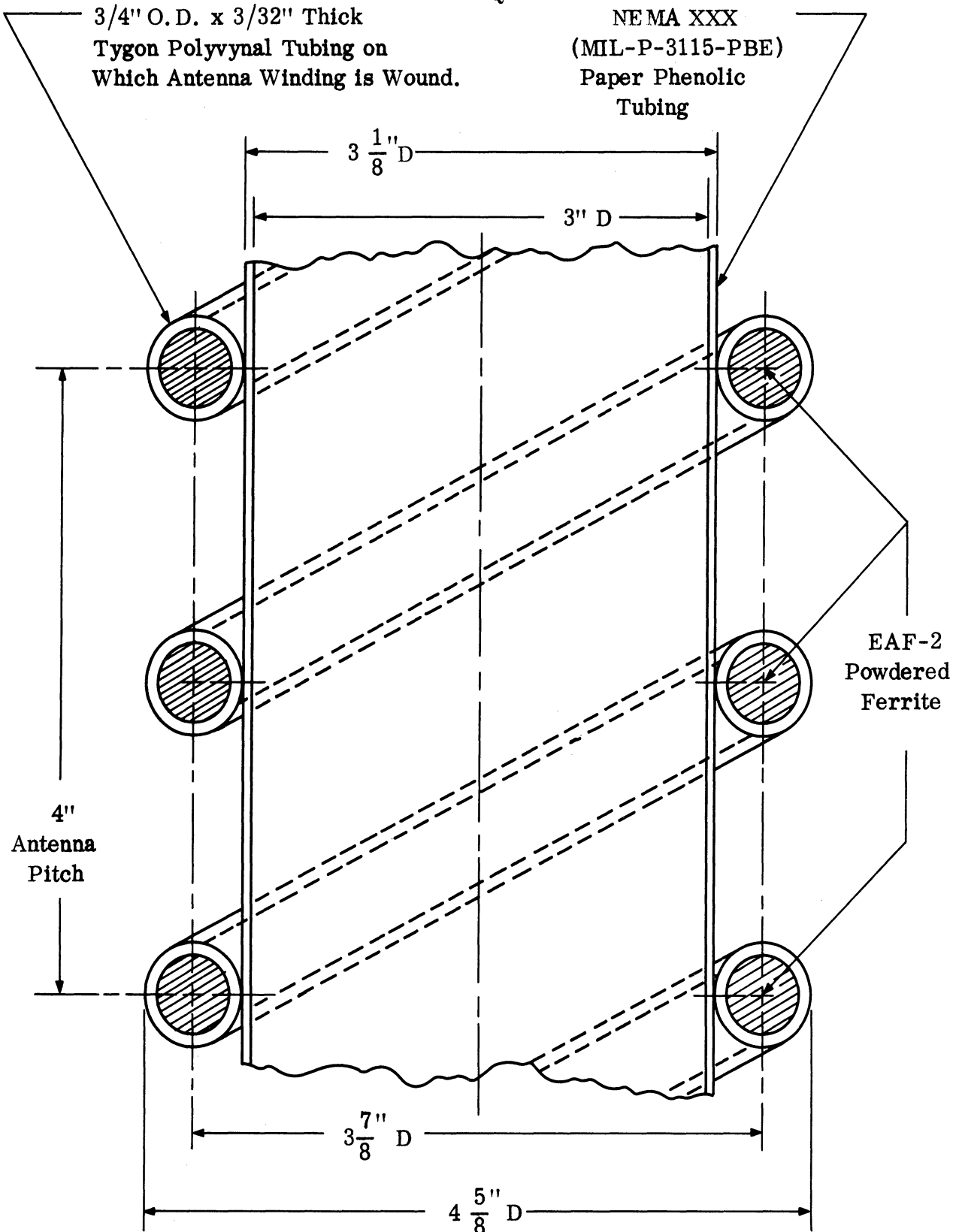
FIG. 2-2: LONGITUDINAL CROSS-SECTION DRAWING OF ANTENNA 232 WITH
THE WINDING HELIX FILLED WITH EAF-2 FERRITE POWDER
SHOWING ALL PERTINENT DIMENSIONS.

160 MHz

170 MHz

175 MHz

180 MHz

190 MHz

200 MHz

210 MHz

220 MHz

$E_\phi{}^2$, Cut 2

$E_\phi{}^2$, Cut 1

$E_\phi{}^2$, Cut 2

$E_\phi{}^2$, Cut 1
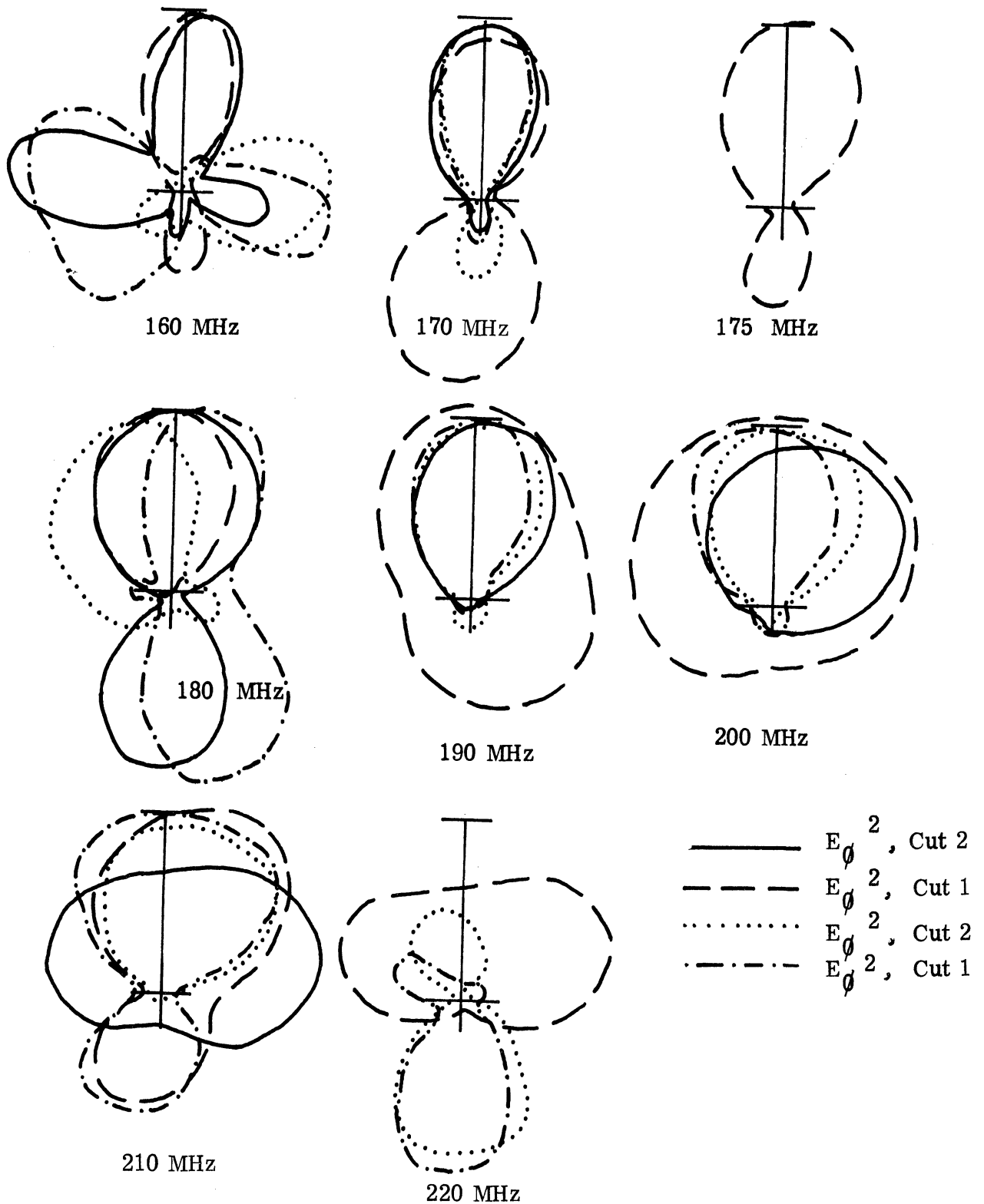
FIG. 2-3: LINEAR POWER RADIATION PATTERNS OF ANTENNA 232, A BIFILAR HELIX WITH A EAF-2 POWDER FERRITE FILLED HELICAL WINDING. CUT 1 IS IN THE PLANE OF THE FEED, CUT 2 IS PERPENDICULAR TO CUT 1.
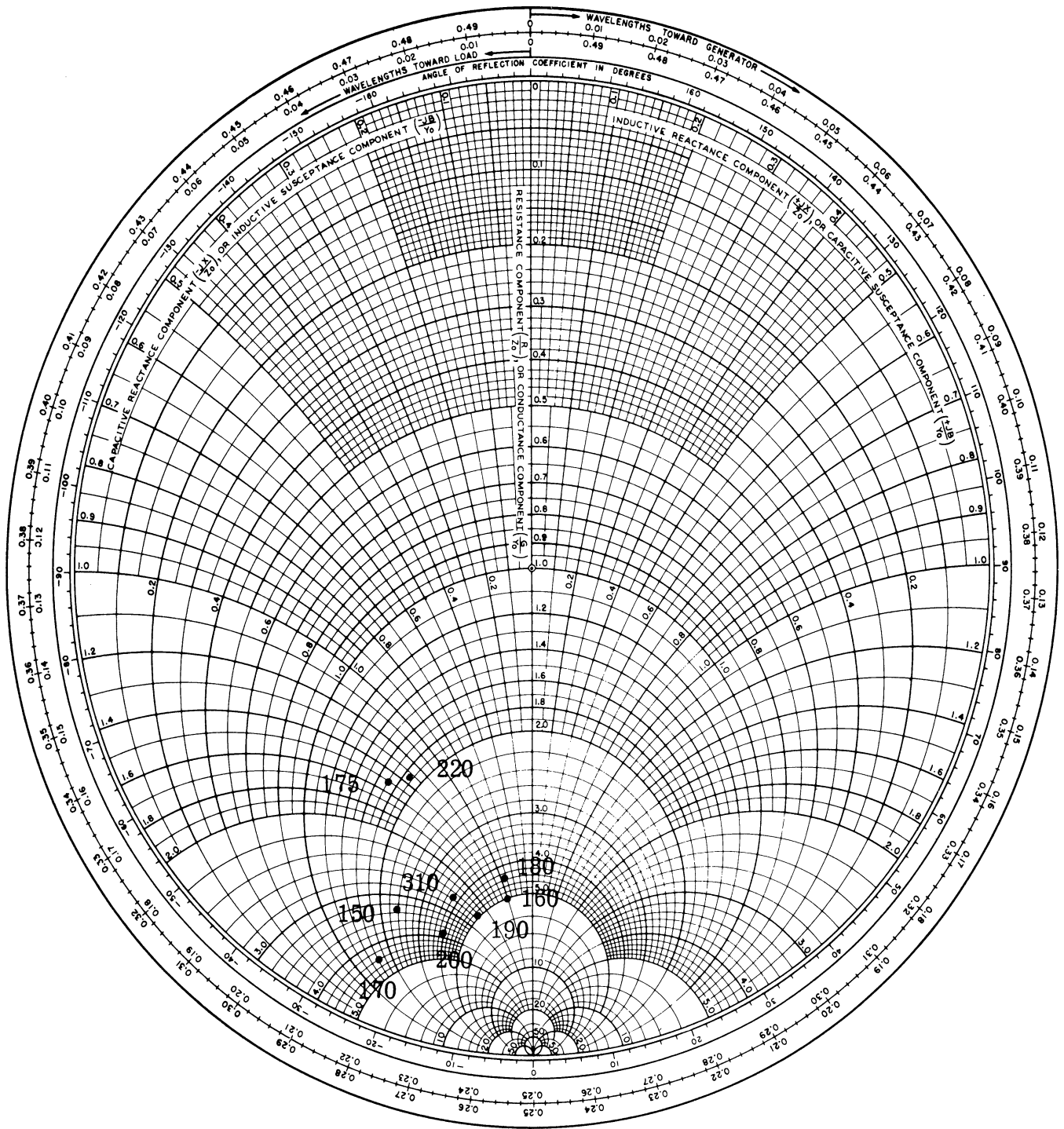
FIG. 2-4: VSWR WITH RESPECT TO 100 Ω FOR ANTENNA 232 WITH THE WINDING FILLED WITH POWDERED EAF-2 FERRITE.

inaccuracy in the magnitude of the reflection should be very small since the cable loss was less than 0.4 db.

Notice that the input impedance of antenna 232 is higher than a conventional helix. This would be expected from the transmission line analogy used to describe some of the properties of a helix antenna, since the coiled conductor is an inductive loading (Lyon et al, 1966, p. 6).

The results of gain measurements on the antenna were not very encouraging. However, additional tests are planned. The loss in the RG-58/U coaxial cable (2 feet) was not used to correct the measured reflection coefficient. At frequencies from 170 MHz to 190 MHz this loss is insignificant.

The polarization ratio was measured at 170 MHz and was 4.5 db. At 190 MHz it was 2.5 db. In both cases, the range of error is ±1 db.

In these last two sets of measurements, the polarization ratio could have been adversely affected by the antenna being only 4 feet above a metal turret. This is 0.68 of a wavelength at 170 MHz and could have contributed to a slight degradation in the value of the polarization ratio measured. The measured values are not, however, unusual for conventional helix antennas. Since the construction of the antenna was not very precise, irregularities may have been the cause of the ellipticity of the polarization.

One reason for the low efficiency of the antenna is apparent from the measured current distribution on the antenna which indicates a standing wave. Figure 2-5 shows the current distribution on the antenna at 170 MHz and Fig. 2-6 shows the current distribution at 190 MHz. In both cases relative amplitude and relative phase were measured.

A small loop (0.131" in diameter) was used to measure the magnetic field at the exterior of the winding as is illustrated in Fig. 2-7. The probe was centered above each winding with the plane of the loop perpendicular to the axis of the antenna as is illustrated. A Hewlett-Packard Vector Voltmeter was used to measure the
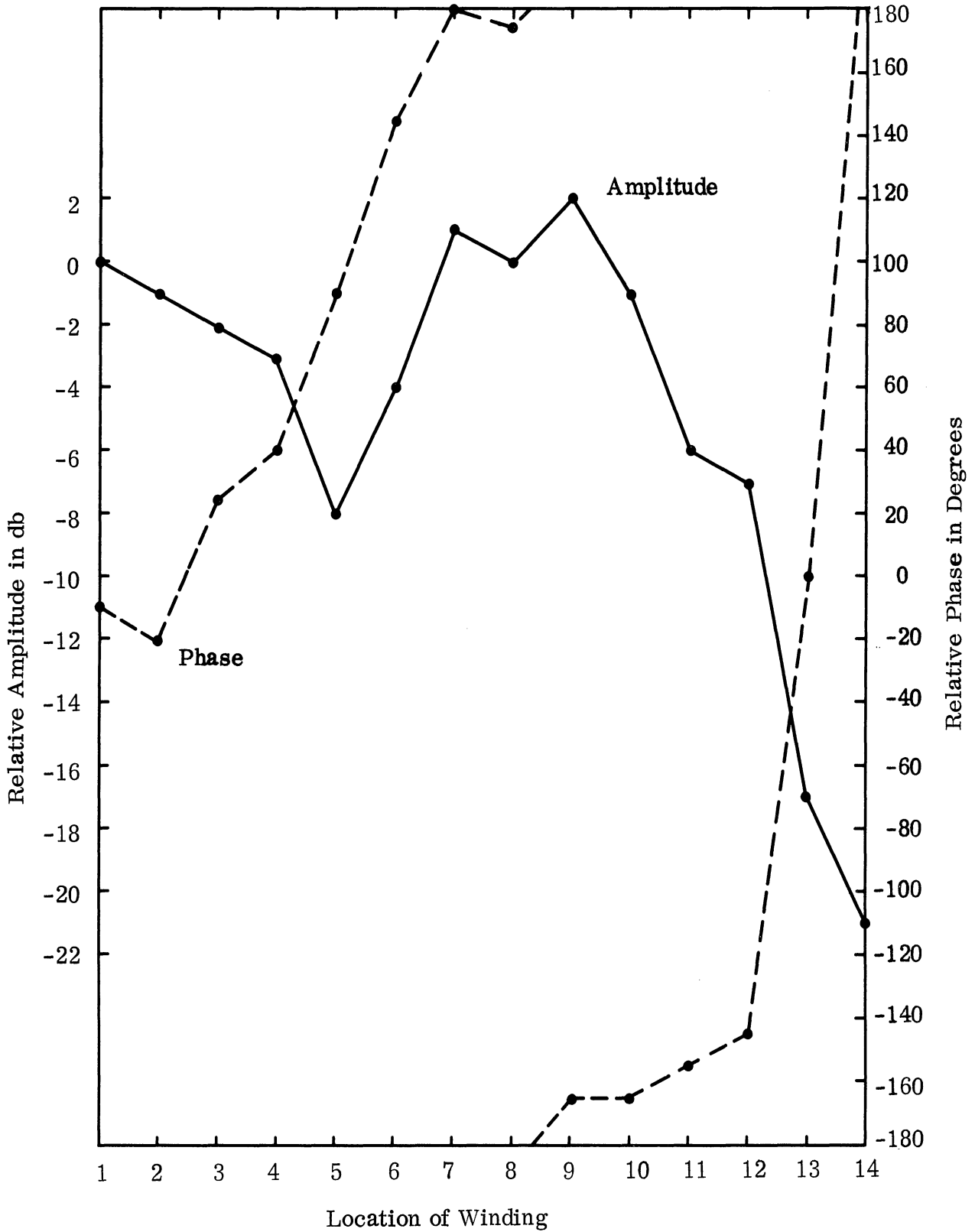
FIG. 2-5: RELATIVE AMPLITUDE AND PHASE OF THE CURRENT ALONG
ANTENNA 232 WITH THE WINDING FILLED WITH EAF-2 POWDERED
FERRITE AT 170 MHz.
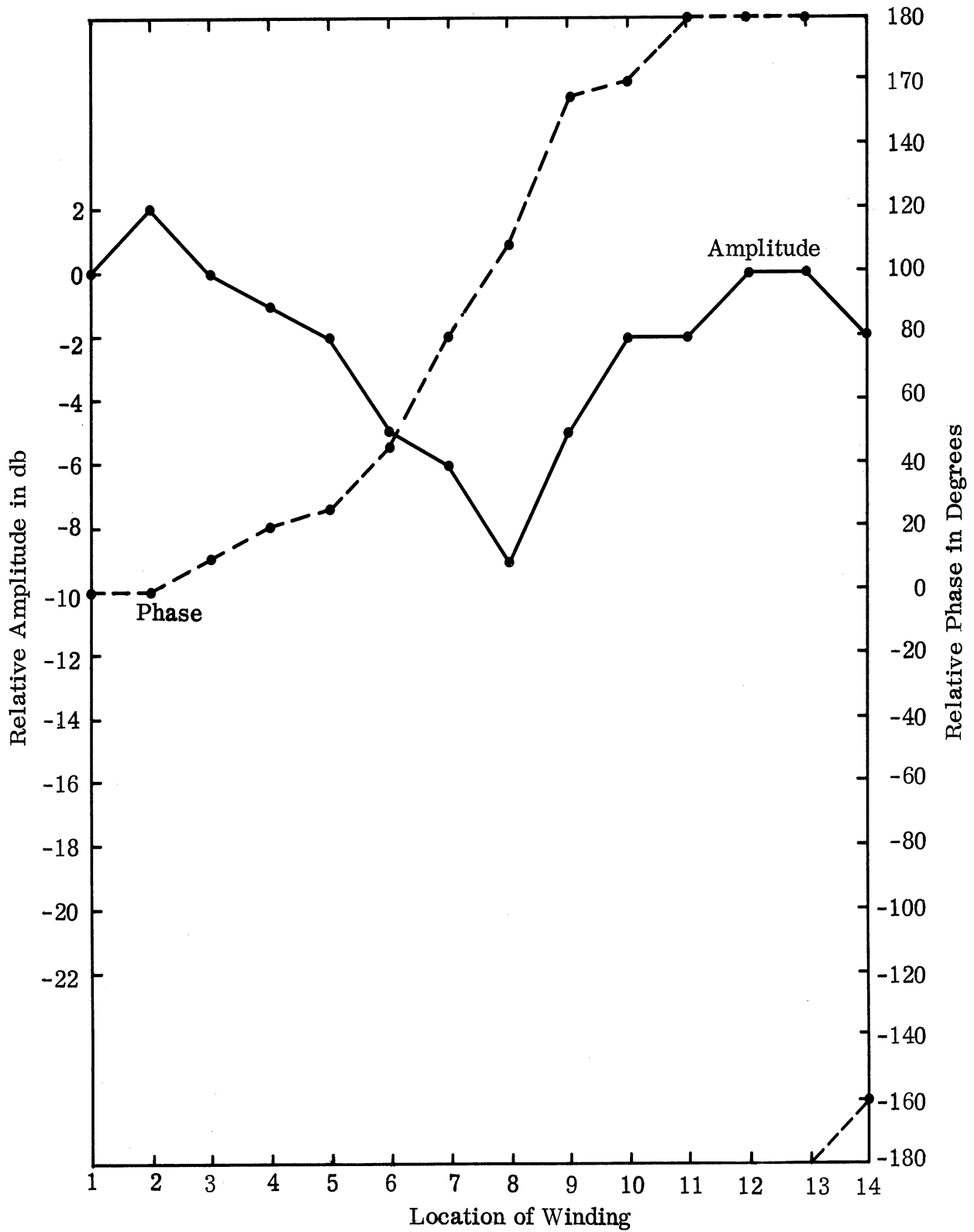
FIG. 2-6: RELATIVE AMPLITUDE AND PHASE OF THE CURRENT ALONG ANTENNA 232 WITH THE WINDING FILLED WITH EAF-2 POWDERED FERRITE AT 190 MHz.
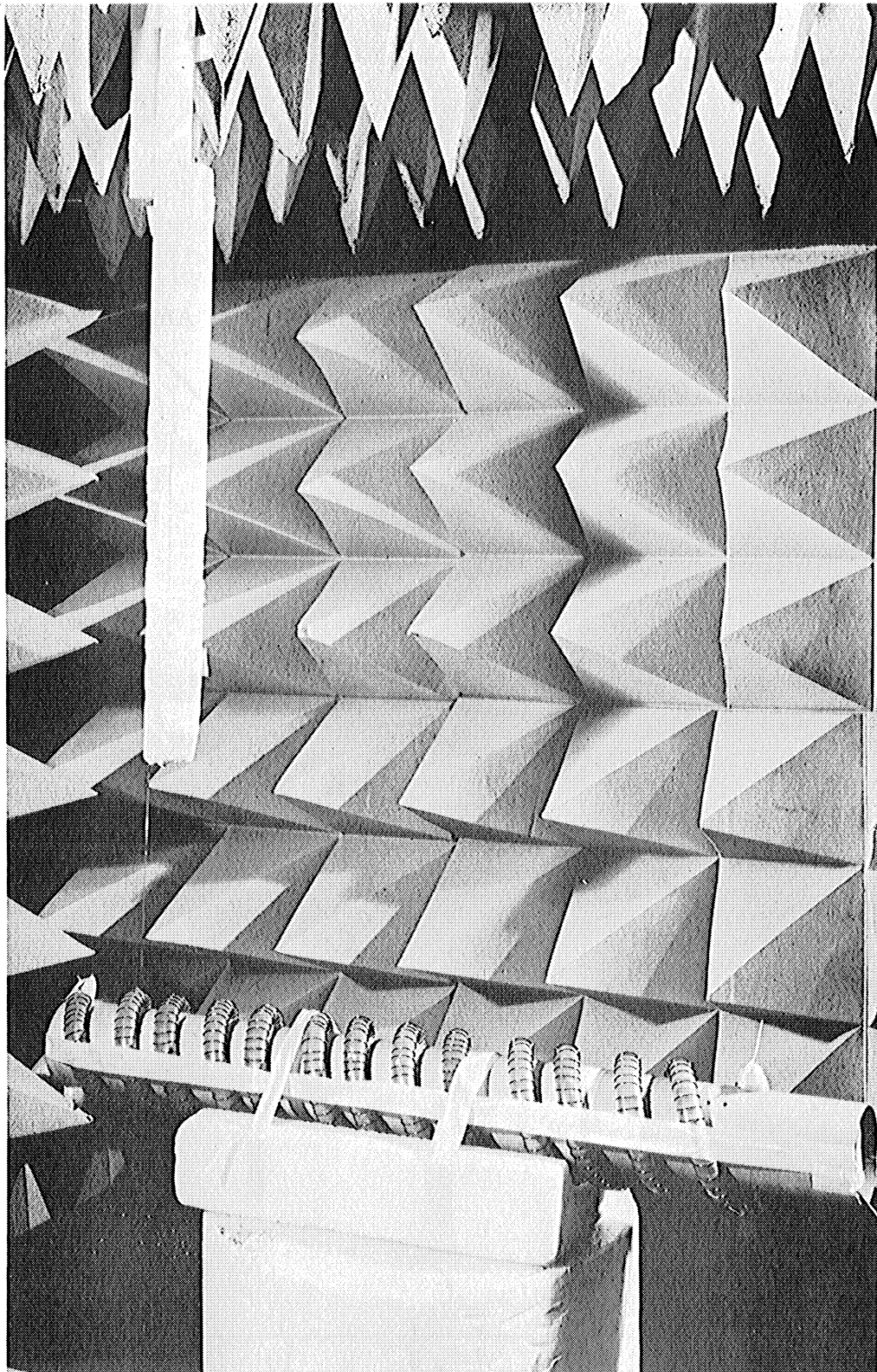
FIG. 2-7: ANTENNA 232, A BIFILAR HELIX ANTENNA WITH A FERRITE FILLED HELICAL WINDING SHOWING THE LOCATION OF THE LOOP PROBE WITH RESPECT TO ANTENNA 232.

relative phase and amplitude of the voltage induced in the probe; the voltage is, of course, proportional to the current in the winding.

As is seen from Figs. 2-5 and 2-6, a standing wave current distribution exists along the antenna with some loss present which fills in the nulls of the amplitude curve and smooths out the phase curve. The numbers along the abscissa of the plots indicate the locations of the winding at each point of intersection as the probe was moved down the axis of the antenna from the tip to the opposite end. Point 1 corresponds to the tip (feed point) and point 14 corresponds to the end of the winding.

III

SLOT ARRAYS

Considerable effort was spent to fabricate a ferrite-loaded slot array to operate at frequency below 200 MHz. For the limited amount of ferrite material available in this Laboratory, a waveguide section (11.5 cm x 1.0 cm x 120 cm) designed to have a cutoff frequency at 126 MHz with Q-3 ferrite sticks filled inside was tested as a transmission line before the slots had been cut in the waveguide. A small current loop located approximately one fourth guide wavelength from the adjustable shorting end was used to obtain an optimum impedance match. The VSWR characteristic as a function of frequency from 180 to 900 MHz is shown in Fig. 3-1. The cutoff frequency is much higher than the designed frequency due to the unavoidable air gaps between the small solid ferrite sticks and the impertion of the material. Measurements of the wave attenuation along the ferrite-loaded waveguide were made with a voltage probe of a Hewlett-Packer Vector Voltmeter moving along a longitudinal slot located at the center of the waveguide. The results are shown in Fig. 3-2. An attenuation of -56 db per free space wavelength at 250 MHz was observed. The experimental study of the ferrite-loaded waveguide slot arrays was discontinued because of the impractically high ferrite loss in the waveguide. However an array of individual ferrite filled slot cavities is now under investigation. The re-oriented program will include the investigation of

1) Impedance characteristics of the array including driving point impedances values;

2) Beam controlability of the array as well as the individual slot cavities by magnetic tuning;

3) Side lobe levels and angles as a function of power distribution;

4) Size reduction and decoupling effects of the array of slot cavity antenna.

5) Use of magnetic bias for frequency band shift.
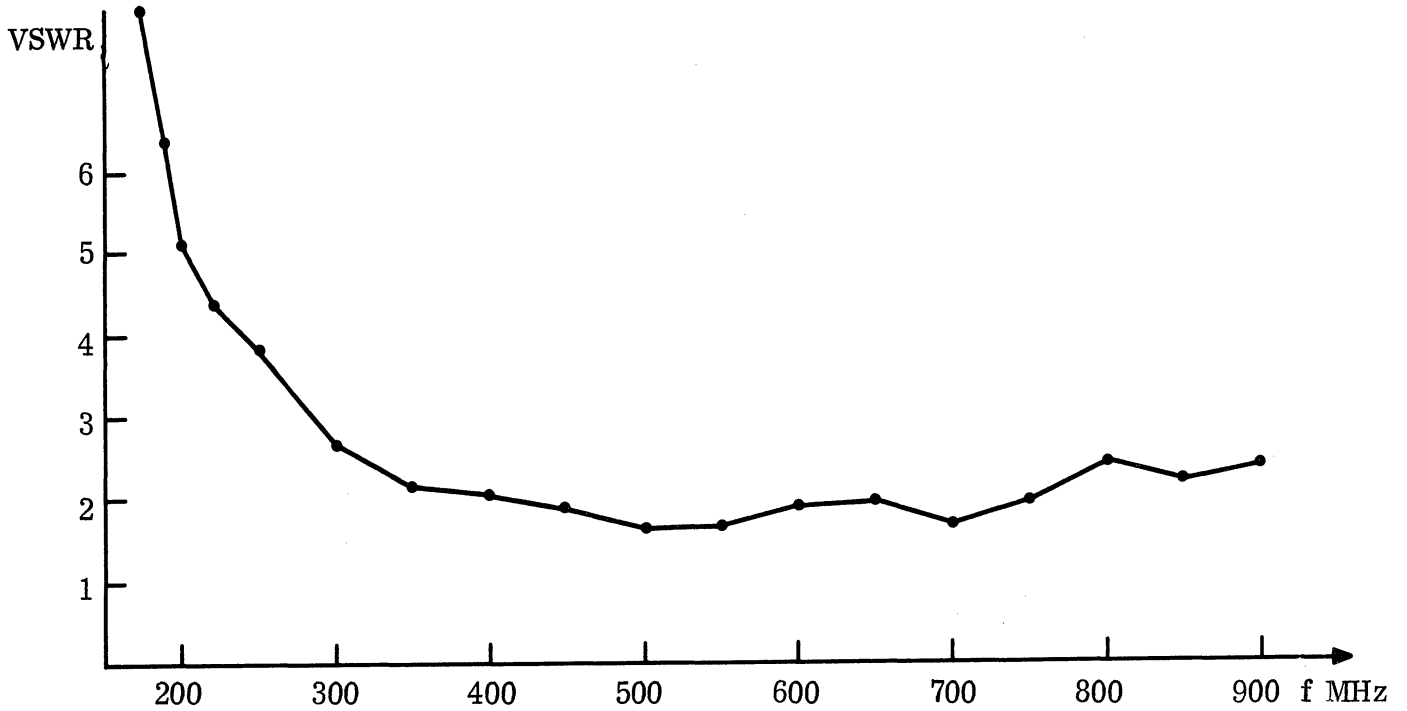
FIG. 3-1: VSWR OF THE 11.5 cm x 1.0 cm CROSS-SECTION Q-3 FERRITE
FILLED WAVEGUIDE WITH A FEEDING LOOP LOCATED
APPROXIMATELY 1/4 GUIDE WAVELENGTH FROM THE
SHORTING END.
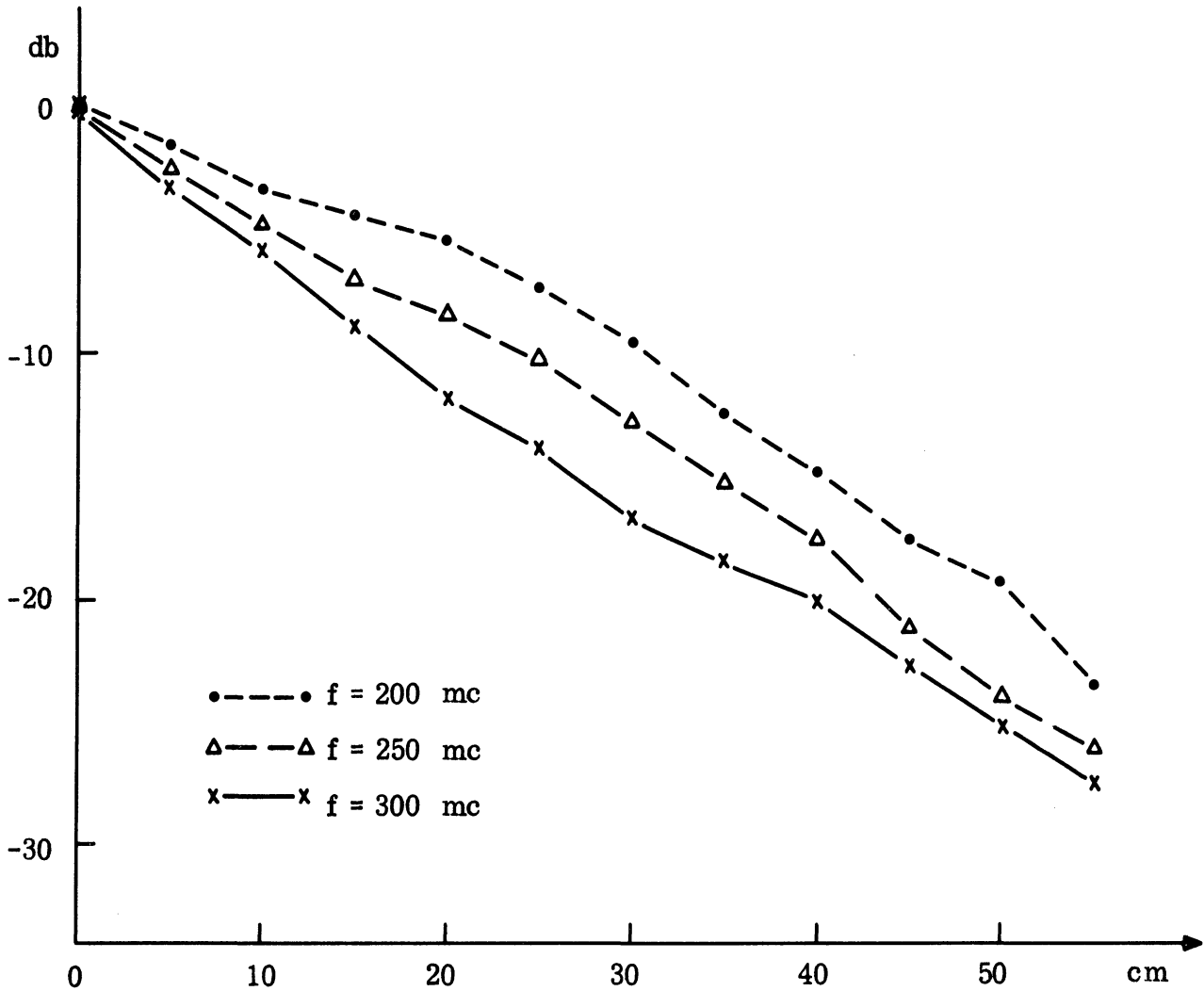
FIG. 3-2: WAVE ATTENUATION ALONG THE LONGITUDINAL DIRECTION OF
THE 11.5 cm x 1.0 cm CROSS-SECTION Q-3FERRITE FILLED
WAVEGUIDE.

IV

FERRITE ROD ANTENNA

4.1 Historical Background

The dielectric analogy will be used to calculate radiation field of an isotropic ferrite rod antenna, the analysis of the dielectric has been already investigated by Horton (1948); Brown and Spector (1957); Fradin (1961); James (1967) and many others, but it continues to be a challenging problem in electromagnetic theory. Thus for all the analysis attempts have been based on various unsupportable assumptions and approximate techniques. Even so, the agreement between these theoretical solutions and experimental results are fairly good.

Arguments on the validity in the application of Schelkunoff's equivalence principle appear in the lattest paper by J.R. James. He states that all treatments of a uniform cylindrical dielectric rod antenna radiating from the radial surface, like a leaky guide are fallacious. He belives that radiation occurs only at discontinuities and the dielectric rod antenna can be treated as a two aperture endfire array. A brief review of three representative analyses by Horton, Fradin and Brown are given below for comparison. This development will indicate a new method to estimate the radiation field of the ferrite rod antenna which is an analog of the dielectric rod. Later this approach will be used to solve the problems of the paraboloidal tapered antenna and the spherical stub antenna.

4.2 Review of the Existing Methods

4.2.1 Horton's Analysis

Horton applied Schelkunoff's equivalence principle to the surface S_d of the dielectric rod as shown in Fig. 4-1 with

$$\bar{J} = \bar{n} \times \bar{H}_t \ , \tag{4.1}$$

and

$$\bar{M} = \bar{E}_t \times \bar{n} \ , \tag{4.2}$$

$$\overline{J} = \overline{n} \times \overline{H}_t$$

$$\overline{M} = \overline{E}_t \times \overline{n}$$
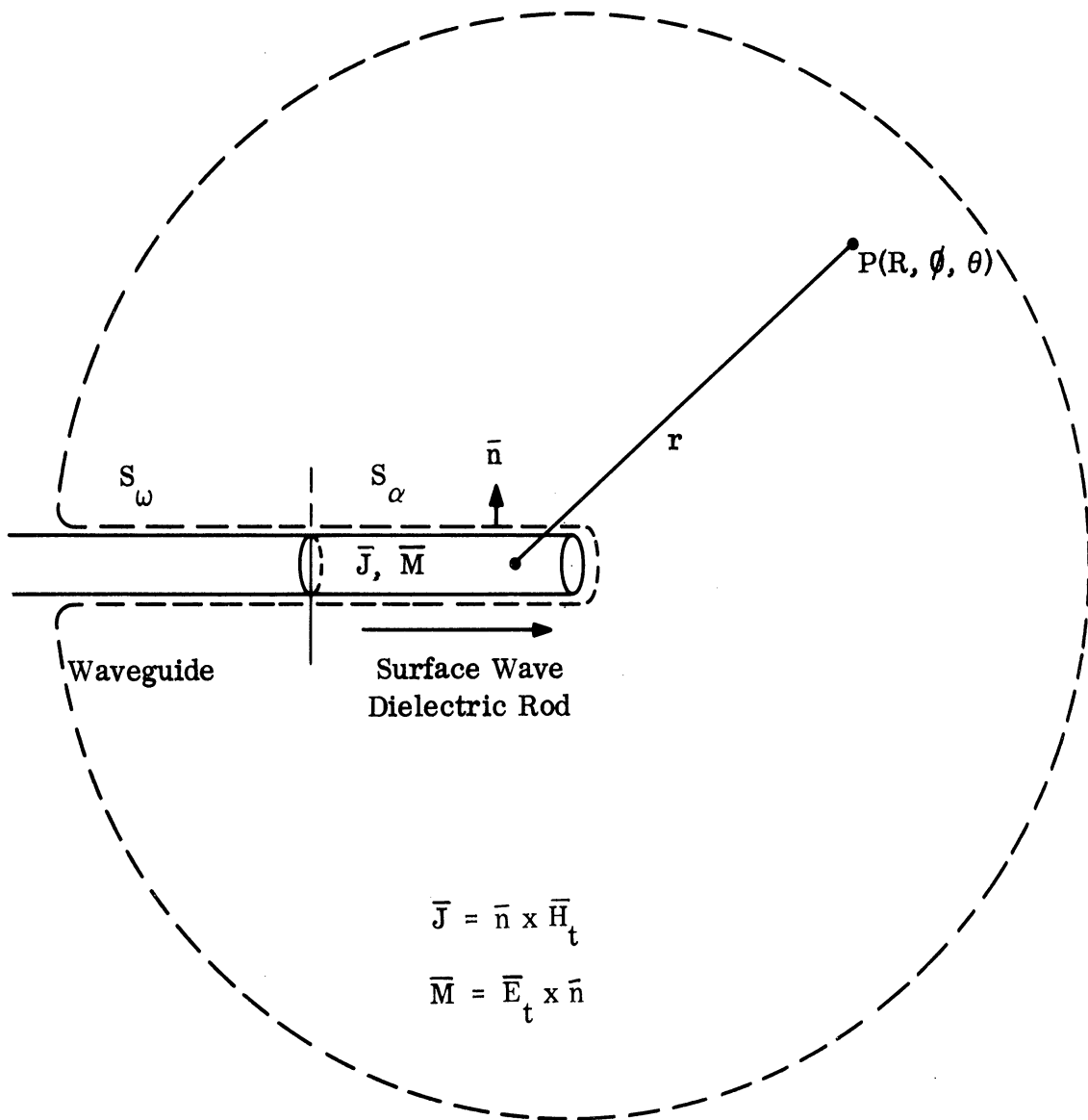
FIG. 4-1: EQUIVALENT SURFACES USED TO ESTIMATE THE RADIATION FIELD OF THE DIELECTRIC ROD ANTENNA IN HORTON'S ANALYSIS.

20

where n is the unit vector directed outward from the rod surface, E_t and H_t are the transverse vector fields on the rod surface. Thus the far field radiation patterns is obtained from the magnetic vector potential A and electric vector potential F in terms of E_t and H_t for the dielectric rod of rectangular cross-section, Horton assumes that the fields E and H on the surface of the dielectric rod are the same as those undisturbed fields in the metal waveguide plus a fictitious magnetic current varying across the width of the guide due to the absence of the metal guide wall. For the dielectric rod of circular cross-section Horton assumes that the field interior to and on the surface of the dielectric rod are the same as those on an infinitely long dielectric rod plus two additional correcting factors. One of these factors is the ratio of the radius of the equivalent integration surface S_d to the radius of the actual dielectric rod. The other factors are the amplitudes of each field component as a function of the distance along the rod. Contributions from the end surface S_o of the dielectric rod and the outer surface S_w of the metal waveguide are negligible.

4.2.2 Fradin's Analysis

The electromagnetic fields assumed on the boundary surface of the dielectric rod antenna are only the approximate values. In addition the far field radiation patterns obtained by the surface integral of the vector Kirchloff formula in the direction normal to the equivalence surface, the endfire direction in which we are interested, are poor. Therefore Fradin applied the second equivalence principle to carry out the volume integral. This principle divided the electric field in the dielectric rod into two components, displacement current in free space and displacement current due to the increase of permittivity by the appearance of the dielectric rod. He replaced the later component by an equivalence volume distribution of conductance current J_{eq} and postulated only this equivalence current in the dielectric rod radiation as shown in Fig. 4-2

P(R, ϕ, θ)

r

Surface Wave

Dielectric Rod

$\bar{J}_{eq}$

Waveguide

$$\bar{J}_{eq} = (\epsilon - \epsilon_o) \frac{\partial \bar{E}}{\partial t}$$
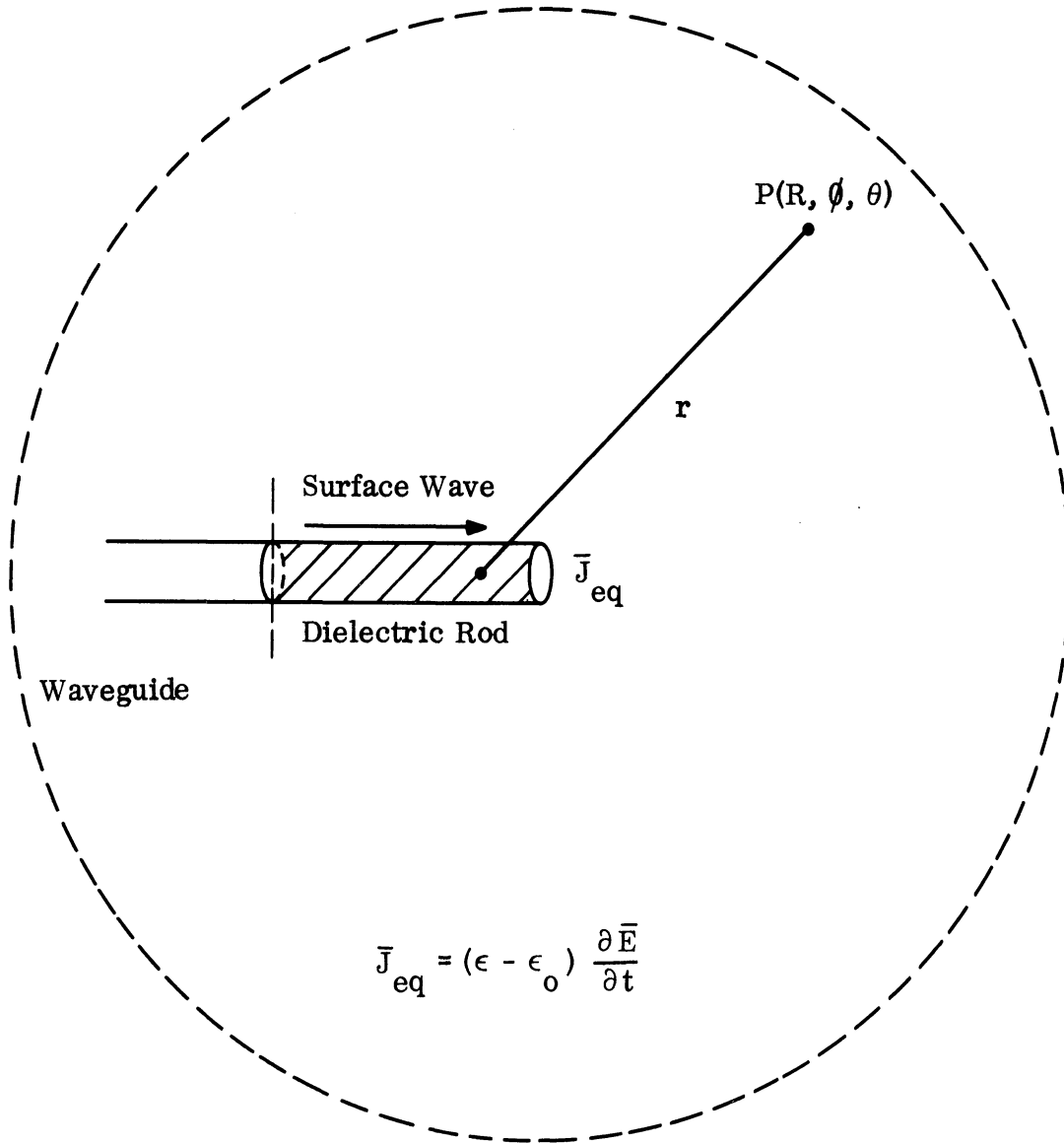
FIG. 4-2: EQUIVALENT VOLUME CURRENT USED TO ESTIMATE RADIATION
FIELD OF THE DIELECTRIC ROD ANTENNA IN FRADIN'S ANALYSIS.

$$\epsilon \frac{\partial E}{\partial t} = \epsilon_o \frac{\partial E}{\partial t} + (\epsilon - \epsilon_o) \frac{\partial E}{\partial t} \tag{4.3}$$

$$J_{eq} = (\epsilon - \epsilon_o) \frac{\partial E}{\partial t} \tag{4.4}$$

The magnetic vector potential A was thus obtained by integrating J_{eq} through the dielectric rod.

4.2.3 Brown's Analysis

Brown and Spector give a physical interpretation of the dielectric rod antenna as a two aperture array. The metal waveguide and the uniform dielectric rod are purely guiding structures like two sections of transmission line with different characteristic impedances. Radiation only occurs at the discontinuities at the free end of the dielectric rod and the junction between the wavegudie feed and the dielectric rod as shown in Fig. 4-3. A wave incident from the far end of the waveguide impinges on the discontinuity at the junction. It generates a surface wave traveling along the dielectric rod, and a reflected wave returning in the waveguide. This results in a reactive field near the junction and a field corresponding to direct radiation from the junction. The field radiated from the junction is assumed to have a radiation pattern similar to the one estimated directly from the junction aperture as if the dielectric rod were absent. Therefore the dielectric rod antenna can be treated as a two aperture array. The relative energy radiatied from the junction aperture and the free end of the dielectric rod can be determined approximately by experimental measurement of the reflection coefficient at the junction (R.H. Clarke, 1957).

4.2.4 Comparison of Prior Methods

In the treatment of the uniform rectangular dielectric rod problem Horton assumed a fictitious magnetic surface current in addition to the undisturbed field in the recatngular dielectric rod. This is essentially the same as as-
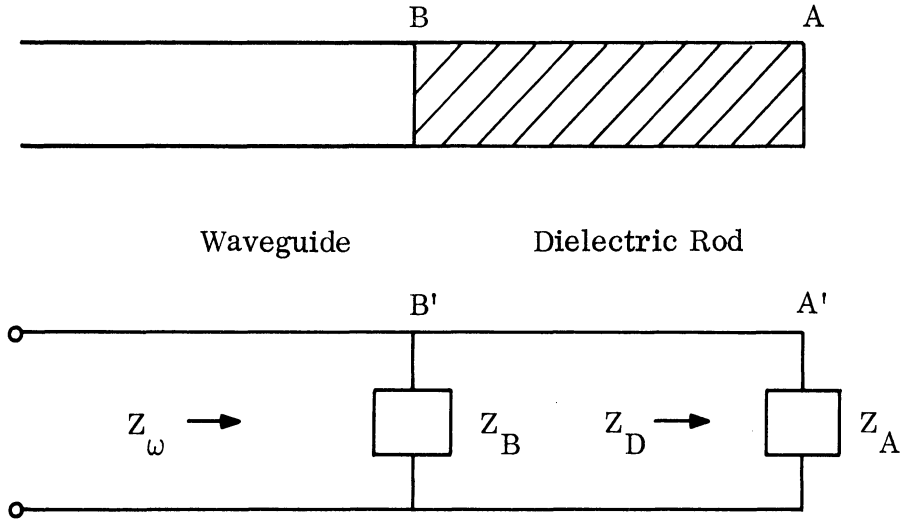
FIG. 4-3: TRANSMISSION LINE ANALOGUE OF THE DIELECTRIC ROD
ANTENNA.

suming an incident wave and a scattered wave due to the discontinuity from the junction. However in the circular dielectric rod problem the equivalent surface used to estimate the radiation fields is incorrect for it contradicts his assumption; since he assumed a surface wave travels along the axis just as for an infinite long dielectric rod. The energy is partly propagated inside the dielectric rod and partly outside. The equivalence surface should be the one that takes account of the contribution from the entire surface wave; i.e., the equivalence surface involves a transverse plane extending to infinity as shown in Fig. 4-4.

Fradin's analysis seems to be reasonable, the equivalence volume current is essentially the motion of atomic particles in vacuum and thus can be treated as a source current radiating into an unbounded free space. If one can estimate J_{eq} in terms of E field in the dielectric rod with reasonable accuracy the Kirchhoff's formula will give an approximate solution.

Brown's two aperture array model is questionable for one still remains essentially ignorant of the field at both apertures of discontinuity. In addition the Kirchhoff's formula and array theory can not apply in the presence of the dielectric rod between them. The transmission line analysis is appropriate for an ideal representation; it doesn't exist in practice. In the latest paper, J.R. James (1967) states that the equivalence principle can not apply to the dielectric rod surface between the two ends of the rod. This statement seems to be incorrect since the discontinuity could be interpreted as due to the absence of the wavequide conductor on the surface of the rod.

In conclusion the surface wave rod antenna is neither a two aperture array nor of infinite length supporting a traveling wave. It seems worthwhile to reinvestigate the field distribution surrounding and inside the rod again.
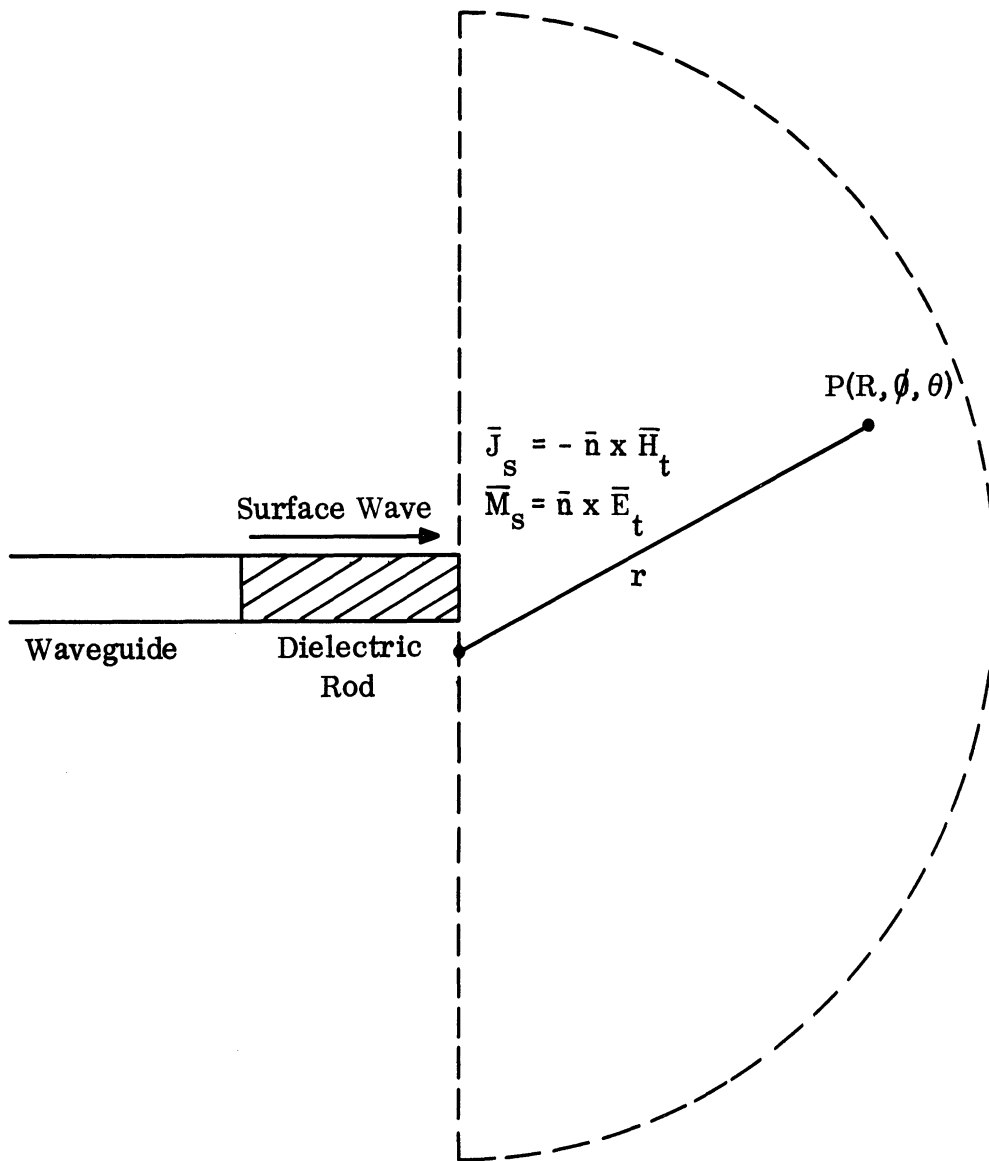
FIG. 4-4: A NEW EQUIVALENCE SURFACE WHICH INCLUDES THE
CONTRIBUTION OF THE ENTIRE SURFACE WAVE.

4.3 Excitation of a Surface Wave on the Ferrite Rod by a Cylindrical Waveguide

A very convenient device to launch a surface wave into a ferrite rod is the cylindrical waveguide. Suppose the semi-infinite circular cylinder is located at $\rho \leq a$, $z \leq 0$. A dielectric rod of radius "a" inside the cylindrical waveguide extends from $z = -\infty$ to $z = +\infty$. Assume the wall-thickness of the cylinder waveguide is negligible. An incident wave from $z = -\infty$ propagation along the rod. As a result of the discontinuity at $z = 0$ where the cylinder waveguide terminates, the energy incident upon the discontinuity will be partly reflected into the waveguide and partly transmitted as surface waves along the dielectric rod with some radiation.

A representation of the discontinuity is shown in Fig. 4-5. Let (ρ, ϕ, z) be the cylindrical coordinates and assume fields inside the ferrite rod or region I and outside the rod or region II. The fields to the left of the discontinuity are directed by the superscript - and to the right denoted by the superscript +. Take the time dependence to be of the form $e^{j\omega t}$. The total electromagnetic fields everywhere are

$$\overline{E} = \overline{E}^i + \overline{E}^S \quad , \tag{4.5}$$

$$\overline{H} = \overline{H}^i + \overline{H}^S \quad , \tag{4.6}$$

where $\overline{E}^i$ and $\overline{H}^i$ are incident fields from $z = -\infty$, $\overline{E}^S$ and $\overline{H}^S$ are the scattered fields due to the discontinuity. The scattered fields obey the homogenous wave equation

$$\left(\nabla^2 + k^2\right)\begin{pmatrix} \overline{E}^S \\ \overline{H}^S \end{pmatrix} = 0 \quad , \tag{4.7}$$

and must satisfy the following conditions:
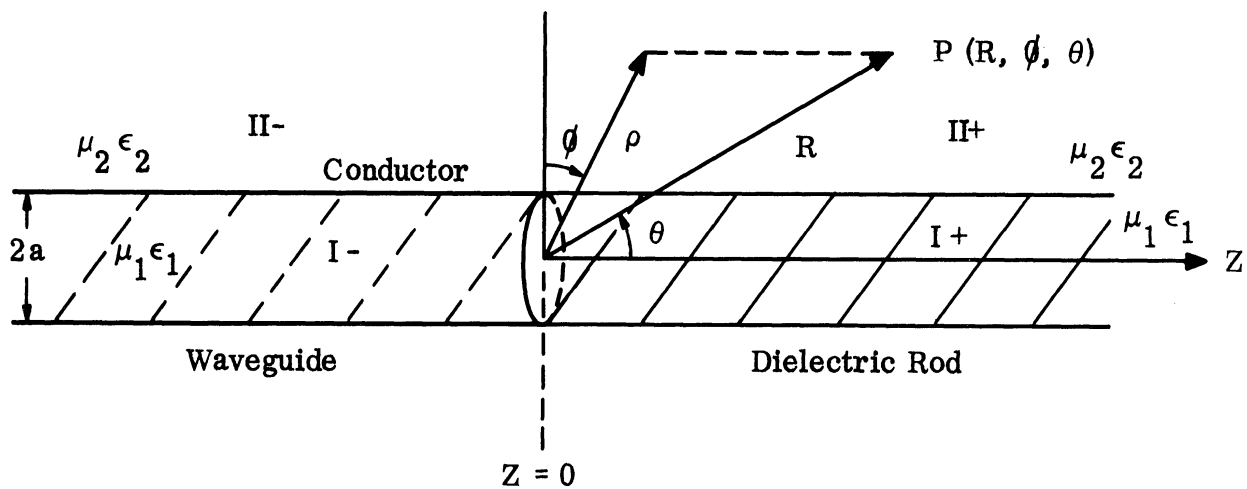
FIG. 4-5: CYLINDRICAL WAVEGUIDE FEED AND DIELECTRIC ROD JUNCTION.
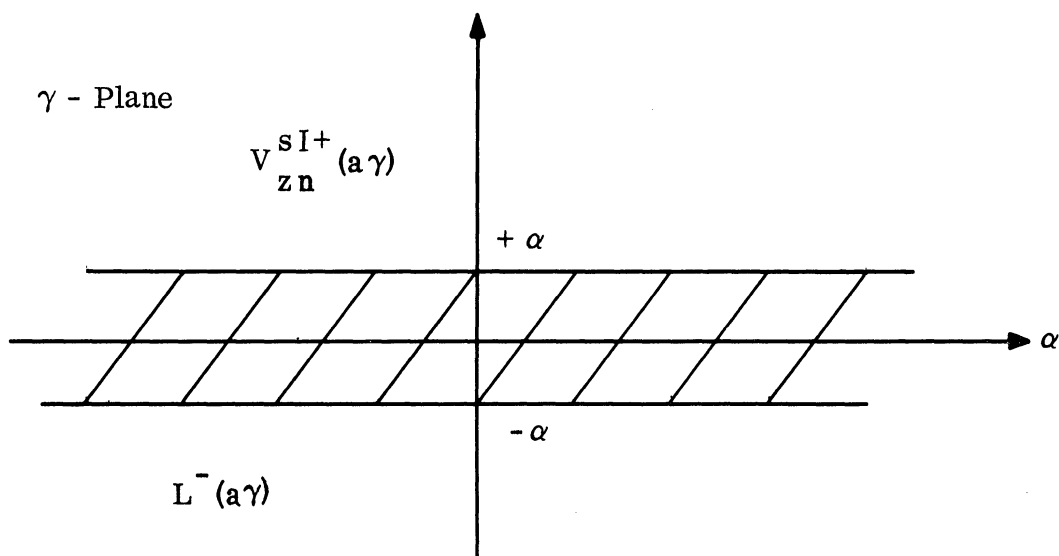
FIG. 4-6: REGIONS OF REGULARITY IN THE COMPLEX γ - PLANE.

1) Tangential field components

$$\begin{cases} E_\phi^{I-} = E_\phi^{II-} = 0 \\ \\ E_\phi^{I-} = E_z^{II-} = 0 \qquad \rho = a, \; z < 0 \end{cases} \tag{4.8a}$$

$$\begin{cases} E_\phi^{I+} = E_\phi^{II+} \\ \\ E_z^{I+} = E_z^{II+} \qquad \rho = a, \; z > 0 \end{cases} \tag{4.8b}$$

$$\begin{cases} H_\phi^{I+} = H_\phi^{II+} \\ \\ H_z^{I+} = H_z^{II+} \qquad \rho = a, \; z > 0 \end{cases} \tag{4.8c}$$

2) E^{II} and H^{II} satisfy the radiation condition at infinity.

Expand all field components in a Fourier series with respect to ϕ and take the Fourier transform with respect to z. Let the transforms of E and H be V and I.

$$V_{zn}(\rho, \gamma) = \frac{1}{2\pi} \int_0^{2\pi} \int_{-\infty}^{\infty} E_z(\rho, \phi, z) e^{+j(\gamma z + n\phi)} \, d\phi \, dz \tag{4.9a}$$

$$E_z(\rho, \phi, z) = \frac{1}{2\pi} \sum_{n=-\infty}^{\infty} e^{jn\phi} \int_{-\infty}^{\infty} V_{zn}(\rho, \gamma) e^{-j\gamma z} \, d\gamma \tag{4.9b}$$

$$I_{zn}(\rho, \gamma) = \frac{1}{2\pi} \int_0^{2\pi} \int_{-\infty}^{\infty} H_z(\rho, \phi, z) e^{+j(\gamma z + n\phi)} \, d\phi \, dz$$

$$H_z(\rho, \phi, z) = \frac{1}{2\pi} \sum_{n=-\infty}^{\infty} e^{jn\phi} \int_{-\infty}^{\infty} I_{zn}(\rho, \gamma) e^{-j\gamma z} d\gamma \quad . \tag{4.10b}$$

The z - components of the wave Eq. (4.7) in cylindrical coordinates can be written:

$$\frac{1}{\rho} \frac{\partial}{\partial \rho} \left(\rho \frac{\partial E_z^s}{\partial \rho} \right) + \frac{1}{\rho^2} \frac{\partial^2 E_z^s}{\partial \phi^2} + \frac{\partial^2 E_z^s}{\partial z^2} + k^2 E_z^s = 0 \quad \text{for TM wave} \tag{4.11a}$$

$$\frac{1}{\rho} \frac{1}{\partial \rho} \left(\rho \frac{\partial H_z^s}{\partial \rho} \right) + \frac{1}{\rho^2} \frac{\partial^2 H_z^s}{\partial \phi^2} + \frac{\partial^2 H_z^s}{\partial z^2} + k^2 H_z^s = 0 \quad \text{for TE wave}. \tag{4.11b}$$

The corresponding differential equations for V_{zn}^s and I_{zn}^s are:

$$\left[\frac{1}{\rho} \frac{\partial}{\partial \rho} \left(\rho \frac{\partial}{\partial \rho} \right) + k^2 - \gamma^2 - \frac{n^2}{\rho^2} \right] \left\{ \begin{matrix} V_{zn}^s (\rho, \gamma) \\ I_{zn}^s (\rho, \gamma) \end{matrix} \right\} = 0 \quad . \tag{4.12}$$

Since the field remains finite within the rod at $\rho = 0$ and must vanish in the infinite external space the solution must be of the form:

For region I, $\rho \leq a$

$$V_{zn}^{sI}(\rho, \gamma_1) = V_{zn}^{sI-}(\rho, \gamma_1) + V_{zn}^{sI+}(\rho, \gamma_1) = A(\gamma_1) J_n(K_1 \rho) \tag{4.13a}$$

$$I_{zn}^{sI}(\rho, \gamma_1) = I_{zn}^{sI-}(\rho, \gamma_1) + I_{zn}^{sI+}(\rho, \gamma_1) = a(\gamma_1) J_n(K_1 \rho) ; \tag{4.13b}$$

For region II, $\rho \geq a$,

$$V_{zn}^{sII}(\rho, \gamma_2) = V_{zn}^{sII-}(\rho, \gamma_2) + V_{zn}^{sII+}(\rho, \gamma_2) = A(\gamma_2) H_n^{(2)}(K_2 \rho) \tag{4.14a}$$

$$I_{zn}^{sII}(\rho, \gamma_2) = I_{zn}^{sII-}(\rho, \gamma_2) + I_{zn}^{sII-}(\rho, \gamma_2) = b(\gamma_2) H_n^{(2)}(K_2\rho) \qquad (4.14b)$$

where

$$K_1^2 = \omega^2 \mu_1 \epsilon_1 - \gamma^2 \qquad \text{and} \qquad K_2^2 = \omega^2 \mu_2 \epsilon_2 - \gamma^2 \ . \qquad (4.15)$$

Then,

$$V_{zn}^+(\rho\gamma) = \frac{1}{2\pi} \int_0^{2\pi} \int_0^{\infty} E_z(\rho, \phi, z) e^{+j(\gamma z + n\phi)} d\phi \, dz \qquad (4.16a)$$

$$V_{zn}^-(\rho\gamma) = \frac{1}{2\pi} \int_0^{2\pi} \int_{-\infty}^{0} E_z(\rho, \phi, z) e^{+j(\gamma z + n\phi)} d\phi \, dz \qquad (4.16b)$$

and similarly for I_{zn}^+ and I_{zn}^-.
Apply the boundary condition on $\rho = a$ for Eq. (4.8)

$$V_{zn}^{sI-}(a\gamma) = V_{zn}^{sII-}(a\gamma) = 0 \ . \qquad (4.17)$$

Then one obtains:

$$\begin{cases} A(\gamma) = \dfrac{V_{zn}^{sI+}(a\gamma)}{J_n(K_1 a)} \\[4ex] B(\gamma) = \dfrac{V_{zn}^{sII+}(a\gamma)}{H_n^{(2)}(K_2 a)} \end{cases} \qquad (4.18)$$

$$\begin{cases} a(\gamma) = \dfrac{I_{zn}^{sI-}(a\gamma) + I_{zn}^{sI+}(a\gamma)}{J_n(K_1 a)} \\[4ex] b(\gamma) = \dfrac{I_{zn}^{sII1}(a\gamma) + I_{zn}^{sII+}(a\gamma)}{H_n^{(2)}(K_2 a)} \ . \end{cases} \qquad (4.19)$$

Substitute Eqs. (4.18) and (4.19) into Eq. (4.13) and (4.14) for $\rho \leq a$ and obtain:

$$V_{zn}^{sI} (\rho, \gamma_1) = \frac{V_{zn}^{sI+}(a\gamma)}{J_n(K_1 a)} J_n(K_1 \rho) \tag{4.20a}$$

$$I_{zn}^{sI} (\rho, \gamma_1) = \frac{I_{zn}^{sI-}(a\gamma) + I_{zn}^{sI+}(a\gamma)}{J_n(K_1 a)} J_n(K_1 \rho) \quad , \tag{4.20b}$$

and for $\rho \geq a$:

$$V_{zn}^{sII} (\rho, \gamma_2) = \frac{V_{zn}^{sII+}(a\gamma)}{H_n^{(2)}(K_2 a)} H_n^{(2)}(K_2 \rho) \tag{4.20c}$$

$$I_{zn}^{sII} (\rho, \gamma_2) = \frac{I_{zn}^{sII-}(a, \gamma) + I_{zn}^{sII+}(a\gamma)}{H_n^{(2)}(K_2 a)} H_n^{(2)}(K_2 \rho) \quad . \tag{4.20d}$$

If $V_{zn}(a\gamma)$ and $I_{zn}(a\gamma)$ are known for $\rho = a$, $-\infty < z < \infty$ then $E_z(\rho, \phi, z)$ and $H_z(\rho, \phi, z)$ can be found by the inverse transform Eqs. (4.9) and (4.10). The remaining field components can then be obtained from Maxwell's equations.

If $\frac{\partial}{\partial z}$ is replaced by $-j\gamma$ and $\frac{\partial}{\partial \phi}$ by $-jn$, the ρ and ϕ components of V and I can be expressed in terms of V_z and I_z components.

$$V_\phi = \frac{1}{K^2} \left[\frac{-n\gamma}{\rho} V_3 + j\omega\mu \frac{\partial I_z}{\partial \rho} \right] \tag{4.21a}$$

$$V_\rho = \frac{-1}{K^2} \left[j\gamma \frac{\partial V_z}{\partial \rho} + \frac{n\omega\mu}{\rho} I_z \right] \tag{4.21b}$$

$$I_\phi = \frac{-1}{K^2} \left[+ j\omega\epsilon \frac{\partial V_z}{\partial \rho} + \frac{n\gamma}{\rho} I_z \right] \tag{4.21c}$$

$$I_\rho = \frac{1}{K^2}\left[\frac{n\omega\epsilon}{\rho} V_z - j\gamma \frac{\partial I_z}{\partial \rho}\right] . \tag{4.21d}$$

Matching the tangential components at the interface $\rho = a$, $V_{zn}(a\gamma)$ and $I_{zn}(a\gamma)$ corresponds to the following conditions:

$$V_{zn}^{s\,I-}(a\gamma) = -V_{zn}^{i}(a\gamma) = 0 , \tag{4.22}$$

$$V_{zn}^{s\,II+}(a\gamma) = V_{zn}^{s\,I+}(a\gamma) , \tag{4.23}$$

$$I_{zn}^{s\,II+}(a\gamma) - I_{zn}^{s\,I+}(a\gamma) = I_{zn}^{i}(a\gamma) , \tag{4.24}$$

$$I_{\phi n}^{s\,II+}(a\gamma) - I_{\phi n}^{s\,I+}(a\gamma) = I_{zn}^{i}(a\gamma) , \tag{4.25}$$

where

$$I_{zn}^{i}(\rho\gamma) = \frac{1}{2\pi}\int_0^{2\pi}\int_0^{\infty} H_z(\rho,\phi,z)\,e^{j(\gamma z + n\phi)}\,d\phi\,dz$$

and

$$V_{\phi n}^{s\,I}(a\gamma) = V_{\phi n}^{s\,II}(a\gamma) \qquad \text{for all } z .$$

Equation (4.21a) gives:

$$\frac{1}{K_1^2}\left\{\frac{-n\gamma}{a}V_{zn}^{s\,I+}(a\gamma) + j\omega\mu_1 K_1 \frac{J_n'(aK_1)}{J_n(aK_1)}\left[I_{zn}^{s\,I-}(a\gamma) + I_{zn}^{s\,I+}(a\gamma)\right]\right\}$$

$$= \frac{1}{K_2^2}\left\{\frac{-n\gamma}{a}V_{zn}^{s\,II+}(a\gamma) + j\omega\mu_2 K_2 \frac{H_n^{(2)'}(aK_2)}{H_n^{(2)}(aK_2)}\left[I_{zn}^{s\,II-}(a\gamma) + I_{zn}^{s\,II+}(a\gamma)\right]\right\} . \tag{4.26}$$

The primes denote the derivative with respect to $K\rho$. Let $L(a\gamma) = I_{\phi n}^{sI-} - I_{\phi n}^{sI-}{}'(a\gamma)$ then

$$I_{\phi n}^{sII}(a\gamma) - I_{\phi n}^{sI}{}'(a\gamma) = L^-(a\gamma) + I_{\phi n}^{i+}(a\gamma) \tag{4.28}$$

then

$$L^-(a\gamma) + I_{\phi n}^{i}(a\gamma) =$$

$$\frac{1}{K_1^2}\left\{j\omega\epsilon_1 K_1 \frac{J_n'(aK_1)}{J_n(aK_1)} V_{zn}^{sI+}(a\gamma) + \frac{n\gamma}{a}\left[I_{zn}^{sI-}(a\gamma) + I_{zn}^{sI+}(a\gamma)\right]\right\}$$

$$- \frac{1}{K_2^2}\left\{j\omega\epsilon_2 K_2 \frac{H_n^{(2)'}(aK_2)}{H_n^{(2)}(aK_2)} V_{zn}^{sII+}(a\gamma) + \frac{n\gamma}{a}\left[I_{zn}^{sII-}(a\gamma) + I_{zn}^{sII+}(a\gamma)\right]\right\}. \tag{4.29}$$

By the relations (4.23) and (4.24), Eqs. (4.26) and (4.27) can be reduced to the form of simultaneous Wiener-Hopf equations.

$$\frac{n\gamma}{a}\left(\frac{1}{K_2^2} - \frac{1}{K_1^2}\right) V_{zn}^{sI+}(a\gamma) - j\omega\left[\frac{\mu_2}{K_2}\frac{H_n^{(2)'}(aK_2)}{H_n^{(2)}(aK_2)} - \frac{\mu_1}{K_1}\frac{J_n'(aK_1)}{J_n(aK_1)}\right] I_{zn}^{sI+}(a\gamma)$$

$$- j\omega\frac{\mu_2}{K_2}\frac{H_n^{(2)'}(aK_2)}{H_n^{(2)}(aK_2)} I_{zn}^{i}(a\gamma)$$

$$= j\omega\left[\frac{\mu_2}{K_2}\frac{H_n^{(2)'}(aK_2)}{H_n^{(2)}(aK_2)} - \frac{\mu_1}{K_1}\frac{J_n'(aK_1)}{J_n(aK_1)}\right] I_{zn}^{sI-}(a\gamma) \tag{4.30}$$

$$j\omega \left[\frac{\epsilon_2}{K_2} \frac{H_n^{(2)'}(aK_2)}{H_n(aK_2)} - \frac{\epsilon_1}{K_1} \frac{J_n'(aK_1)}{J_n(aK_1)} \right] V_{zn}^{sI+}(a\gamma)$$

$$+ \frac{n\gamma}{a} \left(\frac{1}{K_2^2} - \frac{1}{K_1^2} \right) I_{zn}^{sI+}(a\gamma) + \frac{n\gamma}{K_2^2 a} I_{zn}^i(a\gamma) + I_{\phi n}^i(a\gamma) \qquad (4.31)$$

$$= -L^-(a\gamma) - \frac{n\gamma}{a} \left(\frac{1}{K_2^2} - \frac{1}{K_1^2} \right) I_{zn}^{sI-}(a\gamma) \; . \qquad (4.31)$$

Note the unknown quantities are V_{zn}^{sI+}, I_{zn}^{sI+} in the left of Eqs. (4.30), (4.31) and L^- and I_{zn}^{sI-} in the right. The remaining terms involve only known quantities. To make it clearer these equations can be reduced to a single independent equation of the Wiener-Hopf type

$$K(\gamma) V_{zn}^{sI+}(a\gamma) + M(\gamma) L^-(a\gamma) + N(\gamma) = 0 \qquad (4.32)$$

where

$$K(\gamma) = \frac{n^2\gamma^2}{a^2} \left(\frac{1}{K_1^2} - \frac{1}{K_2^2} \right)^2 - j\omega \left[\frac{\mu_1}{K_1} \frac{J_n'(aK_1)}{J_n(aK_1)} - \frac{\epsilon_2}{K_2} \frac{H_n^{(2)'}(aK_2)}{H_n^{(2)}(aK_2)} \right], \qquad (4.33)$$

$$M(\gamma) = -j\omega \left[\frac{\mu_1}{K_1} \frac{J_n'(aK_1)}{J_n(aK_1)} - \frac{\mu_2}{K_2} \frac{H_n^{(2)'}(aK_2)}{H_n^{(2)}(aK_2)} \right], \qquad (4.34)$$

and

$$N(\gamma) = -j\omega \left[\frac{\mu_1}{K_1} \frac{J_n'(aK_1)}{J_n(aK_1)} - \frac{\mu_2}{K_2} \frac{H_n^{(2)'}(aK_2)}{H_n^{(2)}(aK_2)} \right] \left[I_{\phi n}^i(a\gamma) + \frac{n\gamma}{K_2^2 a} I_{zn}^i(a\gamma) \right]$$

$$+ \frac{jn\omega\gamma\mu_2}{aK_2} \left(\frac{1}{K_1^2} - \frac{1}{K_2^2} \right) \frac{H_n^{(2)'}(aK_2)}{H_n^{(2)}(aK_2)} I_{zn}^i(a\gamma) \; . \qquad (4.35)$$

Assume that $\gamma = \beta - j\alpha$ for $\alpha < 0$, and $\beta > 0$. This is equivalent to introducing losses in the surrounding medium and then allowing $\alpha \longrightarrow 0$ to represent the loss-less medium exponentially decreasing and when $z \longrightarrow \infty$ the fields vanish. The Fourier transforms of the fields are analytic in the strip defined by $-\alpha < \operatorname{Im}\gamma < \alpha$ and $-\infty < \operatorname{Re}\gamma < \infty$ of the complex γ plane as shown. $V_{zn}^{sI+}(a\gamma)$ is regular in the half plane $\operatorname{Im}\gamma > -\alpha$, and $L^{-}(a\gamma)$ is analytic in $\operatorname{Im}\gamma < \alpha$. Then decompose the fundtions $K(\gamma)$, $M(\gamma)$, $N(\gamma)$ in the form such that:

$$\frac{K(\gamma)}{M(\gamma)} = \frac{F^{+}(\gamma)}{F^{-}(\gamma)} \ , \tag{4.36}$$

$$\frac{F(\gamma)\,N(\gamma)}{M(\gamma)} = G^{+}(\gamma) + G^{-}(\gamma) \ , \tag{4.37}$$

where $F^{+}(\gamma)$ and $G^{+}(\gamma)$ are regular in the $\operatorname{Im}\gamma > -\alpha$ part of the plane and $F^{-}(\gamma)$ and $G^{-}(\gamma)$ are regular in the $\operatorname{Im}\gamma < +\alpha$ part of the plane.

Rearrange Eq. (4.32) with the relations of (4.36) and (4.37) and define $J(\gamma)$ by

$$J(\gamma) = F^{+}(\gamma)\,V_{zn}^{sI+}(a\gamma) + G^{+}(\gamma) = -F^{-}(\gamma)\,L^{-}(a\gamma) - G^{-}(\gamma) \ . \tag{4.38}$$

The second part of this equation is defined and regular in the $\operatorname{Im}\gamma > -\alpha$ part of the plane; the third part is defined and is regular in the $\operatorname{Im}\gamma < +\alpha$ part of the plane. Thus by analytic continuation $J(\gamma)$ is defined and regular in the whole γ-plane and by Liouville's theorem can be obtained:

$$V_{zn}^{sI+}(a\gamma) = -\frac{G^{+}(\gamma)}{F^{+}(\gamma)} \ , \tag{4.39}$$

and

$$L^{-}(a\gamma) = -\frac{G^{-}(\gamma)}{F^{-}(\gamma)} \ . \tag{4.40}$$

Since V_{zn}^{sI+} is determined, $V_{zn}^{sII+}(a\gamma)$, $I_{zn}^{sI}(a\gamma)$, $I_{zn}^{sII}(a\gamma)$ can be found by Eqs. (4.23), (4.30) and (4.39) respectively. Substituting these boundary values into Eqs. (4.20), (4.21) and applying the inverse Fourier transform, the longitudinal field components E_z and H_z can be found. The remaining field components can then be derived from Maxwell's equations.

V

LOW FREQUENCY FERRITE ANTENNAS

The objective of this task is to investigate the design feasibility of new types of ferrite antennas that are usable at frequencies as low as 30 MHz. An effort has been made to identify realistic applications of ferrite loading to linear radiating elements. Accordingly, the investigation has focused upon applications which improve the performance of antennas that are relatively small. The range of sizes considered are $0.1\lambda < 2h < 0.5\lambda$, where λ = free space wavelength, and h = element half-length. The low end was chosen so as to avoid severe supergain limitations in element performance, while the high end was considered to be a practical size limit for a loaded 30 MHz element. Moreover, the detailed discussion is limited to center fed (or ground plane imaged) elements which support standing wave current distributions.

A generalized analysis of two parallel linear elements was presented in Appendix A of Quarterly Report No. 7848-4-Q. That analysis is the foundation from which ideas for several interesting design concepts are being exploited. Although the formulation was complete, rather limited numerical information was presented for the impedance associated with the symmetric excitation mode. This limitation is eliminated by the addendum which appears in Appendix B. This appendix develops the symmetric mode impedance of a small diameter helical slow wave structure. The formulas are also valid for describing the effects of material loading inside the helix, and are representative of the effects obtainable from other slow wave structures. Due to the general utility of these results, they have been put into a convenient graphical presentation to facilitate usage.

The addendum material in Appendix B, along with the previously developed formulation in Appendix A of the 4th quarterly report, have been incorporated into a general computer program. The computer program will be useful as a diagnostic tool in designing meaningful experiments. Using the computer program to sort

out near optimum designs substantially improves the efficiency of the experimental program. The experimental effort described in the following sections was performed concurrently with the development of the computer program. Hence, the results do not represent any effort toward optimization, but rather serve to demonstrate the feasibility of the various concepts which are described.

5.1 Advantages of Multiple Linear Elements

As pointed out in the 4th quarterly report, the primary advantages of radiating structures using multiple linear elements occur in the transition from one element to two elements. The two advantages pointed out were the inherent properties of impedance matching, and impedance broadbanding. Examples were given which illustrated the mechanism by which each of these properties was achieved. Although the examples cited were for an ordinary folded dipole element, the underlying principles remain entirely applicable to elements foreshortened by distributed loading techniques. In discussing material loadings, the point was made that the presence of ferrite or dielectric material affected the symmetric and asymmetric current modes in a dissimilar fashion. Hence, potentially at least a new degree of freedom was available for controlling the impedance characteristics of such structures. An additional advantage which has been exploited since the previous report is the ability to apply static biasing fields to the material loadings, and thereby alter their RF properties. This technique allows the element to be electrically tuned to resonance without the need of either mechanically moving components, or active circuit components which are characteristically limited in use to low power applications. In principle, both static electric and magnetic fields may be used to advantage; a static electric field to control the increment permitivity, and a static magnetic field to control the incremental permeability. This latter technique has been initially tested on two small diameter helical structures having ferrite cores. The details are described in Section 5.2.

To verify several of the concepts developed through theoretical reasoning, a number of experiments have been performed on small diameter helical slow wave structures. These helices were tested with both hollow and ferrite cores, and excited in several different geometrical configurations. The experiments consisted of measuring the magnitude of the reflection coefficient versus swept frequency, and the resonant input resistance at several discrete frequencies. Results obtained were in reasonable agreement with those anticipated by the theoretical development. The details of the experiments, along with a correlation to the theory, are presented below.

All measurements of reflection coefficients and impedance for the small diameter helix configurations were made with the elements fed against a large aluminum ground plane inserted in the end of an anechoic chamber. Three different geometrical configurations were tested; a single helical monopole, a double helical monopole, and a folded helical monopole. Each of these configurations were tested with the helix having a hollow core, and a partially filled ferrite core. The helix construction is depicted in Fig. 5-1 for the folded helical monopole configuration having a partial core of ferrite. Measurements were made on the magnitude of the reflection coefficient versus swept frequency. These are presented in Fig. 5-2 for the three element configurations and two core conditions. All reflection coefficients are with respect to 50 ohms; the lower trace in each photograph is a reference value of 0.5. In each photograph the second division from the left represents zero frequency, and the top horizontal line corresponds approximately to a 1.0 reflection coefficient. Due to the rapid changes in reflection coefficient near resonance, the limited detector response occasionally prevents the dip from reaching its true null. Also, since the ordinate is not precisely linear in magnitude of reflection coefficient, particular values of interest near the resonance conditions were measured independently.
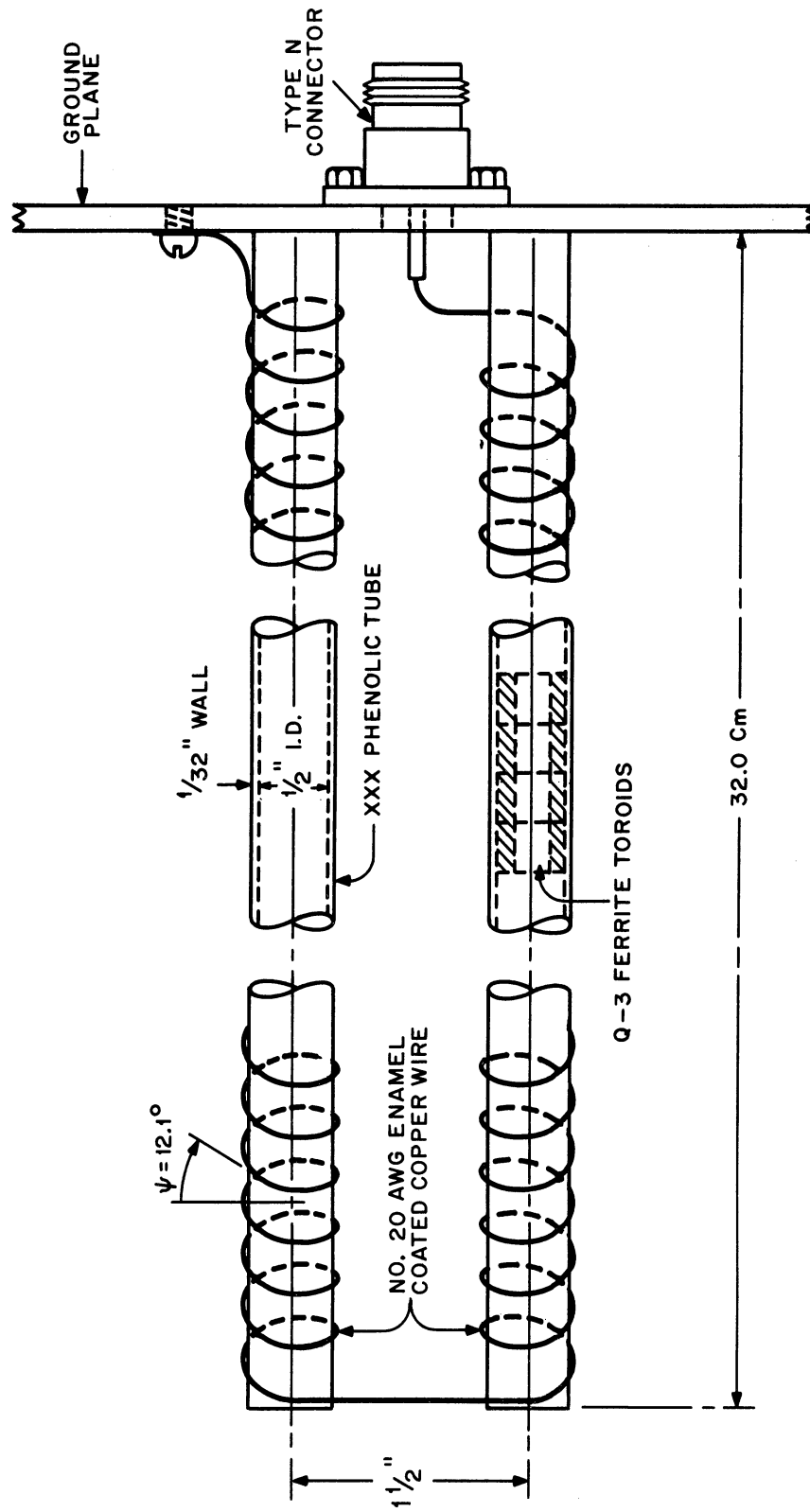
FIG. 5-1: CONSTRUCTION OF FOLDED HELICAL MONOPOLE WITH FERRITE CORE.

Hollow Core   Ferrite Core

Single
Helical
Monopole

(a)   (b)

Double
Helical
Monopole

(c)   (d)

Folded
Helical
Monopole

(e)   (f)
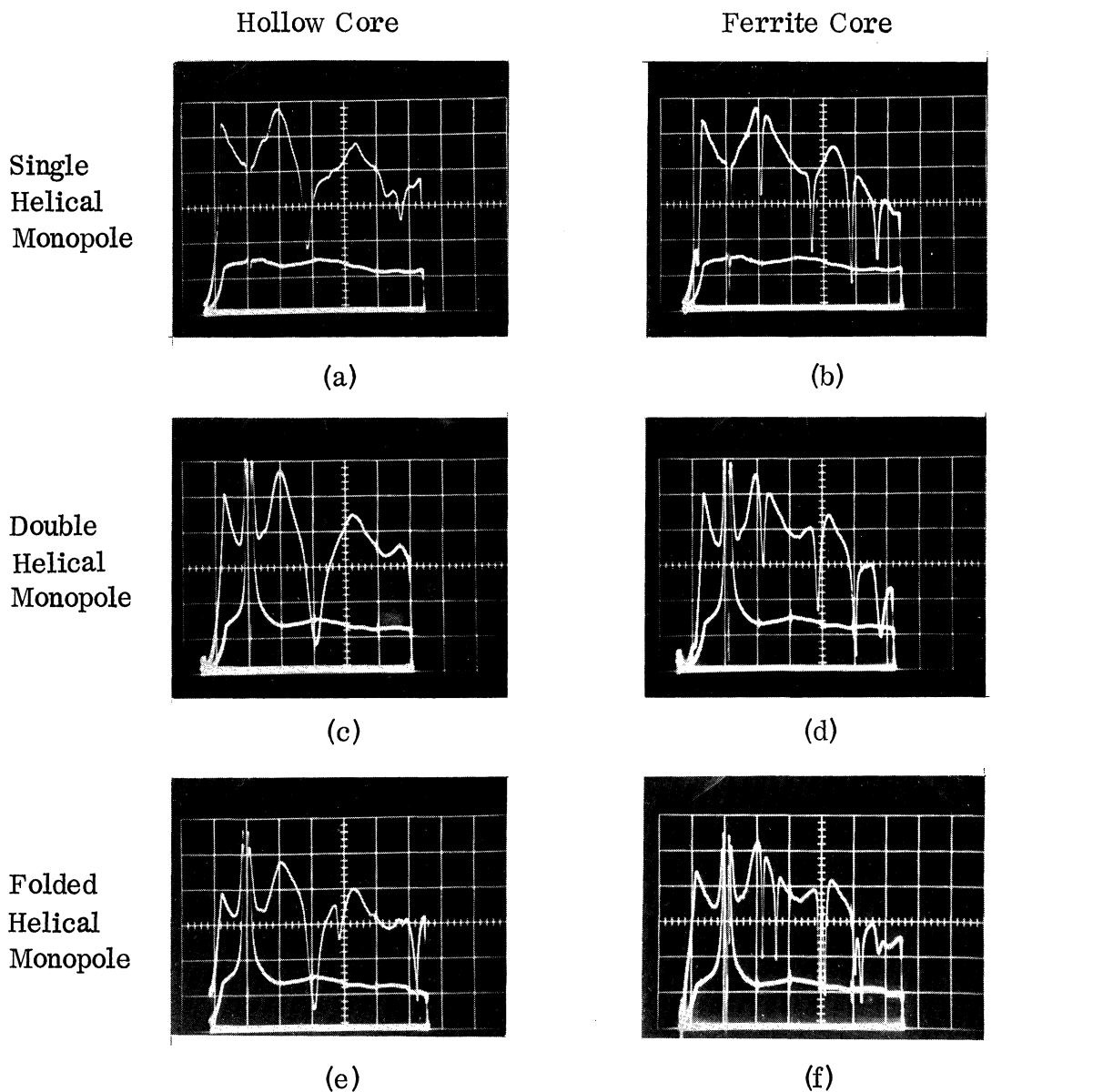
VERTICAL   -   Top Curve $|\rho|$ for Element; Bottom Curve $|\rho|$ = 0.5 Reference

HORIZONTAL -   50 MHz/Square,   Center = 150 MHz

FIG. 5-2: MAGNITUDE OF REFLECTION COEFFICIENT VERSUS FREQUENCY
FOR VARIOUS HOLLOW CORE AND FERRITE CORE HELICAL
ELEMENT CONFIGURATIONS.

Photograph (a) of Fig. 5-2 indicates that the single helical monopole with hollow core has a resonance near 90 MHz. A separate impedance measurement indicated a resonant input resistance of 14 ohms at 88.9 MHz. In photograph (c), two identical helices, except for having opposite pitch angles, were fed in parallel. For this configuration, the resonant resistance was 26 ohms at 102.9 MHz. By comparison with photograph (a) it can be seen that some interaction exists between the helices which results in effectively less phase velocity reduction. For photograph (e) the two helical elements were connected in a folded monopole configuration. The new resonant resistance is 93 ohms at 103.6 MHz. Hence, the folding operation has increased the resonant resistance by a factor of 3.6. The theoretical factor corresponding to the symmetric mode current dividing evenly between the two helical elements would be 4.0. Apparently the slight asymmetry of the feed configuration somewhat altered the division of current. Another theoretically predicted result is the highly mismatched resonance near 142 MHz. The generation of additional resonances slightly above and below the primary resonant frequency is characteristic of the folded configuration. Both additional resonances typically have a large resistive mismatch, the lowest frequency resonance being the most pronounced. The configurations corresponding to photographs (a), (c) and (e) that have ferrite toroids placed in the helix core are presented in photographs (b), (d) and (f), respectively. Photograph (b) indicates that the application of ferrite loading to the single helical monopole significantly lowered the first resonant frequency. The new resonant resistance was 5.3 ohms at 49.6 MHz. Additional resonances due to higher order current excitation modes are also in evidence. Photographs (d) and (f) indicate that each loaded element configuration has characteristics corresponding to those of the unloaded element. In particular there is a slight increase in resonant frequency due to an interaction effect, and the appearance of an additional resonance for the folded configuration. The first resonance in photograph (d) increased to 57.3 MHz and had

an input resistance of 4.3 ohms. The corresponding first resonance at 57.3 MHz of photograph (f) had input resistance of 15 ohms. This represents an increase by a factor of 3.5, which compares well with the factor of 3.6 obtained for the corresponding unloaded configuration.

The conclusions to be drawn from the experimental data may be summarized as follows;

1) Only a slight interaction occurs between two closely spaced small diameter helices, allowing each to function effectively as a linear slow wave structure;

2) The folded helical monopole is an effective configuration for transforming low resonant resistances to higher values;

3) The insertion of ferrite into the core of a small diameter helix substantially reduces the phase velocity;

4) A decrease in phase velocity is accompanied by a proportionately lower value of input resistance at the lowest resonant frequency.

This last point is examined quantitatively in Section B.1 of Appendix B.

5.2 Tuning of Linear Elements Via Magnetic Biasing

The concept of varying the resonant frequency of a linear element configuration utilizing material loading by means of applying a static electric or magnetic field was introduced in Section 5.1. While these ideas are in principle quite sound, certain quantitative aspects may be investigated most expediently through the use of experiments. Accordingly, initial experiments have been made on two separate geometrical configurations in order to ascertain the quantitative effect of static magnetic field biasing. The primary motivation was to establish the feasibility of such concepts. Hence, the experiments represent in no way an optimum design configuration. The results of these initial experiments are encouraging and indicate that the resonant frequency can be shifted several percent. The details of the experiments are described on the following page.

One experiment on static magnetic field biasing was performed using the configuration described in Fig. 5-1. This folded helical monopole having a ferrite toroidal core has a d-c closed circuit path between the center conductor and ground of the input connector. A direct current was applied to this closed path which produced essentially an axial static magnetic field in each of the two loaded helical elements. Due to the opposite pitch angle of the two elements, the axial components of the static magnetic fields were applied to the same vector direction. The change in resonant frequency due to applying magnetic bias was determined through observation of the swept frequency reflection coefficient information, as depicted in Fig. 5-3, first column. Photograph (a) represents the unbiased configuration, and is identical to that of Fig. 5-2, photograph (f). Photograph (b) illustrates with an expanded frequency scale the effect of biasing near the 80 MHz resonance. Two superimposed curves are shown; the right hand curve is the normal unbiased resonance, the left hand curve illustrates the downward shift in resonant frequency with the application of 7.6 amps of bias current. Photograph (c) is a similar presentation of the double resonance near 150 MHz. The left hand curve again represents the downward shift in resonant frequency resulting from the application of a 7.6 amp bias current. The d-c power required to achieve this shift was less than 9 watts.

While these changes in resonant frequency are significant, a more pronounced variation would be desirable. This could be achieved simply by applying a larger bias current, but with the disadvantage of increased d-c power dissipation. A more appealing approach is presently under investigation. Realizing that the principal effect of the static magnetic field is an alteration of the incremental permeability, effort is being directed toward obtaining an element configuration whose resonant frequency has an accentuated sensitivity to incremental permeability. Since the observed resonances result from an interaction between radiation and transmission line modes, alteration of the transmission line frequency behavior can significantly affect the behavior of the resonance. The computer program described previously

Folded Helical Monopole
With Ferrite Core

Helical Monopole With
Ferrite and Copper Core
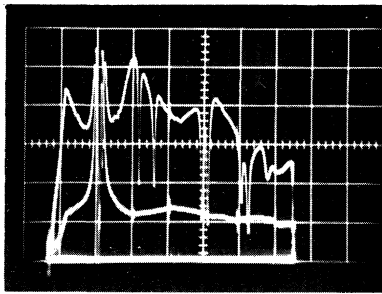
(a)
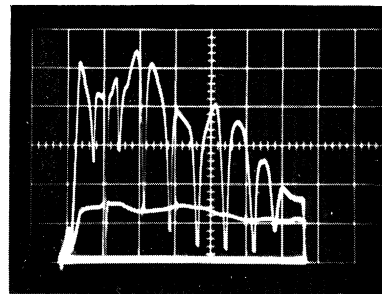
(d)
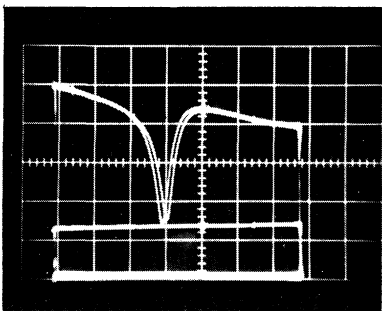
(b)
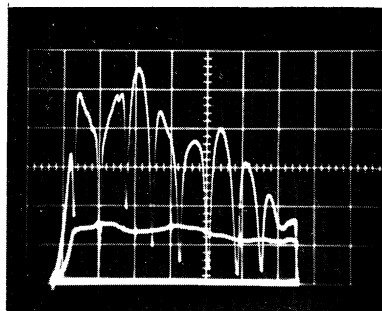
(e)
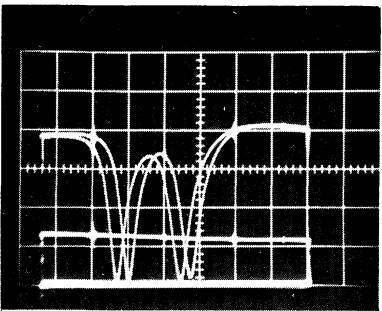
(c)

(f)
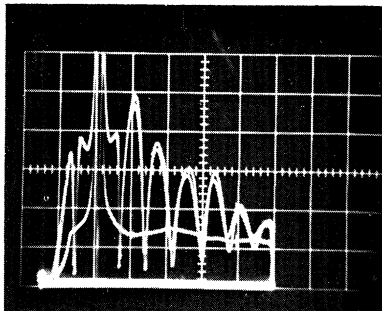
VERTICAL   - Top Curves, $|\rho|$ for Element; Bottom Curve, $|\rho|$ = 0.5 Reference

HORIZONTAL - 50 MHz /Square, Center = 150 MHz, Except as Follows:
(b) Center = 85 MHz ; (c) Center = 155 MHz; Both 5 MHz/Square

FIG. 5-3: EFFECT OF MAGNETIC BIASING ON MAGNITUDE OF REFLECTION
COEFFICIENT VERSUS FREQUENCY FOR TWO DIFFERENT ELEMENT
FERRITE CORE CONFIGURATIONS.

is well suited for a theoretical investigation of various possibilities.

A particular technique of transmission line mode alteration under present investigation involves achieving a significantly greater phase velocity reduction for the transmission line mode compared to the radiation mode. This results in the asymmetric mode impedance being substantially more sensitive to a change in electrical length than the symmetric impedance. While large phase velocity reductions in the symmetric mode are undesirable due to the accompanying severe decrease in resonant radiation resistance, such a phase velocity reduction in the asymmetric mode appears quite desirable. With this line of thinking as motivation, the configuration described in Fig. 5-4 was constructed and tested. The new configuration has several distinctive features. In particular, the concept of symmetric and asymmetric excitation is slightly more difficult to envision. Essentially, symmetric excitation corresponds to feeding a helical slow wave structure having a metal core surrounded by ferrite. Asymmetric excitation corresponds to feeding a type of helical transmission line. Owing to the dissimilar field distributions for the two modes, the phase velocity reduction appears to be substantially greater for the asymmetric mode than for the symmetric mode. The experimental results for this configuration are described below.

Swept frequency reflection coefficient measurements are presented in the second column of Fig. 5-3. Photographs (d) and (e) correspond to the connection between the outer ends of the helix and metal core being open circuited, and short circuited, respectively. The multiple resonances which occur at approximately 40 MHz intervals are seen to shift about 20 MHz corresponding to this change in configuration. Apparently the asymmetric mode impedance repeats itself with a period of 40 MHz. The highly frequency sensitive reactance from this transmission line mode is seen to periodically cancel the radiation mode reactance, thereby causing the multiple resonances. Such a characteristic may in itself be desirable,

GROUND PLANE

TYPE N CONNECTOR

XXX PHENOLIC TUBE

1/4" O.D. COPPER TUBE

Q-3 FERRITE TOROIDS

NO. 20 AWG ENAMEL COATED COPPER WIRE

$\psi = 12.1°$

1/32" WALL

1/2" I.D.

32.0 Cm.
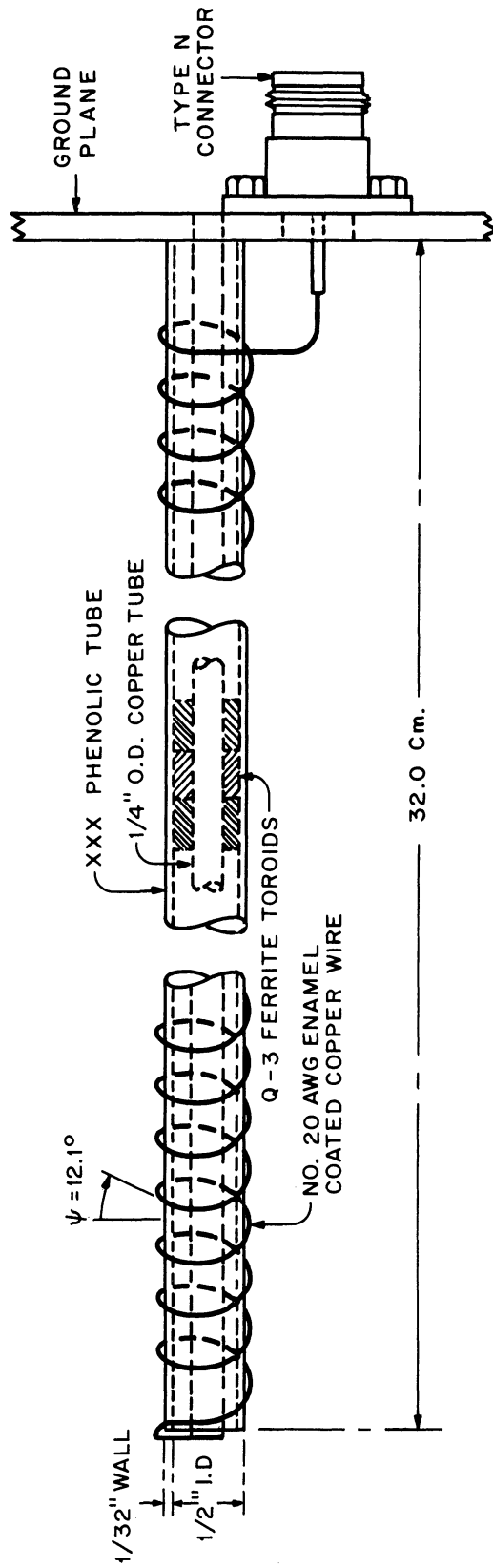
FIG. 5-4: CONSTRUCTION OF HELICAL MONOPOLE WITH FERRITE AND COPPER CORE.

aside from enhancing the resonant frequency sensitivity to magnetic biasing. For this configuration the d-c bias creates a static magnetic field in both the axial and tangential direction. The effect of applying a direct current is illustrated in photograph (f). The trace shifted farthest to the left and having the smallest peak-to-peak variation represents a momentary application of approximately 10 amperes of current. The second curve represents the effect of residual magnetization after the biasing current was removed. A comparison between photographs (e) and (f) indicates that the bias current has lowered the resonant frequency by approximately 7 percent. This represents a substantial improvement over the previous folded helical monopole configuration.

The residual effect suggests the possibility of tuning the elements by means of using pulses of current to establish a specified residual condition. This would remove the necessity of having to continuously apply d-c power to maintain a particular resonance. Such an application would require the ability to demagnetize, and then reapply a different residual condition, when a change in operating frequency is desired. With the presence of a large number of multiple resonant frequencies, the percentage change in frequency required to establish continuous tuning is substantially decreased. It is clear, however, that further modifications will be necessary in order to obtain a capability for continuous tuning. Future effort directed at optimization should yield substantial progress toward achieving this goal. Nevertheless, these present experiments do demonstrate the feasibility of such operation.

5.3 Multiple Resonance Behavior of Composite Slow Wave Structures

The previous section discussed how multiple resonances could result from the interaction between transmission line and radiation type modes of excitation. In this section a discussion is made of a means of generating multiple resonant frequencies when only the symmetric mode of excitation is present. The purpose for considering this topic to two fold. First, from the standpoint of desiring a

continuously tunable radiating element, the larger the number of multiple resonances which exist before applying magnetic biasing techniques, the less stringent the requirements of the biasing technique to shift the resonant frequency. For example, the number of resonances appearing in Fig. 5-4, photograph (e), might be doubled by doubling the number of resonances associated with the symmetric excitation modes. Secondly, it is sometimes desirable to foreshorten elements which are normally excited only in a symmetric mode, as for example in a log periodic dipole array, where the occurrence of multiple resonant frequencies may be detrimental to overall array operation. In this situation it may be necessary to foreshorten the elements in order to control the resonances to an advantage, if possible, without introducing additional multiple resonances. The following describes the mechanism by which multiple resonances occur on structures having only symmetric mode excitation, and then develops a simplified theory for predicting the resonance behavior. The results obtained are useful in the design of composite structures for either of the aforementioned applications.

It is known that to achieve a specified amount of linear element foreshortening, while at the same time minimizing the degradation in impedance bandwidth, a form of "end loading" is needed so as to enhance the current moment of the radiating element. Helical slow wave structures placed at the outer ends of normal linear dipole arms tend to accomplish this goal. In addition to the helices and the normal dipole having dissimilar phase velocities, they also have in general different characteristic impedances. This latter property gives rise to a reflection of the electromagnetic field at the interface between the two structures, in addition to the normal reflection at the dipole ends. The result is that this composite element experiences resonance at generally twice as many frequencies.

To illustrate the effectiveness of a composite element structure in generating multiple resonances, the results of a simple experiment are presented in Fig. 5-5.
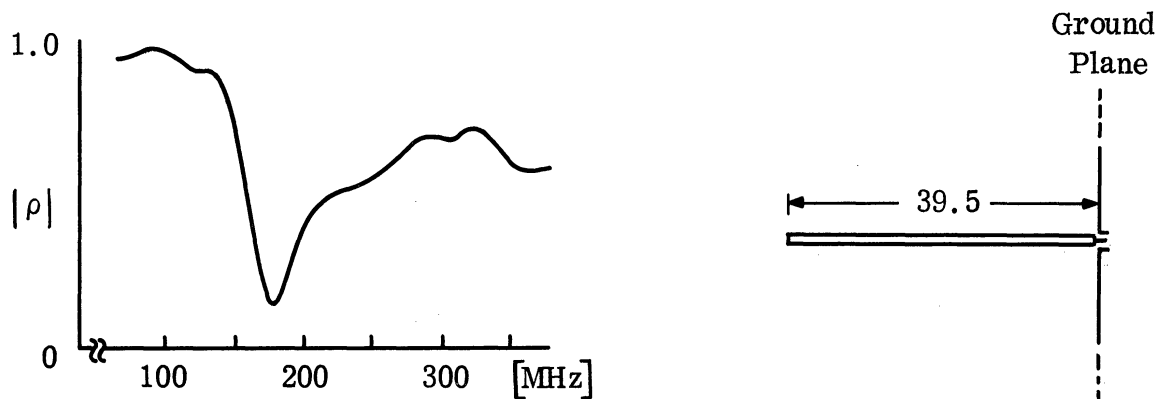
ALL DIMENSIONS IN cm
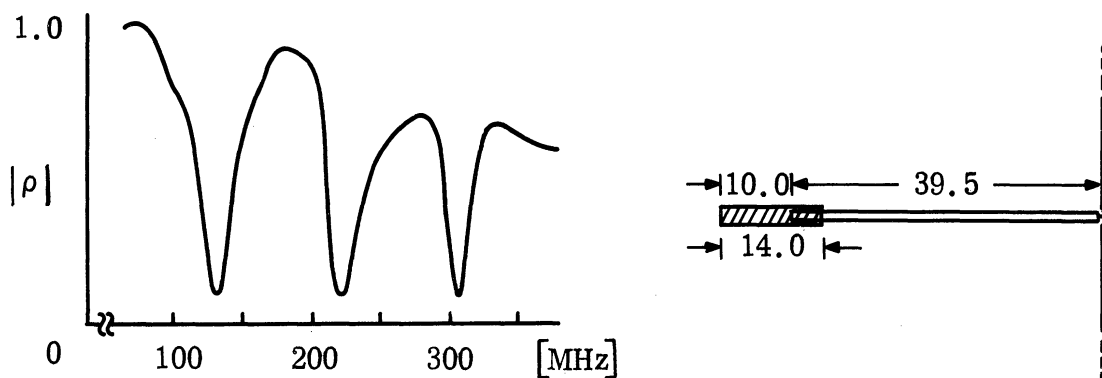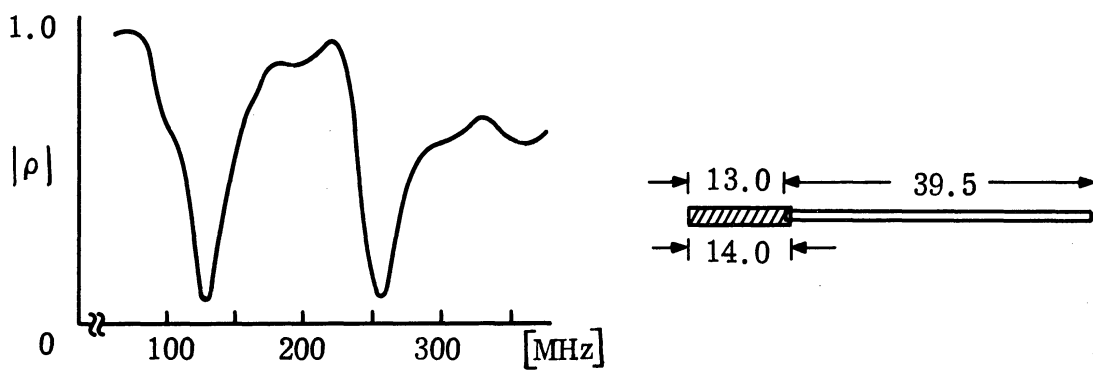
FIG. 5-5: MULTIPLE RESONANCE BEHAVIOR OF VARIOUS COMPOSITE
ELEMENT STRUCTURES.

The left column shows a plot of reflection coefficient versus frequency corresponding to the element configurations shown in the right column. The lengths of the two dissimilar structures are indicated in the figure. The structure nearest the ground plane is 5/32" O.D. brass tube. A helix wound with No. 20 AWG copper wire forming a 10.3 degree pitch angle constitutes the second structure. This helix is supported by a 1/4" O.D. paper phenolic tube which telescopes over the 5/32" O.D. brass structure. A good electrical contact exists between the brass tube and the right hand end of the helix. The first curve shows a single resonance at approximately 180 MHz for the tube structure alone fed against the ground plane. The addition of a relatively short length of helical slow wave structure introduces a double resonance as indicated in the second curve. Along with the expected lowered resonance at 130 MHz, an additional resonance occurs at 260 MHz. By telescoping 4.0 cm of the helical structure back over the brass tube, effectively, a third type of slow wave structure is introduced. The interaction of reflections from the two interfaces between the dissimilar slow wave structures, along with the reflection from the outermost tip all combine to generate three resonant frequencies as shown in the corresponding curve. It is especially significant to note the rather drastic change in resonance behavior between the middle and bottom configuration which resulted from the introduction of only a 3.0 cm segment of a third slow wave structure. Moreover, the electrical length of this third structure had a pronounced influence upon the location of the center resonance. Application of ferrite loading and a variable magnetic bias to control this electrical length might permit positioning this resonance over an appreciable bandwidth. This behavior infers that magnetic biasing may be capable as a substantial alteration in resonance frequency provided that the point of application is judiciously chosen. The theory to describe the behavior of three dissimilar structures follows straightforwordly from the approach used below for two structures.

One can now develop a rather simple theoretical model to describe the multiple resonance behavior of a composite element composed of two dissimilar slow wave structures. To account for the discontinuity in thickness between the two structures, a technique is adapted which has been used successfully in analyzing cylindrical antennas. The zeroth order integral equation formulation for the discontinuous cylindrical antenna yields a solution for input reactance which is identical to that obtained by using a transmission line analogy. Moreover, this solution is known to describe the dominant reactive behavior. Appendix B contains a detailed presentation of the input impedance of a small diameter helical slow wave structure based upon the induced EMF method. The EMF formulation verifies that the dominant behavior of the input reactance for the helix may also be described by a mathematical expression which formally represents that of an equal length of open circuited lossless transmission line. Thus, since the transmission line analogy is applicable to the separate situations of discontinuous thickness, and of a helix having arbitrary axial phase velocity, it should also be applicable to the combined situation. With this motivation, an approximate analysis of a composite slow wave structure will be developed based upon the transmission line analogy. This method will allow the determination of the dominant input reactance behavior, and hence specification of the approximate multiple resonant frequencies. This approach of using a transmission line analogy to approximate the reactance behavior of an element configuration excited by a symmetric mode is to be sharply contrasted with the rigorously developed transmission line mode discussed in Sections 5.1 and 5.2 . For the types of element configurations discussed in those sections, the asymmetric or transmission line excitation was seen to result from a rigorous mathematical decomposition of the source excitation. It should be emphasized that the decomposition into two separate problems is entirely rigorous, even though approximations were invoked to solve the two resulting simpler

problems. This present development is strictly an analogy which is known to give useful approximate results.

Although the experiment presented in Fig. 5-5 contained a segment of normal linear monopole near the ground plane, the following development is generalized to include the possibility of arbitrary phase velocity in this central portion. Realization of such an element is possible using various small diameter helices. The geometry of the corresponding dipole configuration along with its analogous transmission line are shown below. The characteristic impedances Z_1 and Z_2 of the transmission line represent "average" values of the antenna characteristic impedance and will be discussed in greater detail shortly.

Dipole Geometry:
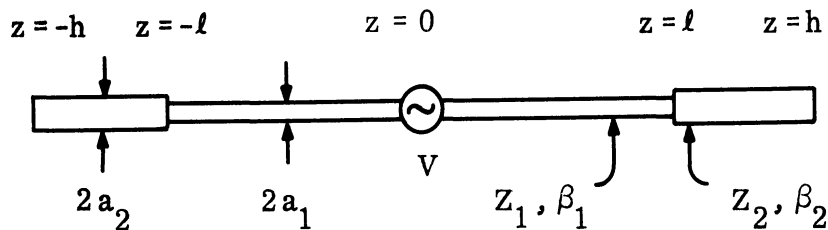
Analogous Transmission Line:
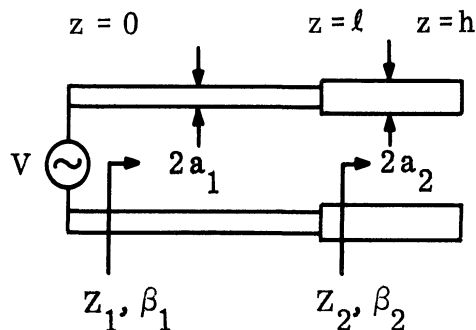
The solution to the analogous transmission line problem is straightforward. First, the general form of the current and voltage distribution is written for each region

$$I(z) = A \sin \beta_2 (h - |z|)$$

$$V(z) = -j Z_2 A \cos \beta_2 (h - |z|)$$

$$\ell \leq |z| \leq h$$

and

$$I(z) = B \sin \beta_1 (\ell - |z|) + C \cos \beta_1 (\ell - |z|)$$

$$V(z) = -j Z_1 B \cos \beta_1 (\ell - |z|) + j Z_1 C \sin \beta_1 (\ell - |z|)$$

$$0 \leq |z| \leq \ell \ .$$

Next, the boundary conditions at $z = \ell$ are applied, i.e.

$$I(\ell -) = I(\ell +) ; \quad V(\ell -) = V(\ell +) \ .$$

It is here that a basic approximation enters. Since voltage may be defined uniquely only for the TEM type waves which exist on a uniform transmission line, the voltage boundary condition precludes from consideration the known existence of higher order modes generated by the discontinuity. Such higher order modes are precisely the terms which contribute to the input resistance R, and the additive reactance correction term X_1. However, since the TEM mode accounts for the dominante term X_2, it is justifiable to exclude the higher order modes from consideration. From the boundary conditions all but one of the unknown constants are determined, and after minor trigonometric manipulation one obtains for the region $0 \leq |z| \leq \ell$:

$$I(z) = A \left\{ \sin \left[\beta_2 (h - \ell) + \beta_1 (\ell - |z|) \right] \right.$$

$$\left. - \frac{Z_1 - Z_2}{Z_1} \cos \beta_2 (h - \ell) \sin \beta_1 (\ell - |z|) \right\} \ .$$

For the special case of $\beta_2 = \beta_1$, this expression reduces to a result given by Schelkunoff and Friis (1952). Below is a drawing of the current distribution for the general result when $Z_2 < Z_1$.

$$A \frac{Z_1 - Z_2}{Z_1} \cos \beta_2 (h - \ell)$$
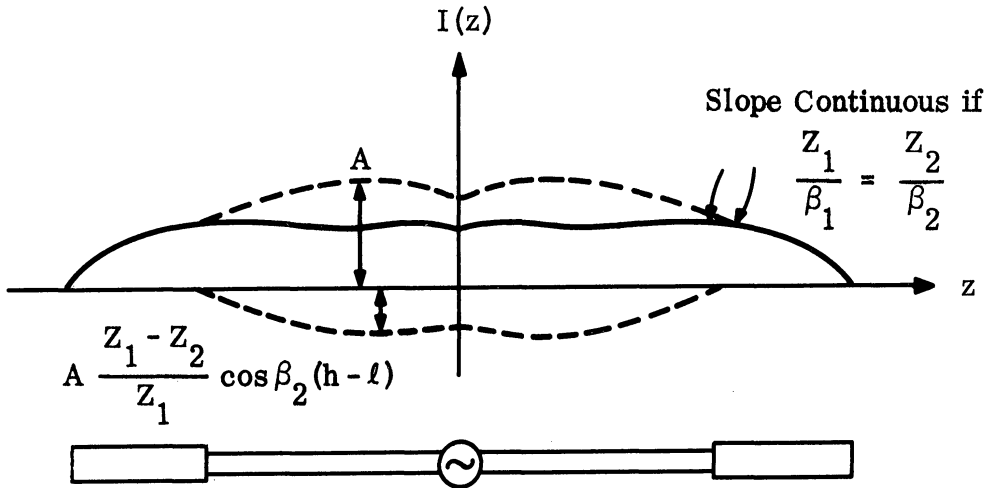
The voltage distribution is found similarly, and the input reactance evaluated as

$$Z_{in} = \frac{V(o)}{I(o)} = j Z_1 \frac{Z_1 \sin\beta_2(h-\ell) \sin\beta_1\ell - Z_2\cos\beta_2(h-\ell)\cos\beta_1\ell}{Z_1 \sin\beta_2(h-\ell)\cos\beta_1\ell + Z_2\cos\beta_2(h-\ell)\sin\beta_1\ell} \equiv j X_2 \ .$$

This expression reduces as a special case to the zeroth order integral equation solution for a cylindrical antenna with discontinuous thickness as given in Wolff (1966). Wolff's result can be obtained from the above expression by setting

$$\beta_1 = \beta_2 = k, \qquad Z_1 = 60 \, \Omega_1, \quad \text{and} \quad Z_2 = 60 \Omega_2 \ ,$$

where the thickness parameter is $\Omega_i = 2\ln\frac{2h}{a_i}$. Thus, the equivalent transmission line characteristic impedances using the thickness parameter concept are given by

$$Z_i = 120 \, \ln \frac{2h}{a_i} \ .$$

The resonance condition for the generalized dipole requires that the input reactance equal zero. Since the numerator and denominator are both real functions, and the denominator is bounded, the resonance condition requires that the numerator equals zero. Hence,

$$Z_1 \sin\beta_2 (h-\ell) \sin\beta_1\ell - Z_2 \cos\beta_2 \cdot (h-\ell) \cos\beta_1 \ell \equiv 0$$

which can be expressed in the more compact form

$$\tan\beta_2 (h-\ell) \tan\beta_1\ell = \frac{Z_2}{Z_1} \ .$$

While this transcendental equation is somewhat awkward to handle in hand computations, it is readily solvable by computer techniques. Recalling that

$$\beta_i = \frac{\omega}{v_i} = \frac{2\pi f}{p_i c} \ ,$$

the parameters which need to be controlled for design purposes are the phase velocity reduction factors p_i, and the characteristic impedances Z_i. Li (1958) presents design data useful for controlling the p_i, and the characteristic impedances for small diameter helices are given by Sichak (1954) as

$$Z_i = 60 \frac{\beta}{k} \ell n \left(\frac{1.123}{\sqrt{\beta^2 - k^2} \ a_i} \right).$$

If a normal linear element is used in place of the center helical structure, an appropriate expression for Z_1 would be

$$Z_1 = 120 \ \ell n \frac{2h}{a_1} \ .$$

VI

MEASUREMENT OF MATERIALS

Two samples of Indiana General Q-4 ferrite were made available to us for measuring the dielectric constant of the material. Because of the small size of the material, it is impossible to fit it into the sample holder made for the transmission line technique used for previous ferrite measurements by the Radiation Laboratory

Until a strip line holder can be made and the material precisely tested, rough checks of the dielectric constant of the material were made by the dielectric sample holder technique described below. This technique indicates that the relative dielectric constant of Q-4 is about 4.2.

Mr. Venerus states that the average value of the relative permeability in the 200 to 500 MHz range is 4.5, and that the Q is 140 at 200 MHz, 100 at 300 MHz, and 80 at 400 MHz. (Venerus, 1967).

6.1 Measurements Technique

The dielectric constant of Indiana General Q-4 ferrite was measured in a General Radio Type 1690 - A Dielectric Sample Holder using the test circuit indicated in Fig. 6-1. The reflection from the dielectric sample holder was noted with the ferrite in place. Then the ferrite was removed and the sample holder adjusted until the same reflection was produced, and both the first and second settings of the micrometer screw of the sample holder were recorded.

Once the micrometer setting is known, the capacitance can be readily determined from the data supplied with the sample holder by General Radio. The difference in the capacitance calculated in this manner is related to the dielectric constant of the material by the formula

$$\Delta C = 0.225 \, \epsilon_r A/t \tag{6.1}$$

where ΔC is the difference in capacitance, in picofarads, for the two micrometer

```
┌──────────┐                                    ┌──────────┐
│          │                                    │          │
│ 1000 ~   │                                    │   SWR    │
│  osc.    │                                    │  Meter   │
│          │                                    │          │
└────┬─────┘                                    └────▲─────┘
     │                                               │
     │                                               │
     ▼                                               │
┌──────────┐      ┌──────────┐      ┌──────────┐    ┌──────────┐
│  G.R.    │      │  20 db   │      │Directional│   │Dielectric│
│  Unit    │ ───▶ │Attenuator│ ───▶ │ Coupler   │◀─▶│ Sample   │
│  osc.    │      │          │      │          │    │ Holder   │
└──────────┘      └──────────┘      └──────────┘    └──────────┘
```
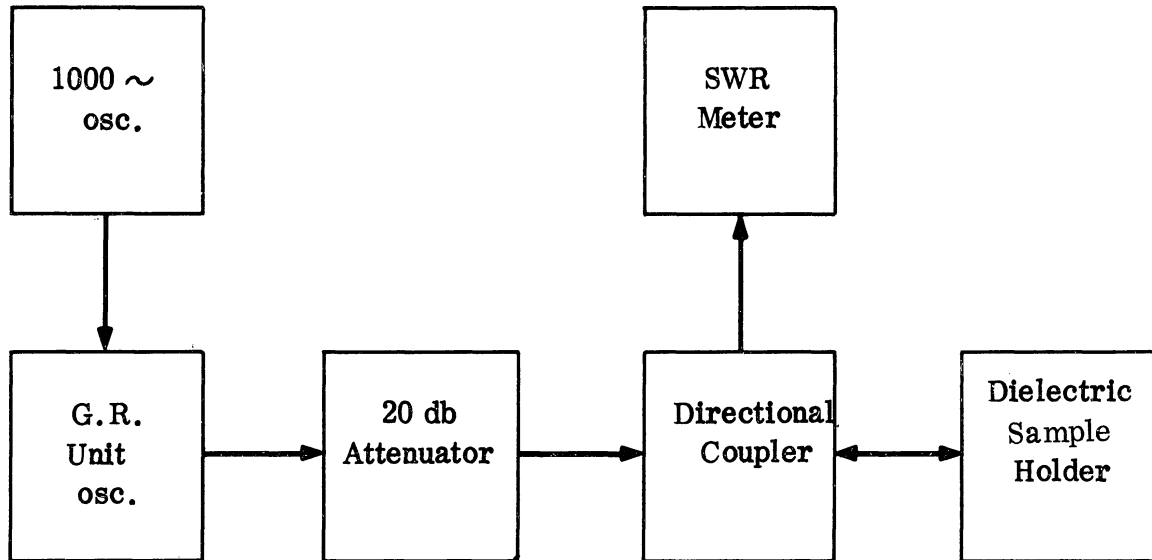
FIG. 6-1: TEST SETUP FOR MEASURING THE DIELECTRIC CONSTANT
           OF INDIANA GENERAL Q-4 FERRITE.

settings, ϵ_r is the relative dielectric constant, and A is the area of the surface of the dielectric sample in square inches, and t is the thickness of the sample expressed in inches. The possibility of the material under test having a relative permeability other than one does not affect the result. A derivation of the formula is given in Section 6.4

6.2 Results

The dielectric constant was measured for several frequencies. The results are summarized in Table VI-1.

TABLE VI-1

THE VALUES OF THE RELATIVE DIELECTRIC CONSTANT
OF INDIANA GENERAL Q-4 FERRITE VERSUS FREQUENCY

Frequency	Dielectric Constant
100 MHz	4.18
125	5.03
150	3.07
175	5.91
200	2.94

The use of the dielectric sample holder is not recommended above 100 MHz. The reason is that stray coupling becomes significant and its random variations with the breathing of the person doing the measurements becomes intolerable.

Another difficulty encountered with the measurements was that the amount of power reflected was an insensitive function of the micrometer adjustment on the sample holder. Consequently, determining the micrometer setting for the second trial was not precise. This hampered accuracy considerably. An attempt to use a tuner to produce a resonant circuit near resonance was a failure because of the inability to desensitize the circuit to mechanical vibrations in the work area.

One additional attempt at improving accuracy was made, but was unsuccessful. More line was inserted between the direction coupler and the sample holder. However, this just made the insensitivity greater.

6.3 Conclusions

Since the ferrite should not be very lossy to an electric field in the UHF-VHF range, and since the effect of stray capacitance became more pronounced at higher frequencies, the value of the relative dielectric constant measured at 100 MHz is probably closest to being correct. Thus the dielectric constant of Indiana General Q-4 ferrite material is about 4.2.

6.4 Theory of Measurement

The measurement procedure is based on the fact that two pure capacitances give the same reflection in a transmission line at the same frequency. Thus, assuming that the material to be measured is lossless and that the power being fed by the generator is constant, the capacitance of the holder with the sample can be determined by removing the sample and re-adjusting the holder until the same reflection is produced. The second micrometer reading determines the capacitance of the sample holder with the test material inserted. Now the first micrometer reading gives the capacitance of the sample holder if the sample were not in place. Thus the difference in the capacitance is the capacitance associated with the presence of the material.

This capacitance can be readily calculated since the sample holder is nothing more than a shielded parallel plate capacitance. The formula relating the geometry of a parallel plate capacitance to its capacitance is well known:

$$C = 0.255 \, \epsilon_r \, A/t \tag{6.2}$$

where A and t are expressed in inches, and C in picofarads. If the sample placed in the holder is a right cylinder, and if the plates of the sample holder are

brought in contact with the faces of the sample in the first trial, then the change in capacitance calculated earlier can be related to the dielectric constant by Eq. (6.1)

6.5 Testing of Ferrite Materials

It is desired that some means be available by which the electrical properties of various ferrite materials can be determined. These materials take several forms. Among these are a solid stick, a donut, and a powder. The desirable frequency range is 100 MHz to 1 GHz. After considering all of these factors, it was decided that a resonant strip-line cavity would be used.

This test method has the following four advantages:

1) It can provide a continuum of test frequencies from 100 MHz to 700 MHz;

2) The cavity does not have to be dismantled in order to insert the test sample;

3) The sample does not have any requirements for a snug fit inside the cavity; and

4) It has an error of only about 10 percent.

The cavity consists of a half-wavelength of strip-line which is short circuited at both ends. So that a continuum of test frequencies can be obtained, these shorts were made adjustable. In constructing the cavity, the ground planes must be wide enough so that they can be considered in finite with respect to the width of the live strip. The live strip must be large enough to facilitate a uniform field over the whole sample width. The sample must be large enough to create a significatnt change in the cavity's Q and resonant frequencies. Ant the cavity must have a low enough impedance so that it will have a high Q.

The final cavity dimensions which were decided upon are as follows. The width of the ground planes is 5.0" . The width of the live strip is 0.5", and its thickness 0.125". The cavity is a half-wavelength long, and can be adjusted from 0.10 m to 1.16 m. The samples have dimensions of 3/16 x .12 x 3/8 ".

The cavity is excited by a "tee" that is composed of a piece of No. 16 s.w.g. wire with a 1 1/2" x 1/8" piece of No. 32 s.w.g. copper foil soldered to the end of it. This cavity is expected to produce a Q of about 500 and a Z_o of about 27 ohms.

The test setup is shown in Fig. 6-2. The cavity is swept through its resonant frequency, and its output is detected and amplified. This output is then displayed on an oscilloscope as a function of frequency. (see Fig.6-3). The fixed signal generator is then used to insert a marker in order to determine the resonant frequency and the half-power frequencies.

To determine dielectric properties, the sample would always be placed in the center of the .12" dimension perpendicular to the cavity axis and the 3/8" dimension is parallel to the cavity axis (see Fig. 6-4). This puts the sample in a position of maximum E-field and minimal H-field. There are three positions in which the sample can be placed in order to measure its μ.

Case 1: The sample is a flat plate against the end wall.

Case 2: The sample is a flat plate with its plane perpendicular to both the end wall and the ground plane.

Case 3: The sample is a flat plate lying on the live strip.

According to other experimenters, Case 3 is the most useful in practice. Case 1 does not allow the use of big enough samples to get measurable frequency shifts. For Case 2, the evaluation equations are too lengthy to be used when a large number of measurements are to be made. However, Case 3 gives easily measurable changes using the same sample as for dielectric measurements, and thus has been adopted as the standard method.

Since the construction of the cavity was only completed near the end of the quarter, complete tests have not yet been run on any ferrite material. However, the Q-3 ferrite was given a test and these tests indicated that the cavity method will work. However, the cavity Q was only about 200 rather than the expected

STRIP - LINE CAVITY

SWEEP GENERATOR

DIRECTIONAL
COUPLER

SWEEP

DETECTOR

MARKER

SCOPE x y

FIXED
SIG.
GEN.

y x
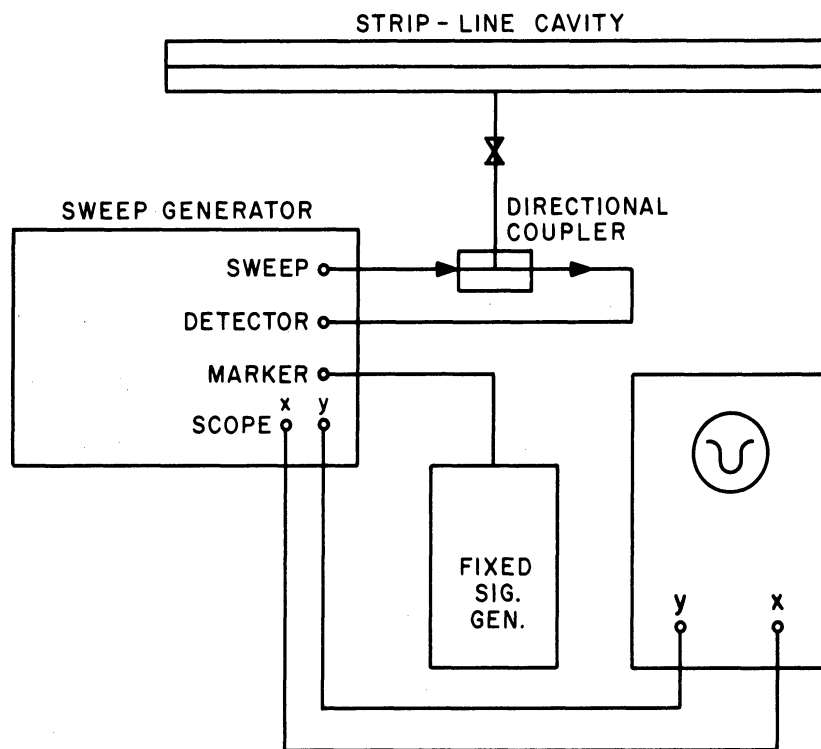
FIG. 6-2: THE TEST EQUIPMENT SET-UP
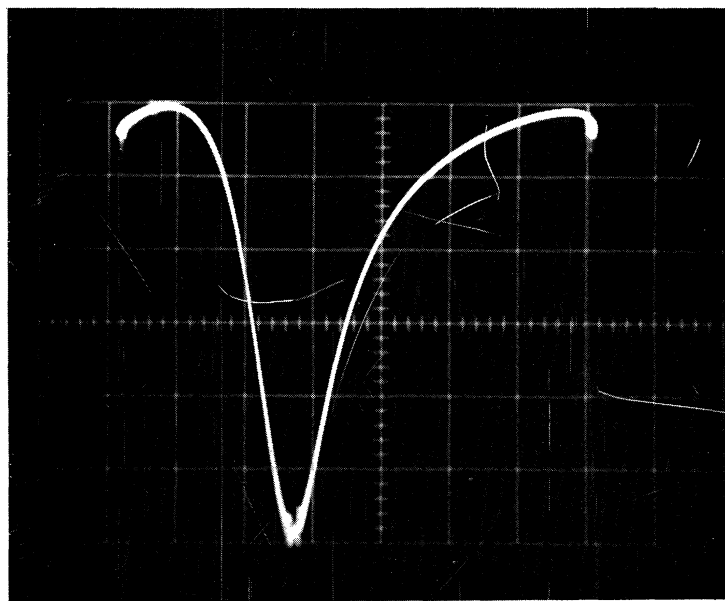
FIG. 6-3: CAVITY OUTPUT VERSUS FREQUENCY
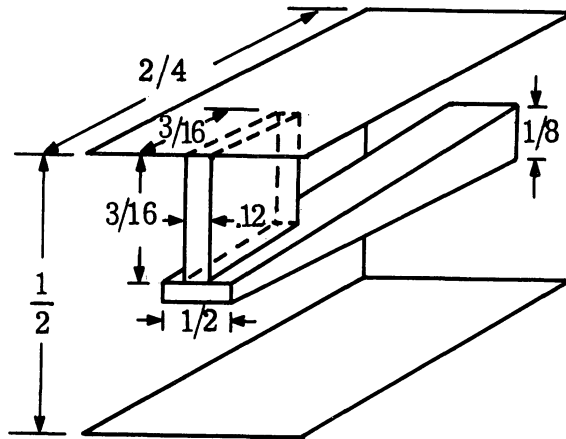
FIG. 6-4: PLACEMENT OF SAMPLE FOR THE DETERMINATION OF THE DIELECTRIC - CONSTANT. HALF THE CAVITY IS SHOWN, THE REMAINDER IS GIVEN BY REFLECTION IN THE PLANE OF SECTION.

500 to 600. Thus, before final tests are performed, there will be an attempt to improve the cavity Q. This will be done by improving the shorts, and possibly by replacing the brass live strip with a copper one.

VII

CONCLUSION

Substantial progress has been made in each of the areas of the four assigned tasks. Under Task 1, the loaded log conical antenna, detailed study has been made of a slow wave winding utilizing a solonoidal winding filled with ferrite material. The radiation properties have been carefully studied. It appears that the backfire radiation observed with a bifilar cylindrical helix wound with such a slow wave structure does not correspond to the usual current distribution on a bifilar cylindrical helix. Current probing methods have shown substantial standing waves of current to be present. It also can be concluded that the utilization of ferrite in the slow wave structure presents an efficiency problem. It has become apparent that reducing the phase velocity through the use of such a loaded structure does not assure good performance as a radiator if this structure is used in winding the radiator, unless a very low loss ferrite is used.

In Task 2, on arrays of physically small ferrite elements, it has been discovered that the characteristics of the available ferrite material interferred substantially with the projected design of a linear radiator made of waveguide and slots in the broadface of this waveguide. Because of this deficiency in material, a comp pletely new design of a linear array of small elements was made. It is recognized that the available ferrite material imposes a considerable limitation on the design of the array and more specifically the ferrite loaded slots of the array.

Under Task 3, the study of ferrite rod radiators, has continued. A careful study of available prior analyses of dielectric rod radiators has shown that each of these analyses have severe limitations. The study on this task has shown that the most appropriate mathematical model will utilize distributions of electric polarization current density over the curved surface of the rod radiator. Current density of these types would also be utilized for the end surface of the rod. The analysis based on these equivalent sources results in a solution different from any prior work.

Under Task 4, concerned with the development of antenna types useful down to 30 MHz an intensive study has been made or the use of multiple linear elements. The advantage of multiple elements has been stated clearly. In addition, linear elements consisting of a small diameter helix loaded with ferrite, have been studied with respect to the influence of steady magnetic bias of the ferrite through the use of a coil carrying a direct current. It has been observed that substantial tuning is possible through such a bias scheme. The magnitude of the shift of center frequency through magnetic bias has been somewhat less than that observed for changes of magnetic bias on the ferrite filled slot antenna described in earlier reports.

Since the electric and magnetic characteristics of ferrites have proved to be in some cases considerably different from published values as shown in the advertising literature, it has been found necessary to ascertain these characteristics for the materials at hand. The discrepancies observed may very well be due to the fact that commercial suppliers of these materials have used measurement methods which are not appropriate for the frequencies involved.

VIII

FUTURE EFFORT

In the continuation of the study under Task 1 on the loaded log conical antenna it is anticipated that a sheath helix transmission line model will be utilized in the analysis of a cylindrical helix filled with an anisotropic ferrite material. This effort will lead to some computer studies.

Under Task 2, this report has indicated a reorientation of the work on arrays involving ferrite loaded elements. An accelerated effort will be carried out utilizing the ferrite loaded slots which have now been constructed. Experiments will now be performed to obtain radiation patterns. The driving point impedances with linear arrays of such slot elements in the two orthogonal directions corresponding to the E and H planes of the slots will be determined.

Under Task 3, the study of ferrite rod radiators, the analysis already begun will be extended to describe the junction of the feed with the radiator proper. Also, the analysis will be extended to include the radiation pattern of the rod. Experimental work on ferrite rod radiators will be performed during the next quarter.

Under Task 4, on antennas useful down to 30 MHz, the information based upon the analysis and impedance measurements will now be supplemented by a substantial experimental program involving radiation patterns of various arrangements of linear elements. It is anticipated also that magnetic bias will be more fully explored with some attention also to an analysis of this problem.

The study of materials will be considerably improved through the use of the TEM mode cavity which has been constructed. After the cavity has been silver plated, it is anticipated that the real and imaginary parts of permeability as well as permittivity will be ascertained for the various materials which the project is utilizing.

APPENDIX
A
GAIN MEASUREMENT BY COMPARISON

In the comparison method of gain measurement the gain of the test antenna can be calculated by the following formula provided the gain of a standard antenna is known:

$$G_t = G_s + C + A_t - A_s + V_t - V_s + L_t - L_s$$

with all terms expressed in db and where:

C   -   Polarization mismatch factor

G_s -   Gain of the standard antenna

G_t -   Gain of the test antenna

A_t -   Attenuator setting for the test antenna

A_s -   Attenuator setting for the standard antenna

V_t -   The mismatch loss for the test antenna

V_s -   The mismatch loss for the standard antenna

L_t -   The cable loss for the test antenna

L_s -   The cable loss for the standard antenna .

The polarization mismatch factor is obtained by measuring the polarization ratio, P, in db and converting this to the numerical polarization ratio, p . Note that P is always assumed to be a positive logarithm. Furthermore, the gain being measured on the test antenna is assumed to be the maximum gain.

The numerical polarization mismatch factor, c , is calculated from the numerical polarization ratio, r , by the formula:

$$c = (p + 1)/p$$

The polarization mismatch factor in db , C , is calculated from c and used in the expression for calculating the gain.

Note that the polarization correction factor in db, C, cannot be greater than 3.01 db (for circular polarization) nor less than 0 db (for linear polarization).

The mismatch loss is calculated by the following formula:

$$V = -10 \log (1 - \Gamma^2)$$

where   is the magnitude of the voltage reflection factor.

For the measurements on antenna 232, a dipole was used as the gain standard and it was assumed to be lossless. Thus G_t was assumed to be 2.16 db. All measurements on the standard dipole and antenna 232 were made with an Anzac H-9 Hybrid that has a specified average insertion loss of 0.5 db. Between the hybrid and antenna 232 was 200 cm of RG-58/U coaxial cable and between the hybrid and the dipole was 128 cm of RG-58/U.

The attenuator settings and reflection coefficients for each antenna at each frequency are given in Table A-1.

TABLE A-1

THE ATTENUATOR SETTINGS AND THE REFLECTION COEFFICIENTS

	170 MHz	196 MHz
Antenna 232 - Vertical Polarization	10 db	12 db
Antenna 232 - Horizontal Polarization	14.5	7.5
Dipole - Horizontal Polarization	34	18
Dipole - Vertical Polarization	33	20
Reflection Coefficient - Antenna 232	0.82	0.70
Reflection Coefficient - Dipole	0.50	0.74

Table A-2 gives the values to be utilized in the gain equation based on the following assumptions:

1) The loss for RG-58/U cable is 6.05 db/100' at 190 MHz and 5.70 db/100' at 170 MHz. This was determined from the data supplied by the Belden wire catalog. (Note that different manufactures claim different attenuations for RG-58/U coaxial cable and there can be a discrepancy of as much as 3 db/100'.)

2) That the reflection coefficient, which was measured at the hybrid with the above stated coaxial cable between the hybrid and the tip of the antennas, is unaltered by losses in this setup (these loses will be taken into account later).

3) The loss in the hybrid is 0.5 db.

The result is that the gain is -4.2 db at 190 MHz and -12.3 db at 170 MHz.

TABLE A-2

TERMS OF THE GAIN EQUATION

	170 MHz	190 MHz
C	1.3	1.93
A_t	14.5	12
A_s	34	20
V_t	4.84	2.92
V_s	1.25	3.44
L_t	0.88	0.91
L_s	0.74	0.76

When the effect of the cable losses and the hybrid loss on the reflection coefficient is taken into account, the gain at 190 MHz changes to -4.4 db. However, at

170 MHz, correcting the reflection coefficient for the losses produces a value that is slightly greater than unity. Although this is possible in lossy transmission lines, (Stannard, 1967) it is improbable in this case. The more likely explanation is that

    1) The losses specified by the manufacturer for the cable and the hybrid are too great and

    2) Since the true value of the reflection coefficient is very close to one, calculation error plus measurement error produce a corrected value greater than one. The results are summarized in Table A-3.

TABLE A-3

CORRECTING THE REFLECTION COEFFICIENT
FOR TRANSMISSION LOSS

	Antenna 232		Dipole	
	170 MHz	190 MHz	170 MHz	190 MHz
Loss	0.88 db	0.91 db	0.74 db	0.76 db
Measured Reflection Reflection Coefficient	0.82	0.70	0.50	0.74
Numerical Loss	1.23	1.23	1.19	1.19
Corrected Voltage Reflection Coefficient	1.01	0.86	0.60	0.88
Correction Factor	——	5.85 db	1.94 db	6.48 db

The correction is made by the following formula:

$$\Gamma_T^2 = L^2 \, \Gamma^2$$

where Γ_T is the true value of the reflection coefficient and L is the numerical value of the loss.

APPENDIX

B

ADDENDUM TO ANALYSIS OF TWO PARALLEL
LINEAR ELEMENTS

A general formulation for the analysis of two parallel linear elements was
presented in Appendix A of Quarterly Report No. 7848-4-Q. The analysis required
a knowledge of two impedance functions, one each for a symmetric and an asymmet-
ric source excitation mode. Asymmetric excitation was shown to correspond to a
transmission line problem, and the solution for Z_a was explicitly stated. Symmet-
ric excitation requires the solution of a radiation problem to obtain Z_s, hence the
solution is more involved. The appropriate method for obtaining Z_s was indicated,
but only limited numerical information was then available. Since that report a
more complete formulation by Li (1958) has been obtained, from which some useful
numerical results have been calculated.

As pointed out previously, the EMF method is approximate to the extent that it
assumes a sinusoidal current distribution along a linear element. Nevertheless, the
results for a normal dipole are known to be accurate enough for most engineering
applications. It would thus seem logical to extend the induced EMF method to an
analysis of a linear slow wave structure used as a dipole. However, a difficulty
arises in that certain integrals which appear due to the generalization have no
known closed form solutions. Li (1958) has been able to obtain an approximation
to the integrals which allows a tenable closed form expression. His result is dis-
cussed below, and then expanded upon to gain further insight into some useful
engineering approximations pertinent to linear slow wave structures.

B. 1 Asymmetric Excitation Impedance by the Induced EMF Method

The EMF method was applied by Li (1958) in his Ph. D. thesis to obtain the
input impedance of a small diameter helical element. This solution is significant
because it is representative of the characteristics of various other linear slow wave

structures. A helical element supports essentially a sinusoidal current distribution in which the axial wave number β_s is controlled by properly choosing the helix pitch angle. The slow wave structure was mathematically modeled using the sheath helix approximation. Although the details of this formulation have been rather carefully studied before preparing this report, the inherent complexity requires that only the primary steps be outlined, the solution quoted, and the limitations discussed.

The input impedance is obtained by the induced EMF method from dividing the complex power contributed to the electromagnetic field through a cylinder enclosing the element by the amplitude squared of the input current. The formulation reduces to an evaluation of the following expression for the input impedance.

$$Z_{11} = \frac{-1}{(I_m \sin\beta_s h)^2} \int_{-h}^{h} \left[E_z(z) + E_\phi(z) \cot\psi \right] I_m \sin\beta_s(h - |z|)\, dz \qquad (B.1)$$

$E_z(z)$ and $E_\phi(z)$ are the longitudinal and traverse components of the electric field on the surface of the enclosing cylinder and are given by

$$E_z(z) = j\, 30\, I_m\, \frac{\beta_s}{k} \left[2\, \frac{e^{-jkR_o}}{R_o} \cos\beta_s h - \frac{e^{-jkR_1}}{R_1} - \frac{e^{-jkR_2}}{R_2} \right.$$

$$\left. + \frac{\beta_s^2 - k^2}{\beta_s} \int_{-h}^{h} \sin\beta_s(h - |z_1|)\, \frac{e^{-jkR}}{R}\, dz_1 \right] \qquad (B.2)$$

and

$$E_\phi(z) = -j\, 60\, I_m\, \frac{\beta_s^2 - k^2}{k} \left[\ln\left(\frac{2}{\sqrt{\beta_s^2 - k^2}\, a} \right) - \gamma \right] \tan\psi\, \sin\beta_s(h - |z|) \qquad (B.3)$$

where

$$R_o = \sqrt{a^2 + z^2} \qquad\qquad R = \sqrt{a^2 + (z - z_1)^2}$$

$$R_1 = \sqrt{a^2 + (z + h)^2} \qquad\qquad R_2 = \sqrt{a^2 + (z - h)^2}$$

$$\gamma = 1.781$$

$$\psi = \text{helix pitch angle} .$$

The last term in E_z containing the integral, along with the entire E_ϕ account for the added complexity in extending the EMF method to the helical slow wave structure. Both these terms are seen to vanish as the phase velocity reduction factor p_s approaches unity, in which case $\beta_s \longrightarrow k$, ($p_s = k/\beta_s$, k being the free space wave number). Finding a suitable closed form approximate solution to the integral term in E_z is the crux to solving the slow wave structure impedance problem.

After some manipulation to facilitate the discussion in the next section, Li's approximate solution yields the following result for the complex input impedance of a small diameter helical slow wave structure.

$$Z_{11} = R + j (X_1 + X_2) \tag{B.4}$$

$$R = \frac{30}{D \sin^2 x} \left\{ 2 \left[\text{Cin } Ax - \text{Cin } Bx \right] \right.$$

$$+ \cos 2x \left[2 \text{ Cin } Ax - 2 \text{ Cin } Bx - \text{Cin } 2 Ax + \text{Cin } 2 Bx \right]$$

$$+ \sin 2x \left[-2 \text{ Si } Ax + 2 \text{ Si } Bx + \text{Si } 2 Ax - \text{Si } 2 Bx \right]$$

$$\left. - \frac{4D}{3} \left[\frac{1}{1 - D^2} (\cos Dx - \cos x)^2 + 2 (1 - D^2)(1 - \cos x)^2 \right] \right\} \tag{B.4a}$$

$$X_1 = \frac{30}{D \sin^2 x} \left\{ 2\left[\text{Si } Ax + \text{Si } Bx - \sin 2x \right] \right.$$

$$+ \cos 2x \left[2 \text{ Si } Ax + 2 \text{ Si } Bx - \text{Si } 2Ax - \text{Si } 2Bx \right]$$

$$\left. + \sin 2x \left[2 \text{ Cin } Ax + 2 \text{ Cin } Bx - \text{Cin } 2Ax - \text{Cin } 2 Bx \right] \right\} \qquad \text{(B.4b)}$$

$$X_2 = \frac{-120}{D} \left(\ln \frac{h}{a} - 1 \right) \cot x \qquad \text{(B.4c)}$$

where: $A = (1 + p_s)$, $B = (1 - p_s)$, $D = p_s$, $x = \beta_s h$ and $0 \le x \le \pi$.
The functions R, X_1 and X_2 have been put into graphical form for easy use
and appear in Figs. B-1a, b through B-3a, b[*] respectively. The functions R
and X_1 are plotted for the family of p_s ranging in 0.1 increments from 0.1 to
1.0. Since X_2 is affected by p_s only as a multiplicative factor, unnecessary
duplication was avoided by plotting the product $X_2 p_s$ for the family of h/a ranging
from 15 to 8000.

A few comments are in order regarding the limitations of this result, along
with its applicability to general slow wave structures. First, the evaluation of
Eq. (B.1), using Eqs. (B.2) and (B.3), to obtain Eq. (B.4) required the usual
assumption that the radius "a" be very small; i.e., $a \ll h$, λ. In addition, a
closed form evaluation of the integral term in Eq. (B.2) required approximations.
After dividing the integral into a real and imaginary part, the real part was inte-
grated exactly, and found to approximately cancel the contribution of Eq. (B.3)
to the input reactance. This approximation allowed the entire effect of E_ϕ
to be removed from the final result, Eq. (B.4). The imaginary part of

---

[*]Each figure is drawn to two scales - a , for an overall presentation, and
b, for an expanded view of the ordinate near the origin.
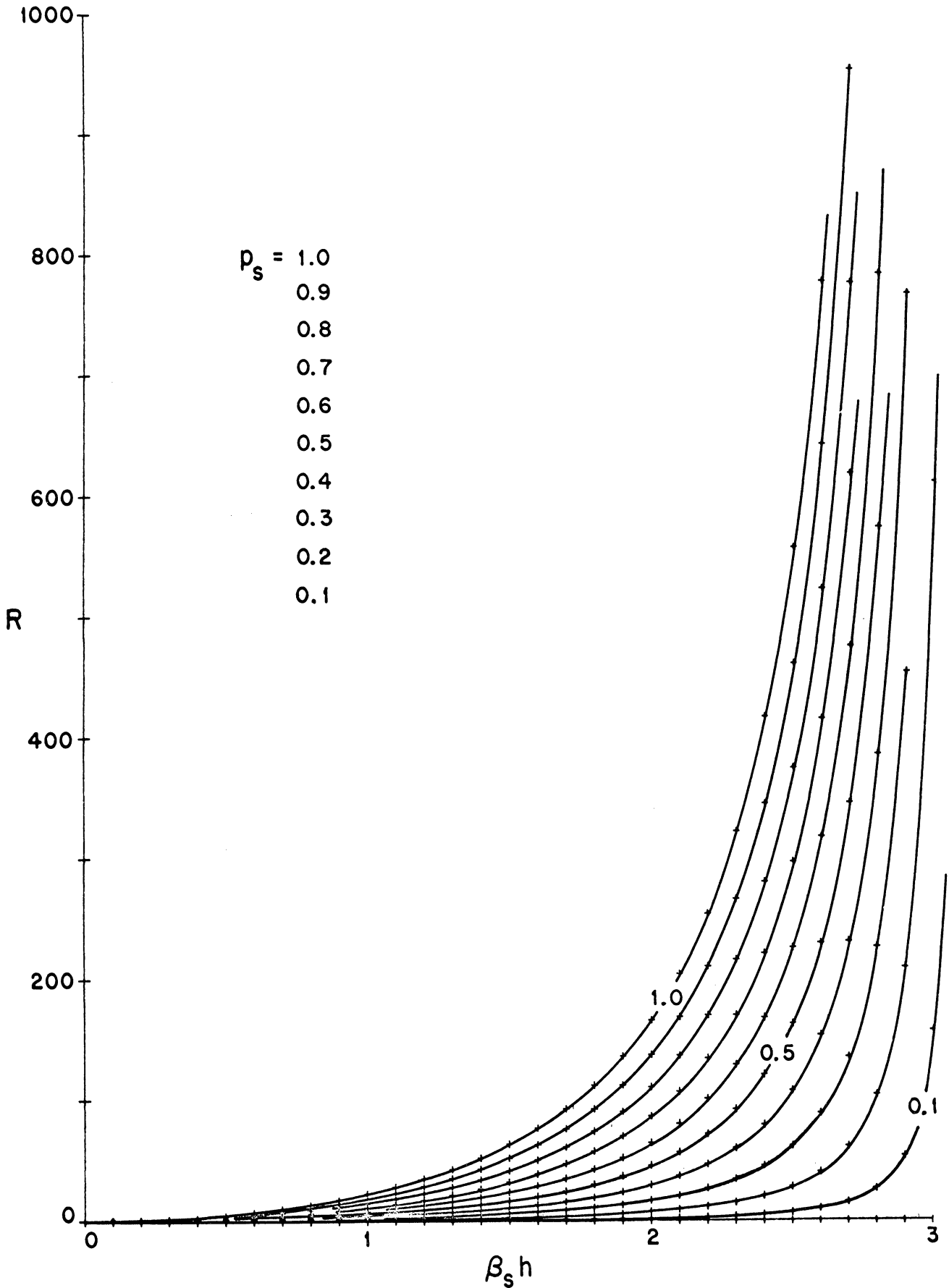
FIG. B-1a: R VERSUS $\beta_s h$ FOR THE PARAMETER p_s (EMF METHOD).
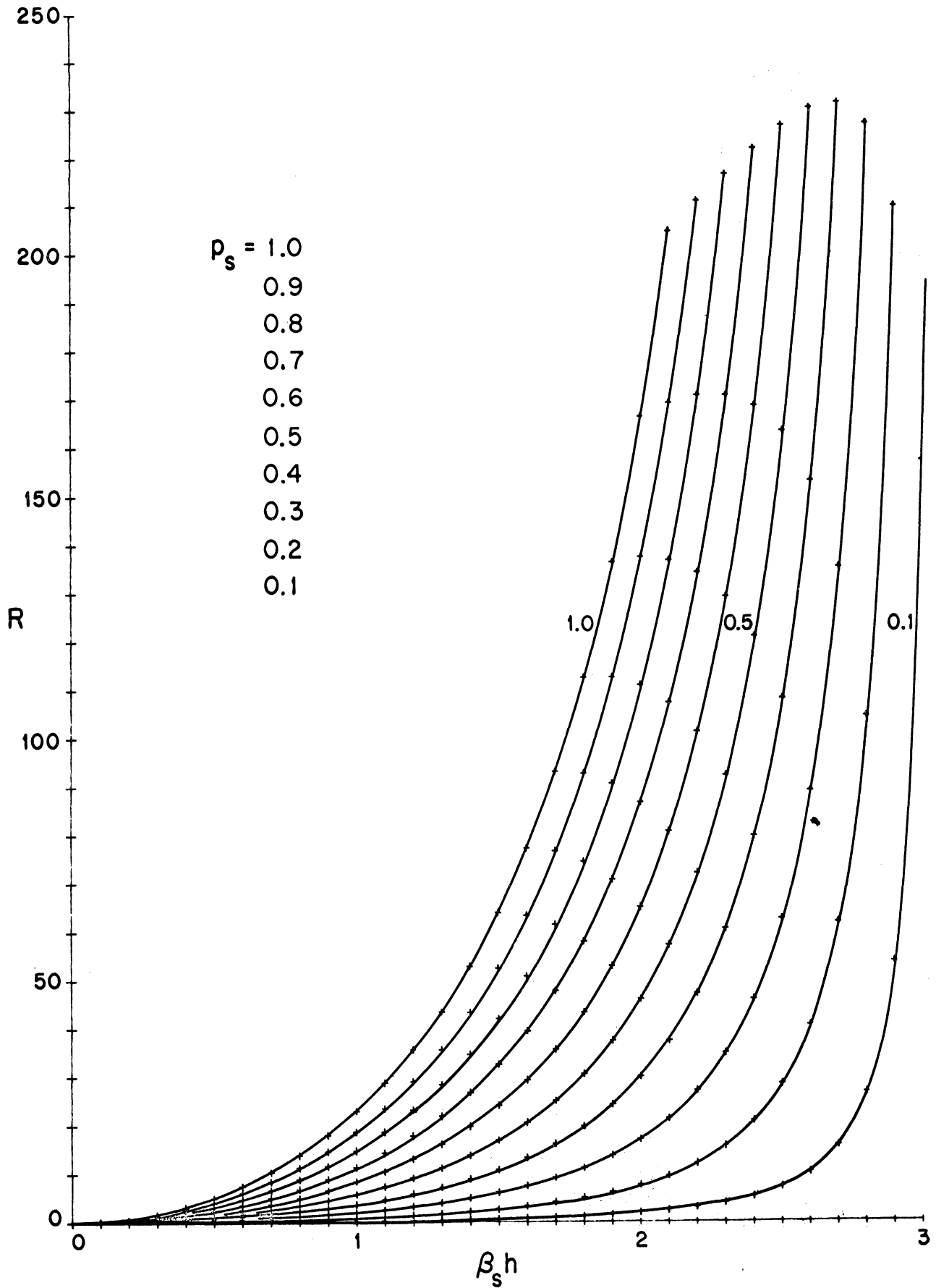
FIG. B-1b: EXPANDED R VERSUS $\beta_s h$ FOR THE PARAMETER p_s (EMF METHOD).
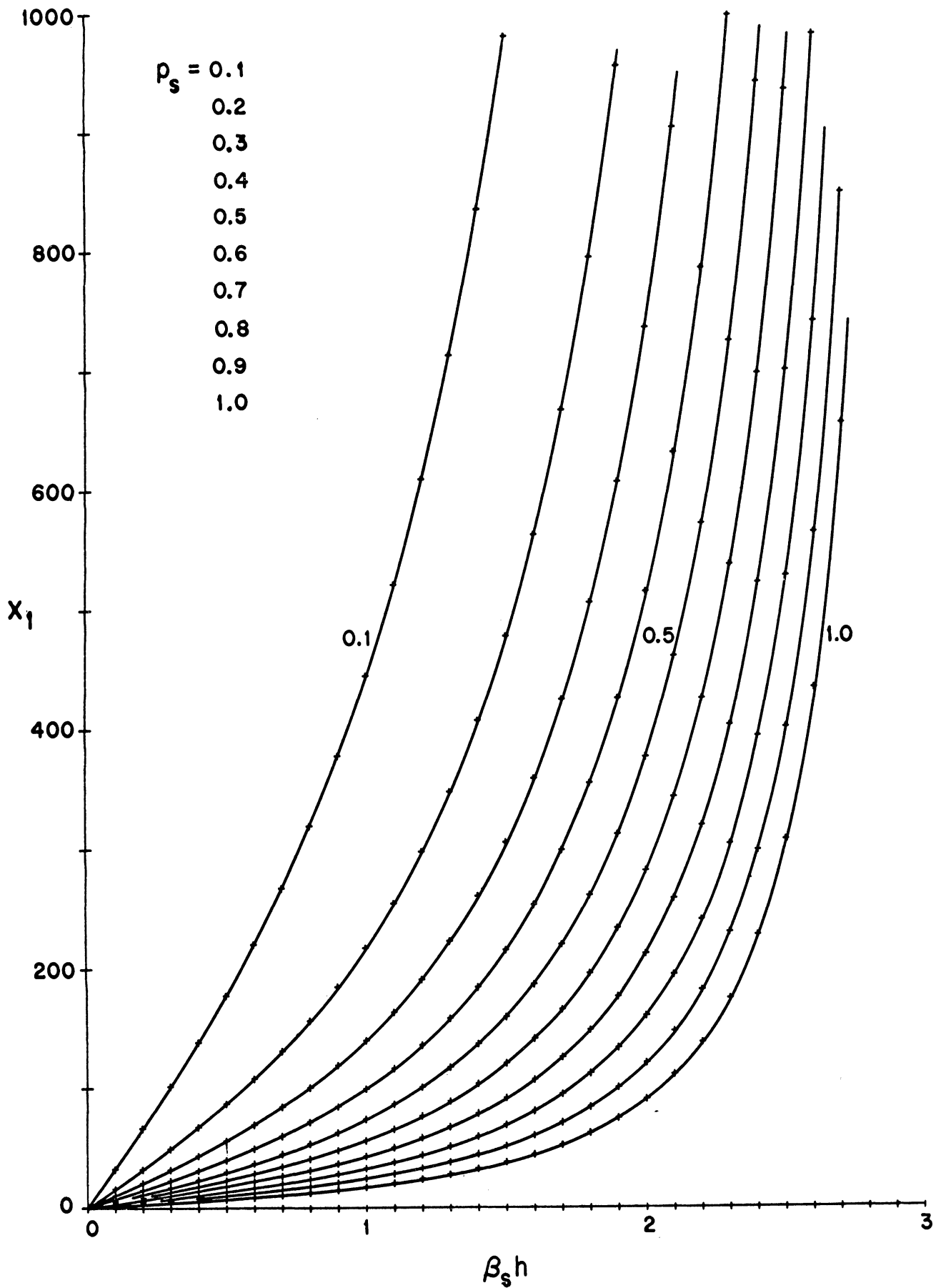
FIG. B-2a: X_1 VERSUS $\beta_s h$ FOR THE PARAMETER p_s (EMF METHOD).
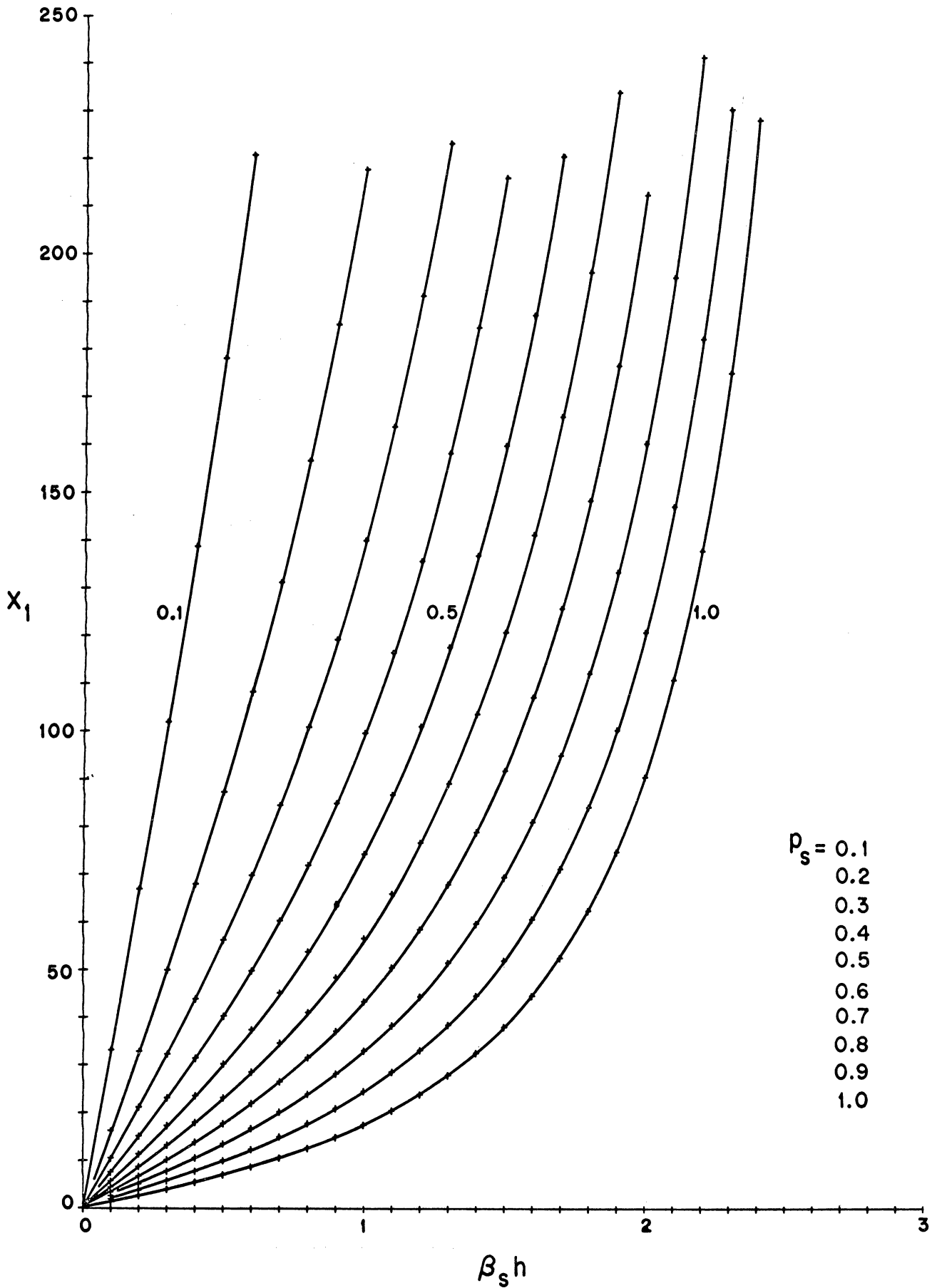
FIG. B-2b: EXPANDED X_1 VERSUS $\beta_s h$ FOR THE PARAMETER p_s (EMF METHOD).
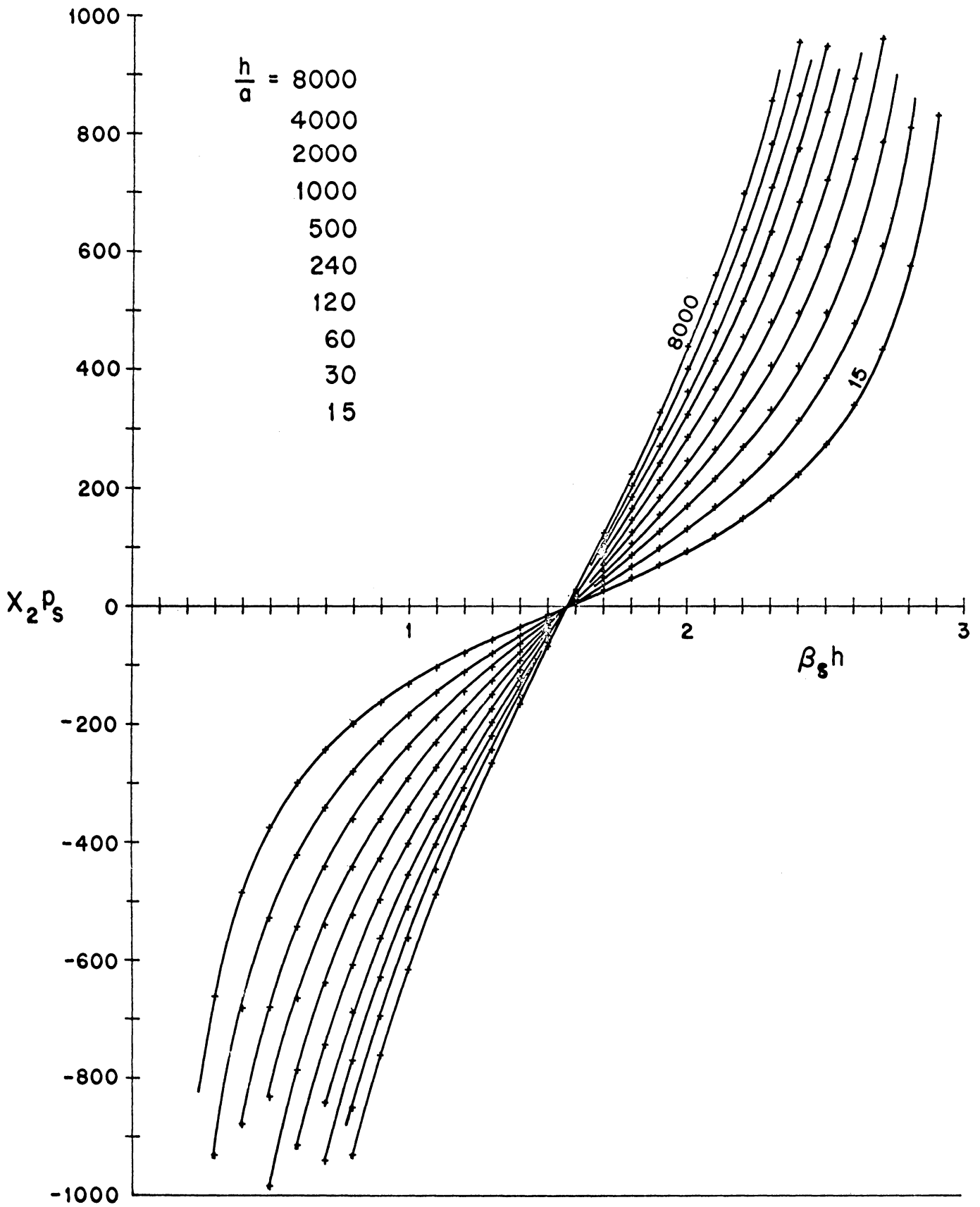
FIG. B-3a: X_2p_s VERSUS $\beta_s h$ FOR THE PARAMETER h/a (EMF METHOD).
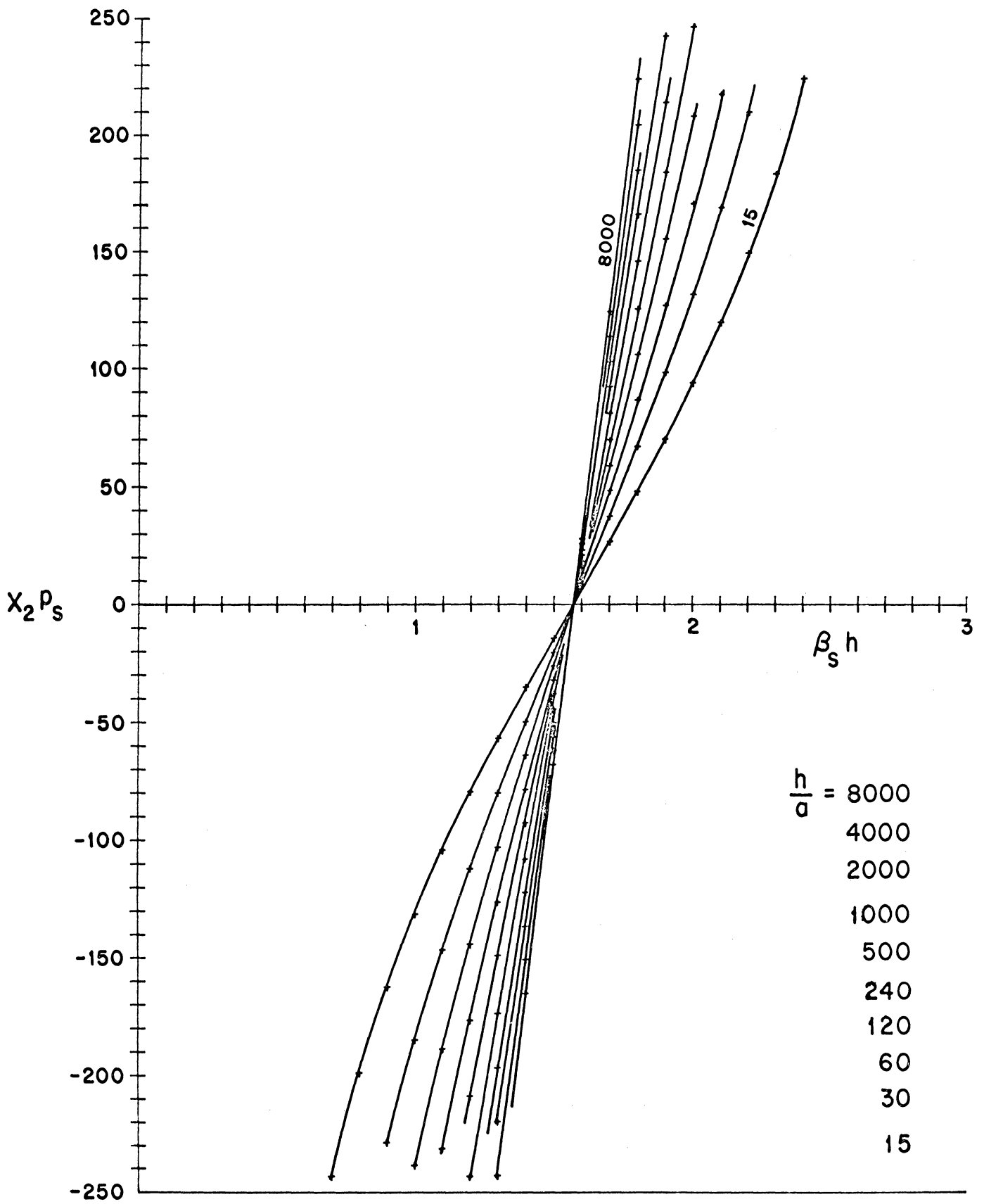
FIG. B-3b: EXPANDED $X_2 p_s$ VERSUS $\beta_s h$ FOR THE PARAMETER h/a (EMF METHOD).

the integral was evaluated using an approximation which becomes poor for $x > \pi$. This influence is felt in the last bracketed terms of Eq. (B.4a), which can become unduely large and force $R < 0$ if x is not restricted. Hence, the impedance expression for the small diameter helical dipole is accurate provided the element is thin and $0 \le x \le \pi$. Moreover, the expression should adequately describe the behavior of a small diameter helix having a ferrite core. The primary effect of the ferrite core is to decrease the current phase velocity, and hence can be accounted for through p_s. The dependence of p_s upon the ferrite core will be discussed later.

B.2   Comparison to Transmission Line Analogy

The above separation of input reactance into two components (X_1 and X_2) was motivated by a similar technique introduced by Tai in connection with the regular dipole ($p_s = 1.0$) as presented in Chapter 3 of Jasik (1961). Tai factored out the terms appearing in X_2 solely for the mathematical reasons of giving X_1 the properties: a) of having no dependence upon the element thickness, and b) of being regular at the origin (i.e. $-X_1 \longrightarrow 0$ as $\beta_s h \longrightarrow 0$). It is intended here to propose a physical interpretation to this so far strictly mathematical separation. Observe that X_2 is in the mathematical form of the input impedance for an open circuited length of lossless uniform transmission line having a characteristic impedance given by

$$Z_o = 120(\beta_s/k)(\ln h/a - 1) \ .$$

Ascribing such an interpretation to the mathematics is of course not new; but, generally the analogy is argued hueristically starting from transmission line theory, dominant mode biconical antenna theory, or the zeroth order in-

tegral equation solution. Here, however, the argument is reversed; a somewhat more credible induced EMF technique reduces formally to contain a familiar term which would otherwise be on somewhat shaky footing. Although it may be rightly argued that the first order integral equation solution is on firm ground, the first order solution obscures the analogy due to an awkward change in its zeroth order functional form, whereas the EMF solution merely introduces additive "correction" terms. This latter notion of R, and in particular X_1 being viewed as correction terms deserves further explanation. Normally one does not think of R, given by either the EMF method or equivalently by the Poynting vector method, as being "corrective" since our familiarity with the result relegates it as "basic". However it is "corrective" when compared with the cruder zeroth order result. More importantly, X_1 is the only readily tractable additive "correction" function available. Despite excellent numerical results from more involved methods, a relatively simple functional expression for the entire reactance is often desirable.

If X_1 is rightly to be considered a correction to X_2, its corrective effect must be small. Tai's results for the normal dipole (p_s = 1.0) showed this to indeed be the case. That this is true for general p_s is verified by examining Figs. B-2 and B-3. Consider as an example a helical slow wave structure for which p_s = 0.5 and h/a = 500. Nominal resonance based upon X_2 = 0 would occur at $\beta_s h$ = 1.57 (= $\pi/2$). However, Fig. B-2b indicates that X_1 = 177 for this value of $\beta_s h$. Actual resonance is achieved when $\beta_s h$ is decreased to where $X_1 + X_2$ = 0. Using Figs. B-2b and B-3b to determine the required decrease in $\beta_s h$, one finds X_1 = 148 = $-X_2$ at $\beta_s h$ = 1.45. Hence, X_1 causes only a 7.6 percent correction to the value of $\beta_s h$ predicted by the use of X_2 alone. In conclusion it may be said that X_2 is a strong

function of frequency, its strength being controlled by the numerical value of Z_o.

X_1 is by comparison a slowly varying function of frequency, its primary influence being a slight lowering of the actual resonant frequency.

There remains the somewhat delicate task of reconciling the above equation for Z_o as representing in some sense a meaningful expression of characteristic impedance. First, for the case when $\beta_s = k$, Z_o reduces to Tai's results. (A typographical error appears in X_2 of Jasik (1961), but has subsequently been noted by Tai (1965)). Throughout the years several differing expressions have appeared to account for characteristic impedance. Siegel and Labus initially suggested the form

$$Z_o = 120 \left(\ln \frac{h}{a} - 1 - \frac{1}{2} \ln \frac{2h}{\lambda} \right) .$$

Later the expression for a biconical line was averaged over the length of a cylindrical antenna to obtain

$$Z_o = 120 \left(\ln \frac{2h}{a} - 1 \right) .$$

It has been stated by Jordan (1950) that both the above expressions when applied to a short antenna yield calculated values which are consistently higher than measured values. He suggests the use of

$$Z_o = 120 \left(\ln \frac{h}{a} - 1 \right)$$

as an "adjusted" characteristic impedance that is empirically picked to give the closest fit to experimentally measured values. Moreover, still another expression results from equating the zeroth order integral equation, which contains the thickness parameter $\Omega = 2 \ln \frac{2h}{a}$, to that of an equivalent transmission line. This results in $Z_o = 60 \, \Omega$, or

$$Z_o = 120 \ln \frac{2h}{a} .$$

While a number of slightly different expressions exist for Z_o, the importance of the numerical differences between them is somewhat over shadowed when one considers the errors introduced by variations due to different feed point terminal conditions. Thus, the degree of uncertainty introduced by measurement technique, and the conditions of actual application suggests that the choice of Z_o is not too critical. Should somewhat greater precision be desired, it would be best to determine Z_o from measurement. This way the above uncertainties would to an extent be taken into account.

In conclusion it is seen that the induced EMF method suggests an expression for Z_o which is identical to Jordan's when $\beta_s = k$. Moreover, the dominant role in describing the impedance behavior is performed by X_2. Thus, it is suggested that R and X_1 may be viewed as correction terms to the zeroth order integral equation solution, to within the limitations of the approximate, but generally adequate, induced EMF formulation. This point of view will prove exceedingly useful in Section 5.3, and is a dominant motivation for the present development.

BIBLIOGRAPHY

Angulo, C. M. and Chang, W.S.C. (1958), "The Launching of Surface Waves by a Parallel Plate Waveguide," IRE Trans., AP-7, pp. 359-368.

Angulo, C. M. and Chang, W.S.C. (1958), "The Excitation of a Dielectric Rod by a Cylindrical Waveguide," IRE Trans., MTT-6, pp. 389-393.

Brown, J. and Spector, J.O. (1957), "The Radiating Properties of Endfire Aerials," Proc. IEE, 104B, pp. 27-34.

Bussey, H.E. (1967), "Measurement of R. F. Properties of Materials," Proc. IEEE, 55, No. 6, pp. 1046-1053.

Clarke, R.H. (1957), "A Method of Estimating the Power Radiated Directly at the Feed of a Dielectric Rod Aerial," Proc. IEE, 104B, pp. 511-514.

Fradin, A. Z. (1961), Microwave Antennas, Pergamon Press, London.

Harrington, R.G. (1961), Time-Harmonic Electromagnetic Fields, McGraw-Hill Book Co., Inc., New York.

Horton, C.W., Karal, F.C. and McKinney, C.M. (1950), "On the Radiation Patterns of Dielectric Rods of Circular Cross-Section — the TM Mode," J. Appl. Phys., 21, p. 1279.

James, J.R. (1967), "Theoretical Investigation of Cylindrical Dielectric Rod Antennas," Proc. IEE, 114, pp. 309-319.

Jasik, H. (1961), Antenna Engineering Handbook, McGraw-Hill Book Co., Inc., New York, Section 3.1.

Jordan, E.C. (1950), Electromagnetic Waves and Radiating Systems, Prentice-Hall, New Jersey, pp. 452-473, p. 512.

Kiely, D.G. (1953), Dielectric Aerials, Methuen Monograph.

Li, Tingye and Robert Beam (1957), "Helical Folded Dipoles and Unipoles," Proc. NEC, XIII, pp. 89-105.

BIBLIOGRAPHY
(Continued)

Li, Tingye (1958), "The Small-Diameter Helical Antenna and its Input Impedance
Characteristics," Ph. D. Thesis, Northwestern University, Evanston, Illinois.

Lyon, J.A.M. et al (1966), "Study and Investigation of a UHF-VHF Antenna," The
University of Michigan Radiation Laboratory, Report No. 07848-2-Q.

Lyon, J.A.M. et al (1967), "Study and Investigation of a UHF-VHF Antenna," The
University of Michigan Radiation Laboratory, Report No. 07848-4-Q.

Noble, B. (1958), The Wiener-Hopf Technique, Pergamon Press,

Schelkunoff, S.A. and Friis, H.T. (1952), Antennas: Theory and Practice, John
Wiley and Sons, Inc., New York, Section 8.28.

Sichak, W. (1954), "Coaxial Line with Helical Inner Conductor," Proc. IRE, 42,
pp. 1315-1319.

Stannard, Georege E. (1967), "Calculation of Power on a Transmission Line,"
Proc. IEEE, 55, No. 1, p. 132.

Tai, C.T. (1965), "Linear Antennas," Electronic Inductries, pp. 75-78.

Venerus, Joseph C. (1967), Private Communication.

Walter, C.H. (1965), Traveling Wave Antennas, McGraw-Hill Book Co., Inc.,
New York.

Watson R.B. and Horton, C.W. (1948), "The Radiation Patterns of Dielectric
Rods — Experiment and Theory," J. Appl. Phys., 19, p. 661.

Watson, R.B. and Horton, C.W. (1948), "On the Calculation of Radiation Patterns
of Dielectric Rods," J. Appl. Phys., 19, p. 836.

Wolff, E.A. (1966), Antenna Analysis, John Wiley and Sons, Inc., New York.

Destination	Number of Copies
Adams-Russell Company Library - Antenna Section 280 Bear Hill Road Waltham, Mass. 02154	1
Aero Geo Astro Security Officer Edsall and Lincolnia Blvd. Alexandria, Va.	1
Aerospace Corporation Robert C. Hansen 2400 E. El Segundo Blvd. Los Angeles, Calif. 90045	1
Cutler-Hammer Division, Airborn Instruments Labs. Librarian - Antenna Section Walt Whitman Road Melville, L.I., New York 11729	1
All Products Company Mr. James Buzbee Mineral Wells, Texas	1
Americal Electronic Laboratories, Inc. Antenna Section Box 552 Lansdale, Pa.	1
Andrew Alfred Consulting Engineers Librarian - Antenna Section 299 Atlantic Ave. Boston, Mass. 02110	1
AVCO Res. and Adv. Development Division Research Library 201 Lowell Wilmington, Mass. 01887	1
AVCO Electronic and Ordnance Division Technical Library 2630 Glendale-Milford Road Cincinnati, Ohio 45241	1
Bell Aircraft Corporation Technical Library - Antennas Buffalo, New York 14205	1
Bell Telephone Laboratories Inc. Technical Reports Library – Room 2A165 Whippany, New Jersey 07961	1

Bendix Radio Division
Technical Library - Dept. 462-4
East Joppa Road
Baltimore, Md. 21204   1

Bendix Research Laboratories
Technical Library
20800 10 1/2 Mile Road
Southfield, Michigan 48076   1

Boeing/Wichita - Antenna Systems Staff Unit
Technical Library
3801 South Oliver
Wichita, Kansas 67201   1

Boeing Aerospace Division
Technical Library - Antenna and Radomes
Box 3707
Seattle, Washington 98124   1

Bunker-Ramo Corporation, Defense Systems Div.
8433 Fall Brook Avenue
Canoga Park, California 91304   1

Canoga Electronics - Advanced Programs Dept
Box 2086
Canoga Park, California 91306   1

Chance-Vought Aircraft, Inc.
BuAer Representative
Technical Library - Antenna Section
Box 1500
Arlington, Texas 75222   1

 Collins Radio Research Division
Technical Library
5200 C   NE
Cedar Rapids, Iowa 52406   1

Collins Radio Corporation
Dr. Robert L. Carrel - Antenna Section
Dallas, Texas 75207   1

Dalmo Victor Company
Technical Library - Antennas
1515 Industrial Way
Belmont, California   1

Dorne and Margolin, Inc.
Technical Library - Antenna Section
29 New York Avenue
Westbury, L.I., N.Y. 11591   1

Douglas Aircraft MSSD Technical Library
Antenna Section
3000 Ocean Park Blvd.
Santa Monica, Calif. 90406   1

Dynatronics, Inc.
Technical Library - Antennas
Hwy 17 and 92 N. Castlebury
Orlando, Florida   1

Electronic Communications Research Division
Technical Library
1830 York Road
Timonium, Md.   1

Emerson and Cuminb, Inc.
E. J. Luoma
869 Washington St.
Canton, Mass. 02021   1

Fairchild Aircraft and Missiles Division
Technical Library - Antennas
Hagerstown, Maryland   1

Fairchild Hiller Corporation
Technical Library
1455 Research Blvd.
Rockville, Md. 20850   1

General Dynamics/Convair
Technical Library - Antennas
Grants Lane
P.O. Box 748
Fort Worth, Texas 76101   1

General Electric Electronics Laboratory
Technical Library
Electronics Park
Syracuse, New York 13201   1

General Electric Light Military Electronics Dept.
901 Broad Street
Utica, New York 13503   1

General Electric General Engineering Laboratory
Building 371, Room 478
Schenectady, New York 12305   1

General Electronics Laboratories, Inc.
Technical Library - Antennas
18 Ames Street
Cambridge, Mass   1

General Precision Laboratory
Technical Library - Antennas
63 Bedford Road
Pleasantville, N. Y.   1

Goodyear Aircraft Arizona Division
Antenna Department
Box. 85
Litchfield Park, Arizona 85340   1

Grumman Aircraft Engineering Corporation
Technical Library - Avionics Engineering
South Oyster Bay Road
Bethpage, N. Y.   1

Hallicrafters Company
Technical Library - Antennas
4401 West Fifth Avenue
Chicago, Illinois 60624   1

Hoffman Laboratories, Inc.
4501 North Arden Drive
El Monte, California 91734   1

Hughes Aircraft Corporation
Technical Library - Antennas
Centinela and Teale Streets
Culver City, California 90232   1

Hughes Aircraft Communications and Videosonics Div.
Antenna Section
1901 West Malvern Avenue
Fullerton, California   1

ITT Federal Laboratories
Technical Library - Antennas
500 Washington Ave.
Nutley, N. J. 07110   1

Laboratory for Electronics, Inc.
Antenna Department
1079 Commonwealth Avenue
Boston, Mass. 02115   1

Ling-Temco-Vought Military Electronics Div.
Librarian - Antennas
1200 Jupiter St.
Garland, Texas   1

Litton Systems, Amecom Division
Technical Library - Antennas
1140 E. W. Highway
Silver Spring, Md. 20910   1

Lockheed Marietta Division
South Cobb Drive
Marietta, Georgia 30061   1

Lockheed Electronic and Armaments System Office
P. O. Box 551
Burbank, California 91503   1

The Martin/Denver Division Headquarters
Antenna Laboratory Mail Nr. T-0453
P. O. Box 179
Denver, Colorado 80201   1

The Martin/Orlando Company
Technical Library - Microwaves
Box 5837
Orlando, Florida   1

The Martin/Baltimore Company
Technical Library - Antennas
Baltimore, Md. 21203   1

Maxon Electronics Corporation
Sunrise Highway
Great River, L. I., New York 11739   1

McDonnell Aircraft Corporation
Technical Library - Antennas
Box 516
St. Louis, Missouri 63166   1

Melpar, Inc.
Technical Library - Antennas
3000 Arlington Blvd.
Falls Church, Va. 22047   1

MITRE Corporation
Technical Library
Electronic Warfare Department D-21
Middlesex Turnpike
Bedford, Mass. 01730   1

Motorola Western Military Electronics Division
8201 E. McDowell
Scottsdale, Arizona 85252   1

North American Aviation, Inc.
Technical Library - Dept. 56
International Airport
Los Angeles, California 90009   1

North American Aviation, Autonetics Division
System Technology Department
3370 Miraloma Avenue
Anaheim, California 92803   1

North American Aviation/Columbus Division
Technical Library - Engineering Dept.
4300 E. Fifth Avenue
Columbus, Ohio 43216   1

Northrop/Norair Division
3901 West Broadway
Technical Information (3924-3)
Hawthorne, California 90250   1

Northrop/Ventura
Technical Information Center
1515 Rancho Conejo Blvd.
Newbury Park, Calfironia 91320   1

Philco Communications and Electronics
Government and Industrial Division
Technical Library - Antennas
4700 Wissachickon Ave.
Philadelphia, Pa. 19144   1

Radiation Systems, Inc..
Engineering Department
440 Swann Avenue
Alexandria, Va.   1

Radiation Products Division
Technical Library
Box 37
Melbourne, Fla. 31511   1

RCA Missile and Service Radar Division
Manager, Antenna Engineering Skill Center
Marne Highway
Moorestown, New Jersey 08057   1

Rantec Corporation
Librarian - Antenna Laboratory
24003 Ventura Blvd.
Calabasas, California 91302   1

Raytheon Equipment Division
Library - Mr. J. Portsch
P. O. Box 520
Waltham, Mass. 02154   1

Raytheon Missile Systems Division
Research Library
Hartwell Street
Bedford, Mass.   1

Raytheon Space and Information Systems Div.
528 Boston Post Road
Sudsbury, Mass.   1

Sanders Associates
Librarian - Antennas
95 Canal Street
Nashua, New Hampshire   1

Sichak Associates.
Mr. W. Sichak
518 Franklin Ave.
Nutley, New Jersey   1

HRB Singer Corporation
Attn: Library - Antennas
Box 60, Science Park
State College, Pa. 16801   1

Southwest Research Institute
Librarian - Antenna Laboratory
8500 Culebra Road
San Antonio, Texas 78206   1

Space Technology Laboratory
Research Library
One Space Park
Redondo Beach, California 90278   1

Sperry Gyroscope Division
Librarian - Antenna Laboratory
Great Neck, L. I., New York 11020   1

Sperry Microwave Electronics Division
Librarian - Antenna Laboratory
Box 1828
Clearwater, Florida   1

Stanford Research Institute
Librarian - Antennas
333 Ravenswood Street
Menlo Park, California 94025   1

Sylvania Electronic Products
Librarian - Antennas
Box 188
Mountain View, California   1

Sylvania Electronic Systems Division
Librarian - Antennas and Microwaves
40 Sylvan
Waltham, Mass 02154   1

Teledyne Communications System Division
12964 Panama Street
Los Angeles 66, California   1

Texas Instruments, Inc.
Librarian - Antennas
13500 N. Central Expressway
Dallas, Texas 75209   1

A. S. Thomas, Inc.
Librarian - Antennas
355 Providence Highway
Westwood, Mass. 02091   1

Westinghouse Aerospace Division
P. O. Box 746
Baltimore, Md. 21203   1

Wheeler Laboratories
Librarian - Antennas
Box 561
Smithtown, New York 11787   1

AFCRL
C. J. Sletten CRD
L G Hanscom Field
Bedford, Mass. 01731   2

AFETRL - Technical Library
Patrick AFB, Bla. 32925   1

AFMDC - Technical Library
Holloman AFB, New Mexico 88330   1

APGC, Hq. 3208 Test Group
Eglin AFB, Fla. 32542   1

ASD - ASEP B. Brooks
Wright-Patterson AFB, Ohio 45433   1

RADC - EMATA,
Griffiss AFB, New York 13442   1

RADC EMLT-1
Griffiss AFB, New York 13442   1

RADC EMIAD - R F Davis
Griffiss AFB, New York 13442   1

SEG - SEAEM Mr. Mulligan
Wright-Patterson AFB, Ohio 45433   1

SEG - SEACC Y. E. Stahler
Wright-Patterson AFB, Ohio 45433   1

SEG - SEPIE
Wright-Patterson AFB, Ohio 45433   1

AFSC - SCSE
Andrews AFB, Wash. D. C. 20331   1

RTD - RTGS
Bolling AFB, Washington, D. C. 20332   1

Hq, USAF, AFRDR, Lt. Col. B. Lieber
Washington, D. C. 20330   1

Hq, USAF AFXSAI, Air Battle Analysis Center
Dep. Dir. Plans for War Plans
Washington, D. C. 20330   1

RTD RTHR
Bolling AFB, Washington, D. C. 20332   1

FTD TD-EE
Wright-Patterson AFB, Ohio 45433   1

U. S. Army Electronics Command
SIGRA/NAI
Ft. Monmouth, N J   1

U. S. Army White Sands Missile Range
Technical Library ORDBS-OM   RR-312
White Sands, New Mexico 88002   1

Ballistic Research Laboratory
Technical Library - Antennas
Aberdeen Proving Ground, Md. 21005   1

Harry Diamond Laboratories
Connecticut Ave., and Vann Ness Street, NW
Attn: 240
Washington, D. C. 20438   1

U S Army Electronics R and D Activity
SELWS-ED
White Sands Missile Range, N. Mexico 88002   1

USAFSS
ESD/ESG Mr. A. Martinez
San Antonio, Texas 78241   1

Director, Surveillance Dept.
Evans Area
Technical Document Center
Belmar, New Jersey   1

ONR Branch Office
Box 39
FPO, New York 09510   1

Chief, Bureau of Ships
Code 312
Main Navy Building
Washington, D. C. 20360   1

Naval Research Laboratory
Code 5200
Washington, D. C. 20390   1

U S Naval Air Test Center
WSST-54, Antenna Section
Patuxent River, Md. 20910   1

Materials Laboratory
New York Naval Shipyard
Code 932
Brooklyn, N. Y. 11201   1

U. S. Navy Electronics Laboratory Code 3220 - Library San Diego, California 92152	1
U. S. Naval Ordnance Test Station Mr. J. A. Mosko - Code 4021 China Lake, California 93557	1
U. S. Naval Ordnance Laboratory Technical Library Corona, California 91720	1
Office, Assist. Sec'y Def. R and D Technical Library 3E1065, Pentagon Washington, D. C. 20330	1
Air University Library 3T-AUL-59-30 Maxwell AFB, Alabama 36112	1
NASA Goddard Space Flight Center Antenna Branch Greenbelt, Md. 20771	1
V. DeSanti, Exchange Section DCD Scientific/Technical Information Facility P O Box 5700 Bethesda, Md.	1
GIT Engineering Experiment Station Technical Library - Electronics Division Atlanta, Ga. 30313	1
JHU Applied Physics Laboratory 8621 Georgia Avenue Silver Springs, Md. 20910	1
JHU Carlyle Barton Laboratory Charles and 34th Streets Baltimore, Md. 22218	1
MIT-Lincoln Laboratory Document Room Box 73 Lexington, Mass. 02173	1
New Mexico State University Antenna Department Physical Science Dept. University Park, New Mexico	1

Northeastern University
Dodge Library
Boston, Mass. 02115   1

Ohio University
Technical Library - EE Dept.
Athens, Ohio   1

Ohio State University Research Foundation
Technical Library - Antenna Laboratory
2024 Neil Ave.
Columbus, Ohio 43210   1

Ohio State University Antenna Laboratory
Technical Library
1320 Kinnear Road
Columbus Ohio 43212   1

PIB Microwave Research Institute
Professor A. A. Oliner
55 Johnson St.
Brooklyn, N. Y. 11201   1

Stanford Electronics Laboratory
Librarian - Antennas
Stanford, California 94025   1

Syracuse University
Dr. Jose Perihi - Electrical Engineering Dept.
Syracuse, N. Y. 13210   1

University of Dayton Research Institute
Professor Douglas Hanneman
300 College Park
Dayton, Ohio 45409   1

University of Southern California
W. V. Trusch - EE Dept.
University Park
Los Angeles, California 90007   1

University of Texas - EE Res. Lab.
Route 4
Box 189
Austin, Texas   1

Cornell Aeronautical Laboratory
Research Library
Buffalo, New York 14221   1

University of Illinois EE Res. Laboratory
Engineering Experiment Station
Urbana, Illinois   1

Air Force Avionics Laboratory
AVWE-3
Wright-Patterson AFB, Ohio 45433   5 + reproducible

Defense Documentation Center
Alexandria Virginia 22314   20 + card

                                                                          163 + reproducible

DOCUMENT CONTROL DATA - R&D

(Security classification of title, body of abstract and indexing annotation must be entered when the overall report is classified)

1. ORIGINATING ACTIVITY *(Corporate author)*	2a. REPORT SECURITY CLASSIFICATION
The University of Michigan Radiation Laboratory	Unclassified
Department of Electrical Engineering	2b. GROUP
Ann Arbor, Michigan 48108	

3. REPORT TITLE

Study and Investigation of a UHF-VHF Antenna

4. DESCRIPTIVE NOTES *(Type of report and inclusive dates)*

Quarterly Report No. 6 1 April 1967 through 30 June 1967

5. AUTHOR(S) *(Last name, first name, initial)*

Lyon, John A. M., Chen, Chao-Chun, Greene, Edward S., Parker, James C., and Smith, Dean L.

6. REPORT DATE	7a. TOTAL NO. OF PAGES	7b. NO. OF REFS
August 1967	89	26

8a. CONTRACT OR GRANT NO.	9a. ORIGINATOR'S REPORT NUMBER(S)
AF 33(615)-3609	7848-6-Q
b. PROJECT NO. 6278	
c. Task 627801	9b. OTHER REPORT NO(S) *(Any other numbers that may be assigned this report)*
d.	Quarterly Report No. 6

10. AVAILABILITY/LIMITATION NOTICES

Subject to special Export Controls (DoD Dir. 203. 4A FR 400-10); not to be disseminated to OTS. Qualified requestors may obtain copies from DDC

11. SUPPLEMENTARY NOTES	12. SPONSORING MILITARY ACTIVITY
	Air Force Avionics Laboratory
	Research and Technology Division, AFSC
	Wright-Patterson AFB, Ohio 45433

13. ABSTRACT This report discusses the activity and accomplishment of the various aspects of four assigned tasks of this project for a three month period. Under Task 1, studies have centered upon the development of a helical slow wave structure utilizing ferrite. The objective is to use this helical structure as a winding on a log conical spiral. In this way, the ferrite loading material would be associated with the conductor of the log conical spiral rather than as a core.

A ferrite loaded slot array is being studied under Task 2. Some preliminary results are given utilizing type Q-3 ferrite sticks in transmission line fed slots. As a result, the type of ferrite loaded slot arrays will be completely changed in future work. Individually ferrite slots will be used rather than those fed by a waveguide. The objectives under the new program of ferrite loaded arrays are described in some detail.

Under Task 3, studies have been made on ferrite rod antennas. Most of the work has been on analysis of such antennas. Simple experimental models have been fabricated, but test data are not yet available. Various analytical approaches are considered in the report. A review has been made of such analyses by other workers. An analysis more complete than any hertofore, is now underway. Principal considerations of this analysis are given.

Various types of antenna configurations useful down to 30 MHz are studied under Task 4. A discussion and analysis is given on the advantages of multi-linear elements. Experimental data are recorded upon the tuning of linear elements utilizing magnetic biasing. Multiple resonance behavior of composite slow wave structures is considered both experimentally and analytically.

Additional information is reported on the testing of ferrite materials. For the frequency ranges involved, previous test methods have not been entirely satisfactory. For this reason, a strip line cavity was fabricated.

DD $_{1 \text{ JAN } 64}^{\text{FORM}}$ **1473**

14. KEY WORDS	LINK A		LINK B		LINK C	
	ROLE	WT	ROLE	WT	ROLE	WT
FERRITE ROD ANTENNA						
LOADED SMALL HELIX						
FERRITE LOADING TECHNIQUES						
PHYSICALLY SMALL ANTENNAS						

INSTRUCTIONS

1. ORIGINATING ACTIVITY: Enter the name and address of the contractor, subcontractor, grantee, Department of Defense activity or other organization (corporate author) issuing the report.

2a. REPORT SECURITY CLASSIFICATION: Enter the overall security classification of the report. Indicate whether "Restricted Data" is included. Marking is to be in accordance with appropriate security regulations.

2b. GROUP: Automatic downgrading is specified in DoD Directive 5200.10 and Armed Forces Industrial Manual. Enter the group number. Also, when applicable, show that optional markings have been used for Group 3 and Group 4 as authorized.

3. REPORT TITLE: Enter the complete report title in all capital letters. Titles in all cases should be unclassified. If a meaningful title cannot be selected without classification, show title classification in all capitals in parenthesis immediately following the title.

4. DESCRIPTIVE NOTES: If appropriate, enter the type of report, e.g., interim, progress, summary, annual, or final. Give the inclusive dates when a specific reporting period is covered.

5. AUTHOR(S): Enter the name(s) of author(s) as shown on or in the report. Enter last name, first name, middle initial. If military, show rank and branch of service. The name of the principal author is an absolute minimum requirement.

6. REPORT DATE: Enter the date of the report as day, month, year; or month, year. If more than one date appears on the report, use date of publication.

7a. TOTAL NUMBER OF PAGES: The total page count should follow normal pagination procedures, i.e., enter the number of pages containing information.

7b. NUMBER OF REFERENCES: Enter the total number of references cited in the report.

8a. CONTRACT OR GRANT NUMBER: If appropriate, enter the applicable number of the contract or grant under which the report was written.

8b, 8c, & 8d. PROJECT NUMBER: Enter the appropriate military department identification, such as project number, subproject number, system numbers, task number, etc.

9a. ORIGINATOR'S REPORT NUMBER(S): Enter the official report number by which the document will be identified and controlled by the originating activity. This number must be unique to this report.

9b. OTHER REPORT NUMBER(S): If the report has been assigned any other report numbers (either by the originator or by the sponsor), also enter this number(s).

10. AVAILABILITY/LIMITATION NOTICES: Enter any limitations on further dissemination of the report, other than those imposed by security classification, using standard statements such as:

  (1) "Qualified requesters may obtain copies of this report from DDC."

  (2) "Foreign announcement and dissemination of this report by DDC is not authorized."

  (3) "U. S. Government agencies may obtain copies of this report directly from DDC. Other qualified DDC users shall request through

    _____."

  (4) "U. S. military agencies may obtain copies of this report directly from DDC. Other qualified users shall request through

    _____."

  (5) "All distribution of this report is controlled. Qualified DDC users shall request through

    _____."

If the report has been furnished to the Office of Technical Services, Department of Commerce, for sale to the public, indicate this fact and enter the price, if known.

11. SUPPLEMENTARY NOTES: Use for additional explanatory notes.

12. SPONSORING MILITARY ACTIVITY: Enter the name of the departmental project office or laboratory sponsoring (paying for) the research and development. Include address.

13. ABSTRACT: Enter an abstract giving a brief and factual summary of the document indicative of the report, even though it may also appear elsewhere in the body of the technical report. If additional space is required, a continuation sheet shall be attached.

It is highly desirable that the abstract of classified reports be unclassified. Each paragraph of the abstract shall end with an indication of the military security classification of the information in the paragraph, represented as (TS), (S), (C), or (U).

There is no limitation on the length of the abstract. However, the suggested length is from 150 to 225 words.

14. KEY WORDS: Key words are technically meaningful terms or short phrases that characterize a report and may be used as index entries for cataloging the report. Key words must be selected so that no security classification is required. Identifiers, such as equipment model designation, trade name, military project code name, geographic location, may be used as key words but will be followed by an indication of technical context. The assignment of links, rules, and weights is optional.